Library Declaration and Deposit Agreement

1. STUDENT DETAILS

Please complete the following:

Full name: …………………………………………………………………………………….

University ID number: …………………………………………………………………………

2. THESIS DEPOSIT

2.1 I understand that under my registration at the University, I am required to deposit my thesis with the University in BOTH hard copy and in digital format. The digital version should normally be saved as a single pdf file.

2.2 The hard copy will be housed in the University Library. The digital version will be deposited in the University's Institutional Repository (WRAP). Unless otherwise indicated (see 2.3 below) this will be made openly accessible on the Internet and will be supplied to the British Library to be made available online via its Electronic Theses Online Service (EThOS) service.
[At present, theses submitted for a Master's degree by Research (MA, MSc, LLM, MS or MMedSci) are not being deposited in WRAP and not being made available via EthOS. This may change in future.]

2.3 In exceptional circumstances, the Chair of the Board of Graduate Studies may grant permission for an embargo to be placed on public access to the hard copy thesis for a limited period. It is also possible to apply separately for an embargo on the digital version. (Further information is available in the *Guide to Examinations for Higher Degrees by Research*.)

2.4 *If you are depositing a thesis for a Master's degree by Research, please complete section (a) below. For all other research degrees, please complete both sections (a) and (b) below:*

(a) Hard Copy

I hereby deposit a hard copy of my thesis in the University Library to be made publicly available to readers (please delete as appropriate) EITHER immediately OR after an embargo period of ………..................... months/years as agreed by the Chair of the Board of Graduate Studies.

I agree that my thesis may be photocopied.   YES / NO (*Please delete as appropriate*)

(b) Digital Copy

I hereby deposit a digital copy of my thesis to be held in WRAP and made available via EThOS.

Please choose one of the following options:

EITHER   My thesis can be made publicly available online.   YES / NO (*Please delete as appropriate*)

OR   My thesis can be made publicly available only after…..[date] (Please give date)
                                                       YES / NO (*Please delete as appropriate*)

OR   My full thesis cannot be made publicly available online but I am submitting a   separately identified   additional, abridged version that can be made available online.
                                                       YES / NO (*Please delete as appropriate*)

OR   My thesis cannot be made publicly available online.   YES / NO (*Please delete as appropriate*)

3. **GRANTING OF NON-EXCLUSIVE RIGHTS**

    Whether I deposit my Work personally or through an assistant or other agent, I agree to the following:

    Rights granted to the University of Warwick and the British Library and the user of the thesis through this agreement are non-exclusive. I retain all rights in the thesis in its present version or future versions. I agree that the institutional repository administrators and the British Library or their agents may, without changing content, digitise and migrate the thesis to any medium or format for the purpose of future preservation and accessibility.

4. **DECLARATIONS**

    (a) I DECLARE THAT:

    - I am the author and owner of the copyright in the thesis and/or I have the authority of the authors and owners of the copyright in the thesis to make this agreement. Reproduction of any part of this thesis for teaching or in academic or other forms of publication is subject to the normal limitations on the use of copyrighted materials and to the proper and full acknowledgement of its source.

    - The digital version of the thesis I am supplying is the same version as the final, hard-bound copy submitted in completion of my degree, once any minor corrections have been completed.

    - I have exercised reasonable care to ensure that the thesis is original, and does not to the best of my knowledge break any UK law or other Intellectual Property Right, or contain any confidential material.

    - I understand that, through the medium of the Internet, files will be available to automated agents, and may be searched and copied by, for example, text mining and plagiarism detection software.

    (b) IF I HAVE AGREED (in Section 2 above) TO MAKE MY THESIS PUBLICLY AVAILABLE DIGITALLY, I ALSO DECLARE THAT:

    - I grant the University of Warwick and the British Library a licence to make available on the Internet the thesis in digitised format through the Institutional Repository and through the British Library via the EThOS service.

    - If my thesis does include any substantial subsidiary material owned by third-party copyright holders, I have sought and obtained permission to include it in any version of my thesis available in digital format and that this permission encompasses the rights that I have granted to the University of Warwick and to the British Library.

5. **LEGAL INFRINGEMENTS**

    I understand that neither the University of Warwick nor the British Library have any obligation to take legal action on behalf of myself, or other rights holders, in the event of infringement of intellectual property rights, breach of contract or of any other right, in the thesis.
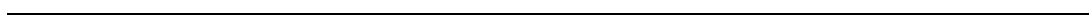
Please sign this agreement and return it to the Graduate School Office when you submit your thesis.

Student's signature: ....………… Date: ....

JHG 05/2011
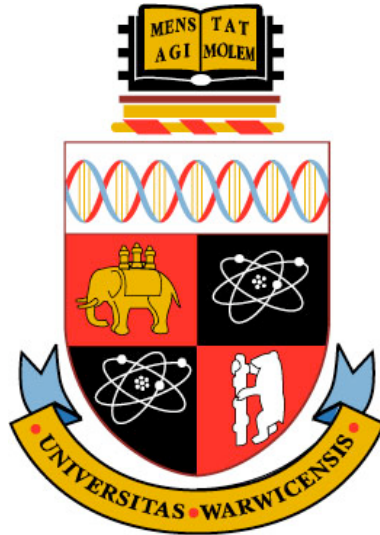
Aperiodically forced oscillators

A Hau Gin

A thesis submitted in fulfilment of the requirements for the
degree of Doctor of Philosophy

Mathematics Department, University of Warwick

28 January 2012

THE UNIVERSITY OF

WARWICK

Contents

Dedication

I dedicate this thesis to You God. Thank You for your faithfulness and providence. You gave me the strength and the will to keep going and stay focussed on the goal. You blessed me with incredibly kind people at every step! Thank You for forgiving me for thinking that I can make it without You and teaching me the valuable lesson that pride comes before a fall. Thank You God that in your Fatherly love You still receive this far from perfect thesis as an offering! I say this in Jesus' name, the name above all names, Amen!

Acknowledgements

I thank my thesis supervisors for their help and support throughout the course of my doctoral study. In particular, it has been an inspiration to work with Robert MacKay and I am very grateful for his direction. I am indebted to him for his time, care and interest in my research. I am also thankful for Magnus Richardson for his supervision and especially his encouragement when I needed it most. I would like to express my gratitude to him for setting up the Theoretical Neuroscience Group which has been stimulating and motivating for us all. I would like to thank those in TNG who have contributed to my research experience, especially Azadeh Khajeh-Alijani, Naveed Malik and Robert Gardner who gave me much enjoyment and interesting conversation in the field. Special thanks to Rupert Swarbrick and Michael Korotyaev for their valuable support in computer programming and Yi Chan for general proof–reading of this thesis.

Many thanks to those family members and friends who have given me moral support and spurred me on to the completion of this thesis. I would also like to thank Jianwen Zhang for her support in many ways.
I would also like to mention those Ph.D friends such as Yuxin Yang, Wu Bo, Patrick O'Callaghan and Umar Hayat who have made my study an enjoyable experience. Thanks to the Warwick University Badminton team, in particular team mates such as Andy Hotchen, Nikko Cheung and Matthew Seeley, for providing me much enjoyment in training and games. Special thanks to the Coventry Chinese Christian Church and the youth group for giving me memorable times during my study.

Declaration

I declare that, to the best of my knowledge, the material contained in this thesis is original and my own work except where otherwise indicated, cited, or commonly known.

Chapter 1

Motivation and introduction

1.1 Motivation

The motivation of this project is synchronisation at the network level. The emerging behaviour of synchronisation is ubiquitous in science, nature and engineering. It is found in systems as diverse as clocks, flashing fireflies, cardiac pacemakers, bursting neurons and applauding audiences (PRK01).

This phenomenon has received much attention from many generations of researchers dating as far back as 1665 when Christiaan Huygens recognised it in his clocks. However, possibly the earliest record of synchronisation may be found in the book of Joshua in the Bible when the Israelites besieged the ancient city of Jericho around 1200 B.C. In brief, the Israelite army was ordered to surround the city wall and at a trumpet signal, shouted out in unison. It is possible that the soldiers synchronised with their nearest neighbours to produce a powerful output of synchronised sound, which forced the wall to crumble down and the city was subsequently captured. It is unlikely that the ancient generation knew or understood synchronisation to the extent that they would have been able to exploit it.

The beauty of this phenomenon is that it is very easily recognised by the human mind and yet it is immensely puzzling. It is certainly not obvious how the network with no leader can self-organise into coherence. Insight into this phenomenon is highly important to scientific and technological progress.

For example the Pre–Bötzinger complex, a unit in our brain containing roughly

300 neurons, works rhythmically helping us to breathe subconsciously in a robust and controllable way. However, there can be neuronal dysfunctions such as in sleep apnoea and possibly sudden infant death syndrome (FN06). Thus to be able to understand and control this dysfunction would be highly beneficial to humanity.

The Millennium Bridge in London has shown an undesirable effect termed Synchronous Lateral Excitation where, as the number of walkers on the bridge increases, the bridge reaches a critical mass and starts to sway causing danger to the walkers (Mil). It was due to subsequent research taken that a sensible solution was found and modification of the bridge was made by placing lateral dampers under the bridge deck.

The advancement of computer technology has provided us valuable tools to observe what happens at the network level. For example, we can take a very complicated neuron model and wire many of them together using a computer program to see what properties can arise (BRS99). However, to gain real understanding we need to tackle the problem using analytical tools (Str01). This is a highly difficult task and simplification is inevitable. Reducing the network to just two oscillators is a natural first step. However, for the case of many oscillators, major advancement was made by Kuramoto when he considered a simplified phase model with all-to-all autonomous coupling (Kur84). The system was shown to synchronise as it passes a critical mass which provides greater understanding for the Millennium bridge problem.

However, the Kuramoto phase model is too simplistic and a more realistic approach can be taken which includes the change in amplitude. This motivated my thesis project and led me to consider aperiodically forced oscillators. This is of great interest because the oscillator can receive inputs from other oscillators in the network with unknown architecture and these inputs are unlikely to be periodic and can be treated as time–dependent. This will be very useful for the study of synchronisation of non–autonomous oscillators at the network level.

1.2 Introduction

Oscillations are ubiquitous in nature (Str04, Win80) and the theory of nonlinear oscillators is very useful in the study of these phenomena (GH83, HS74). Autonomous systems of ordinary differential equations that possess a limit cycle are commonly employed to model the individual oscillator. In reality, these systems are invariably subjected to time-dependent influences. The case of time-periodic forcing has been extensively studied giving rise to the phenomenon of Arnol'd

tongues (PRK01). However, periodic forcing is a poor representation of many real situations and relatively little attention has been paid to the case of general bounded time-dependent forcing.

For weak time-dependent forcing, not necessarily periodic, the response of a hyperbolic limit cycle oscillator is clear from the theory of normal hyperbolicity (HPS77, Fen71). In the time–extended space, the limit cycle becomes a normally hyperbolic cylinder which persists when weakly forced.

To be more specific let us first take the following phase coordinate system based at the unperturbed limit cycle of period, T, say. For every point γ on the cycle we give it an angle $\theta \in \mathbb{R}/T\mathbb{Z}$ which is the time it takes for the trajectory to reach γ from a reference point on the cycle. To extend this away from the cycle we can take a tubular neighbourhood of any transverse bundle (a possible choice is the vector bundle defined by taking the tangent space to the invariant foliation, a.k.a "isochron", at the base point on the cycle). Then any point that lies on the transverse fibre based at γ can be assigned the same angle as that of γ and we can take its relative position $r \in \mathbb{R}^n$ from γ to complete the coordinate system, where the dimension of the system is $n+1$. The unperturbed limit cycle is given by $r = 0$ and we can write the perturbed system in the neighbourhood of the unperturbed limit cycle as

$$\dot{\theta} = \Theta(\theta, r, t)$$
$$\dot{r} = R(\theta, r, t). \tag{1.1}$$

In the unperturbed case, Θ and R are independent of t, $\Theta(\theta, 0, t) = \omega = 1/T$ and $R(\theta, 0, t) = 0$. We assume that Θ and R are C^1. The unperturbed limit cycle is *hyperbolic* if the time-T map of the linearised unperturbed dynamics

$$\dot{\xi} = R_r(\omega t, 0, t)\xi, \qquad \xi \in \mathbb{R}^n \tag{1.2}$$

has no eigenvalue on the unit circle. The application here will be to stable oscillators, thus the case of interest is when the spectrum is inside the unit circle but the theory applies equally well even if there is some spectrum outside too. Since we are studying non-autonomous systems it is convenient to extend the state space to include time, t, as an additional coordinate. As a result the straight cylinder, $r = 0$, in the time–extended space, which represents the product of the unperturbed limit cycle with time, is normally hyperbolic. By (HPS77, Fen71) it follows that the straight cylinder persists to a C^1- nearby normally hyperbolic invariant submanifold $r = \rho(\theta, t)$ under bounded C^1 perturbation, i.e. the perturbed system has the invariant submanifold given by ρ. The vector field on the perturbed cylinder is C^1- close to $\dot{\theta} = \omega$, $\dot{t} = 1$. Strictly speaking, a

non–compact version of (HPS77, Fen71) is required.

This is fine as theory, but in practice one would like to know how close the cylinder is to the unperturbed one and to what extent the dynamics on the cylinder change. To achieve realistic estimates, I shall present an path–wise approach to computing the perturbed invariant manifold which has the advantage that there is no graph transform involved and the operator it uses can be made an arbitrarily strong contraction if coordinates are chosen appropriately, see Theorem 3.2.2. It could be a persistence theory in itself, however this would require a result on smoothness which is not shown here. A hybrid approach is also proposed here in a conjecture which has a graph transform that is potentially a strong contraction if coordinates are chosen appropriately.

The outline of the thesis is as follows. In Chapter 2 we include the theory of uniform hyperbolicity which captures the behaviour of the dynamic transverse to the submanifold. We will see that a set of uniformly hyperbolic trajectories is robust to perturbation of the vector field that generate these trajectories. This will be used to prove invertibility for a Newton step in Chapter 3, which outlines the path–wise approach to computing the normally hyperbolic invariant manifold and the hybrid approach. The graph transform method due to (HPS77) will also be briefly covered and a comparison between their method and ours is given. Given that the invariant manifold can be approximated the next step is to investigate the dynamics on it, for example synchronisation, which is the subject of Chapter 4. Pseudo–codes and C++ header files based on the theories of Chapter 3 will be given in Chapter 5 for attracting systems. These are implemented for a simple aperiodically forced oscillator with numerical results for both methods. These methods are also tested on a physiologically relevant oscillator described in Chapter 6 where periodic, two–frequency and Poisson spike train forcing were explored. Finally the thesis ends with Chapter 7 which summarises each chapter with conclusions and discussions.

Chapter 2

Uniform hyperbolicity

We are primarily interested in normal hyperbolicity of invariant manifolds, whose analysis includes the dynamics in the centre direction as well as the transverse direction to the manifold. This will require the theory of uniform hyperbolicity, which restricts attention to the transverse direction only. Uniform hyperbolicity can be stated in a functional form, in particular the invertibility of the associated linear operator (BM03). This is equivalent to the concept of exponential dichotomies which gives the existence of splittings of exponentially contracting and expanding complementary linear spaces through time (Cop78).

Viewing Uniform Hyperbolicity in terms of exponential dichotomy is more intuitive as it can be used to describe the linearised transverse direction of nonlinear systems. However, the functional form is useful to us as it provides invertibility of an operator which will be employed in a Newton operator as seen in Chapter 3. We will show one direction of the equivalence, in particular, invertibility implies exponential dichotomy. See (Cop78) for more details on the subject of exponential dichotomy where exponential on "half" lines, $\mathbb{R}_-$ and $\mathbb{R}_+$, were dealt with individually. Here we deal with the entire real line $\mathbb{R}$.

Uniformly hyperbolic sets of system arising from a time dependent vector field u in the centre direction is developed here which is not studied in (Cop78). Each system in the set is given by a matrix evaluated at a trajectory of u which has initial value y_0 at t_0. It is shown that the projections, thus the splittings, in the exponential dichotomy vary Hölder continuously with the initial value y_0. Moreover, a perturbation result is also achieved here where if $\tilde{u}$ is a small enough perturbation of u, the set of systems arising from $\tilde{u}$ is also a uniformly hyperbolic set.

2.1 Preliminaries

The following two lemmas are applied to general linear operators which I include without proof. They concern the invertibility of perturbed linear operators and their bounds, which can be useful here. See (Kat76) for details. We denote the space of bounded linear operators from Banach space X to Banach space Y by $\mathcal{B}(X,Y)$.

Lemma 2.1.1 *Assume the linear operator $P \in \mathcal{B}(X,Y)$ is such that $||P|| < 1$. Then the Neumann series $Q = (I - P)^{-1} = \sum_{n=0}^{\infty} P^n$ is well defined and we have the following bounds*

$$||Q|| \leq (1 - ||P||)^{-1}, \qquad ||Q - I|| \leq \frac{||P||}{1 - ||P||}. \tag{2.1}$$

Lemma 2.1.2 *Consider the linear operators $T, \mu \in \mathcal{B}(X,Y)$ and assume $T^{-1} \in \mathcal{B}(Y,X)$ exists and μ is T-bounded, i.e. $|\mu u| \leq a|u| + b|Tu|$ for all u with constants $a, b \geq 0$. If we have $a||T^{-1}|| + b < 1$ then a perturbation of T given by $S = T + \mu$ is invertible and we have the following bounds*

$$||S^{-1}|| \leq \frac{||T^{-1}||}{1 - a||T^{-1}|| - b}, \qquad ||S^{-1} - T^{-1}|| \leq \frac{||T^{-1}||(a||T^{-1}|| + b)}{1 - a||T^{-1}|| - b}. \tag{2.2}$$

We will make use of the special case $b = 0$.

2.2 Linear non–autonomous systems

Take the following free (unforced) system,

$$\dot{x} = A(t)x \qquad \text{for } t \in \mathbb{R} \quad \text{and } x \in V \tag{2.3}$$

where V is an n–dimensional vector space and $A(t)$ a bounded $n \times n$ matrix function. This system has a matrix solution $X(t,s)$ with $X(s,s) = I$ for all $s \in \mathbb{R}$, i.e. it satisfies

$$\partial_1 X(t,s) = A(t)X(t,s). \tag{2.4}$$

Note that by differentiating the identity $X(t,s)X(s,t) = I$ with respect to s,

$$\partial_2 X(t,s)X(s,t) = -X(t,s)\partial_1 X(s,t), \tag{2.5}$$

and thus $X(t,s)$ also satisfies $\partial_2 X(t,s) = -X(t,s)A(s)$.

We will be considering the forced system

$$\dot{x} = A(t)x + f(t) \qquad (2.6)$$

with the forcing, f, lying in the space of bounded continuous functions

$$C^0 = \{f : \mathbb{R} \to V \mid |f|_0 < \infty\} \qquad (2.7)$$

where $|f|_0 := \sup_{s \in \mathbb{R}} |f(s)|$. We will take the space of response to a forcing to be the space of continuously differentiable functions

$$C^1 = \{x : \mathbb{R} \to V \mid |x|_1 < \infty\} \qquad (2.8)$$

where $|x|_1 := \max\{|x|_0, \ \tau|\dot{x}|_0\}$. A timescale $\tau > 0$ is included to make the norm scalable with respect to changes in time unit and typically will be chosen to satisfy $\tau|A| \leq 1$, which is chosen to simplify estimates.

The matrix function A in the free system (2.3) has an associated linear operator given by

$$L : C^1 \to C^0 \qquad (2.9)$$
$$\xi \mapsto \dot{\xi} - A(t)\xi.$$

Note that the operator L is invertible if and only if the forced system (2.6) has a unique bounded response for each forcing $f \in C^0$.

A simple example is given by $A(t) = v_y(y(t), t)$, v_y denoting the partial derivative, which gives the linearised dynamics around a solution, $y()$, of a vector field, $\dot{y} = v(y, t)$, thus typically, A belongs to a set of matrix functions defined by the set of solutions $y()$.

We will work with the set of bounded continuous matrix functions $\mathcal{F}$. Since every matrix $A \in \mathcal{F}$ has an associated linear operator L as described above we can view $\mathcal{F}$ to be the set of those linear operators.

Definition 2.2.1 (Uniformly hyperbolic linear system) *The free linear system (2.3) given by a bounded matrix function A is uniformly hyperbolic with bound $K > 0$ if the associated operator, L, is invertible with $||L^{-1}||^{-1} \geq K$ using the operator norm.*

Note that since τ is used to define the norm of the range of L^{-1}, K depends on the choice of τ. Due to invertibility, a small perturbation of a uniformly hyperbolic system has a bounded inverse. This is the case for any general invertible linear operator from one Banach space to another as seen in Lemma

2.1.2. The following special case is useful.

Lemma 2.2.1 *Assume L is uniformly hyperbolic and $||\Delta L|| < ||L^{-1}||^{-1}$. Then $L' = L - \Delta L$ is invertible and $||L'^{-1}||^{-1} \geq ||L^{-1}||^{-1} - ||\Delta L||$.*

Definition 2.2.2 (Uniformly hyperbolic set) *A set $\mathcal{F}$ of bounded matrix functions is a uniformly hyperbolic set with bound $K > 0$ if for each member $A \in \mathcal{F}$ the associated operator L is invertible with $||L^{-1}||^{-1} \geq K$ using the operator norm.*

2.3 Functional analysis and exponential dichotomy

2.3.1 Exponential dichotomy

Here we will see that invertibility of the linear operator L implies exponential dichotomy. In fact the reverse is also true (Cop78).

Definition 2.3.1 *A matrix P is a projection if $P^2 = P$. The range and kernel of P are denoted by $\mathcal{R}(P)$ and $\mathcal{N}(P)$ respectively.*

Definition 2.3.2 (Exponential Dichotomy) *The free linear system (2.3) has an exponential dichotomy if there are complementary invariant projections $P_{\pm}(s)$, exponent $\mu > 0$ and constant $C(\mu, \tau)$ such that for $x_{\pm}(s) \in \mathcal{R}(P_{\pm}(s))$*

$$\left| X(t,s)x_+(s) \right| \leq Ce^{-\mu(t-s)}|x_+(s)| \qquad for \quad s \leq t,$$
$$\left| X(t,s)x_-(s) \right| \leq Ce^{-\mu|t-s|}|x_-(s)| \qquad for \quad t \leq s. \qquad (2.10)$$

for every $s \in \mathbb{R}$.

Let us now state and prove a theorem which states that uniform hyperbolicity implies exponential dichotomy.

Theorem 2.3.1 *If the free linear system (2.3) is uniformly hyperbolic then it has an exponential dichotomy.*

The proof is adapted from (Cop78) where the major change is that we are dealing with the entire real line $\mathbb{R}$ and not just the half line $\mathbb{R}_+ = [0, \infty)$.

Proof: Given the associated linear operator L is invertible with $||L^{-1}||^{-1} \geq K$ we will show that there are complementary projections $P_{\pm}$ at each point $s \in \mathbb{R}$, bounded uniformly in s. Moreover, for any $\mu \in [0, K)$ there is $C(\mu, \tau) \in \mathbb{R}$, such that for $x(s) \in E_{\pm}(s) = \mathcal{R}(P_{\pm}(s))$ the trajectory of $x(t)$ satisfies

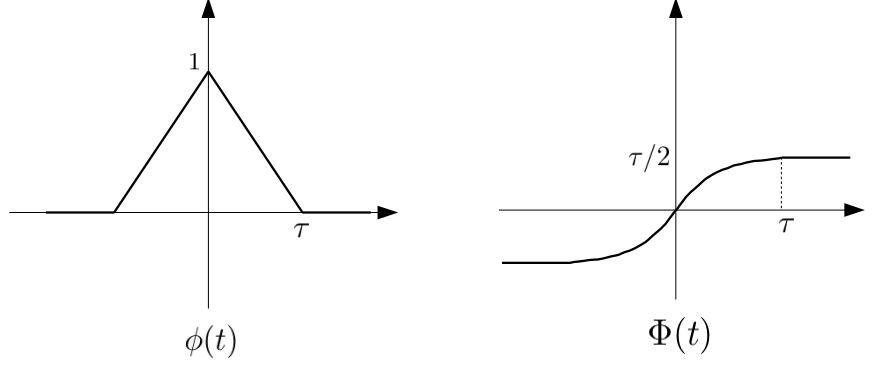$$|x(t)| \leq Ce^{-\mu|t-s|}|x(s)| \qquad for \qquad s \lessgtr t, respectively.$$

Figure 2.1: A sketch of the tent map ϕ and its integral Φ.

Obtaining $P_\pm$

Choose timescale $\tau > 0$ such that $|A| \leq 1/\tau$. Given time $s \in \mathbb{R}$, for any vector x_0 at s we wish to split x_0 into two components, one with a bounded forward orbit and the other with bounded backward orbit. Let x be the unbounded solution of the free linear system (2.3) from the initial condition $x(s) = x_0 \neq 0$. Without loss of generality, we take $s = 0$. Now consider the tent map and its integral as follows

$$\phi(t) = \begin{cases} 1 - |t|/\tau & \text{for } |t| < \tau \\ 0 & \text{otherwise} \end{cases}$$

$$\Phi(t) = \int_0^t \phi(t) = \begin{cases} t - sgn(t)\frac{t^2}{2\tau} & \text{for } |t| < \tau \\ sgn(t)\frac{\tau}{2} & \text{otherwise} \end{cases}$$

For a sketch of ϕ and Φ see figure 2.1. Let $\zeta = \Phi x$ and $\eta = \phi x$, then differentiation ζ with respect to time we have $\dot{\zeta} = A(t)\zeta + \eta$. By the definition of uniform hyperbolicity there is a unique bounded solution $\beta = L^{-1}\eta$. Now let

$$x_+ = (\beta - \zeta)/\tau + \frac{1}{2}x$$

$$x_- = (\beta - \zeta)/\tau - \frac{1}{2}x \tag{2.11}$$

and note that x_+ satisfies $\dot{x}_+ = Ax_+$ and equals β/τ for $t > \tau$, so is bounded for $t \geq s = 0$. Similarly, x_- satisfies $\dot{x}_- = Ax_-$ and equals β/τ for $t < -\tau$, so is bounded for $t \leq s = 0$. See figure 2.2 for a sketch of $x_\pm(s)$ and their forward and backward orbit respectively. Then $x = x_+ - x_-$ and we define

$$P_+ x_0 = x_+(0)$$
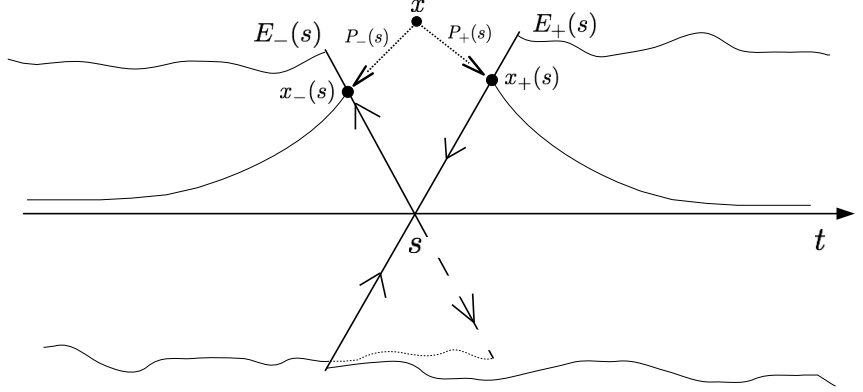
$$P_- x_0 = -x_-(0).$$

15

Figure 2.2: A sketch showing the vector spaces $E_{\pm}(s)$ as the range of the respective projections $P_{\pm}(s)$ varying through time. The arrows from the origin at time s on $E_{\pm}(s)$ indicate the respective vector space contracts forward and backward in time respectively. Also shown, at time s, the point x is projected to $x_{\pm}(s)$ by $P_{\pm}(s)$ respectively.

By construction, since L^{-1} is linear, $P_{\pm}$ are linear and sum to the identity. The ranges of $P_{\pm}$ have intersection $\{0\}$ since the free linear system has no non–trivial bounded solution on the whole of $\mathbb{R}$. To see they are projections, take $P_{+}x_0 = x_{+}(0)$ as new initial condition and define η_{+}, ζ_{+}, β_{+} to be the corresponding functions above. Then $(\beta_{+} - \zeta_{+})/\tau - \frac{1}{2}x_{+}$ is bounded not only for $t < 0$ but also for $t > 0$ since each of its terms is bounded for $t > 0$. But the free linear system has no non–trivial bounded solution, thus $(\beta_{+} - \zeta_{+})/\tau - \frac{1}{2}x_{+} = 0$, i.e. $P_{-}P_{+}x_0 = 0$. From $P_{+} + P_{-} = I$ we deduce that $P_{\pm}^2 = P_{\pm}$. To obtain uniform bounds for $P_{\pm}$, note that from the choice of τ, $|x(t)| \leq e^{|t|/\tau}|x_0|$,

$$|\beta(0)| \leq |\beta|_0 \leq |\beta|_1 \leq K^{-1}|\eta|_0 = K^{-1} \sup_{|t|<\tau} (1 - \frac{|t|}{\tau})|x(t)| \leq K^{-1}|x_0| \quad (2.12)$$

since $(1 - \frac{|t|}{\tau})e^{|t|/\tau}$ is a decreasing function of $|t|$. Also noting $\zeta(0) = 0$ we have

$$|x_{+}(0)| = |(\beta(0) - \zeta(0))/\tau + \frac{1}{2}x(0)| \leq (\frac{1}{K\tau} + \frac{1}{2})|x_0| \quad (2.13)$$

Thus $|P_{+}| \leq \frac{1}{K\tau} + \frac{1}{2}$ and similarly $|P_{-}| \leq \frac{1}{\tau K} + \frac{1}{2}$.

To show invariance of $P_{\pm}$ under the linear flow, let $\tilde{P}_{\pm}(t) = X(t,0)P_{\pm}(0)X(0,t)$. They are complementary projections at t and the forward orbits from $\mathcal{R}(\tilde{P}_{+}(t))$

16
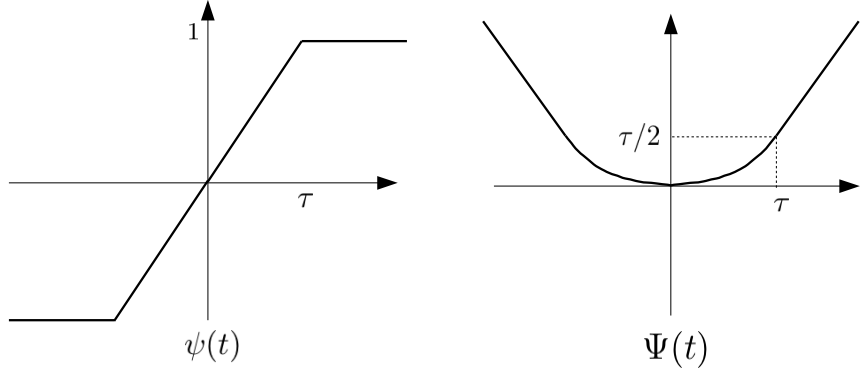
Figure 2.3: A sketch of the "switch" map ψ and its integral Ψ.

are bounded while the backward orbits from $\mathcal{R}(\tilde{P}_-(t))$ are bounded. The latter condition determines $P_\pm(t)$ uniquely, so $P_\pm(t) = \tilde{P}_\pm(t)$. Hence, the invariance condition $P_\pm(t)X(t,0) = X(t,0)P_\pm(0)$.

Obtaining $C(\mu, \tau)$

To obtain the exponentially decaying bounds for $x_\pm$ we make use of the "switch" map and its integral, see figure 2.3 for a sketch,

$$\psi(t) = \begin{cases} \frac{t}{\tau} & \text{for } |t| < \tau \\ sign(t) & \text{otherwise} \end{cases}$$

$$\Psi(t) = \int_0^t \psi(u)du = \begin{cases} \frac{t^2}{2\tau} & \text{for } |t| < \tau \\ |t| - \frac{\tau}{2} & \text{otherwise.} \end{cases} \tag{2.14}$$

Consider the following perturbed linear operator

$$L_\mu : C^1 \to C^0 \tag{2.15}$$

$$\zeta \mapsto \dot{\zeta} - A\zeta - \mu\psi\zeta.$$

For $\mu \in [0, K)$, L_μ is invertible with $||L_\mu^{-1}||^{-1} \geq K - \mu$ (applying Lemma 2.2.1 with $b = 0$). Let $\tilde{x} = xe^{\mu\Psi}$, $\tilde{\beta} = \beta e^{\mu\Psi}$ and $\tilde{\eta} = \phi\tilde{x}$. Then

$$L_\mu\tilde{\beta} = \tilde{\eta} \quad \Rightarrow \quad |\tilde{\beta}|_1 \leq \frac{1}{K - \mu}|\tilde{\eta}|_0. \tag{2.16}$$

We show that $|\tilde{\eta}|_0 = |x_0|$. Note that $K^{-1} \geq \tau$ (otherwise by Lemma 2.1.2 $L + A = \partial_t$ would be invertible, which is not the case) so $\mu < 1/\tau$ since $K \leq$

17

$|A| \le 1/\tau$. We have

$$|\tilde{\eta}|_0 \le \sup_{|t|<\tau} |\phi(t)x(t)e^{\mu\Psi(t)}| = \sup_{|t|<\tau} (1 - |t|/\tau)|x_0|e^{\frac{|t|}{\tau}} e^{\frac{t^2}{2\tau^2}} \le |x_0| \qquad (2.17)$$

since $(1 - |t|/\tau)e^{\frac{|t|}{\tau}} e^{\frac{t^2}{2\tau^2}}$ is a decreasing function of $|t|$. But $\tilde{\eta}(0) = x_0$, so we have the required equality. Then $|\tilde{\beta}|_1 \le \frac{1}{K-\mu}|x_0|$ and so

$$|\beta(t)| \le \frac{1}{K - \mu}|x_0|e^{-\mu\Psi(t)}. \qquad (2.18)$$

Now if $x_0 \in \mathcal{R}(P_+)$ then $x_+ = \frac{\beta}{\tau} + (\frac{1}{2} - \frac{\Phi}{\tau})x_+$, so

$$x_+ = \frac{\beta}{\Phi + \tau/2} \qquad (2.19)$$

and thus

$$|x_+(t)| \le \frac{e^{-\mu\Psi}|x_0|}{(K - \mu)(\Phi + \tau/2)}. \qquad (2.20)$$

So

$$|x_+(t)| \le C'(t)e^{-\mu t}|x_0| \text{ with } C'(t) = \frac{e^{\mu(t-\Psi)}}{(K - \mu)(\Phi + \tau/2)}. \qquad (2.21)$$

For $t \ge 0$, $t - \Psi(t) = \Phi(t)$ and C' is non–increasing so we have the bound

$$C(\mu, \tau) \le \frac{2}{(K - \mu)\tau} \text{ for } t \ge 0. \qquad (2.22)$$

Proceed similarly for $x_0 \in \mathcal{R}(P_-)$ and negative time.
Note that this bound can be improved to

$$C(\mu, \tau) \le \frac{e^{\mu\tau/2}}{(K - \mu)\tau} \text{ for } t \ge \tau. \qquad (2.23)$$

$\blacksquare$

Remarks 1

(i) *One can optimise the decay estimate (2.21) over μ by using the bound (2.23). The optimum over μ is at $\mu = K - \frac{1}{t-\tau/2}$ which is valid for $t \ge \frac{3}{2K}$ if we set $\tau > 1/K$. Then the following bound can be obtained*

$$|x_+(t)| \le (\frac{t}{\tau} - \frac{1}{2})e^{1-K(t-\tau/2)}|x_0| \text{ for } t \ge \frac{3}{2K}. \qquad (2.24)$$

18

(ii) The functions ϕ and ψ could be chosen asymmetrically, and different values of μ could be used for positive and negative time; if the resulting operator (call it L_{μ_+, μ_-}) happens to remain invertible for larger values of one or both of $\mu_\pm$ then stronger decay estimates follow. In particular, in the attracting case, $P_- = 0$.

2.3.2 Green functions and bounds on response for certain types of forcing

The following definition can be found in (Cop78).

Definition 2.3.3 *The Green's function for a uniformly hyperbolic linear system is the matrix on $\mathbb{R}^2$ defined by*

$$G(t,s) = \begin{cases} X(t,s)P_+(s) & \text{for } s < t \\ -X(t,s)P_-(s) & \text{for } t < s. \end{cases}$$

Fixing s, $G(t,s)$ is the unique bounded solution of $\dot{x}(t) = A(t)x(t)$ for $t \neq s$ with $G(s+,s) - G(s-,s) = I$. Note that by invariance of the projections, $G(t,s)$ can also be written as

$$G(t,s) = \begin{cases} P_+(t)X(t,s) & \text{for } s < t \\ -P_-(t)X(t,s) & \text{for } t < s \end{cases}$$

and that $\partial_2 G(t,s) = -G(t,s)A(s)$ for $s \neq t$,

$$G(t,t+) - G(t,t-) = I \tag{2.25}$$

Theorem 2.3.2 *If the linear system (2.3) is uniformly hyperbolic then it has the following properties.*

(i) *The unique bounded response $x = L^{-1}[f]$ of (2.6) to the forcing, f, can be written as*

$$x(t) = \int_{-\infty}^{+\infty} G(t,s)f(s)ds. \tag{2.26}$$

(ii) *For any $\mu \in [0,K)$ there exists $D(\mu)$ such that $|G(t,s)| \leq De^{-\mu|t-s|}$.*

(iii) *If $|f(s)| \leq \varepsilon e^{\mu|s|}$ for some $\mu \in [0,K)$ then $|x(t)| \leq \frac{\varepsilon e^{\mu|t|}}{(K-\mu)}$.*

(iv) *If $T > 0$ and f is a bounded function with $f(s) = 0$ for all $s \in (-T,T)$ then $|x(t)| \leq \frac{e^{-\mu(T-|t|)}}{K-\mu}|f|$; optimising over $\mu \in [0,K)$ yields*

$$|x(t)| \leq (T - |t|)e^{1-K(T-|t|)}|f| \text{ for } |t| \leq T - 1/K. \tag{2.27}$$

Proof:

(i) We can verify this by differentiating (2.26) w.r.t. t, taking care to first split the integral at $s = t$ where the integral is not differentiable:

$$\dot{x}(t) = \int_{-\infty}^{+\infty} A(t)G(t,s)f(s)ds + P_+(t)f(t) + P_-(t)f(t)$$

$$= A(t)x(t) + f(t). \tag{2.28}$$

But $L^{-1}[f]$ is the unique bounded solution of $\dot{x} = Ax + f$, thus it is given by (2.26).

(ii) A bound on $|G(t,s)|$ can already be obtained by composition of those of the previous theorem for the projections and the evolution of vectors in their ranges, but it will be useful to sharpen the estimate as follows. Repeat the estimates using L_μ as in the proof of the previous theorem to obtain (2.18). Then $x_+ = \frac{\beta}{\tau} + (\frac{1}{2} - \frac{\Phi}{\tau})x$ implies

$$e^{\mu t}|x_+(t)| \leq \left(\frac{e^{\mu(t - \Psi(t))}}{\tau(K - \mu)} + (\frac{1}{2} - \frac{\Phi(t)}{\tau})e^{\mu t}e^{t/\tau} \right)|x_0| \text{ for } t \geq 0. \tag{2.29}$$

Note that for $t \geq 0$, $t - \Psi(t)$ attains its sup value of $\frac{\tau}{2}$ at $t \geq \tau$; $(\frac{1}{2} - \frac{\Phi(t)}{\tau})e^{(\mu + \frac{1}{\tau})t}$ attains its sup value of $\frac{1}{2}$ at $t = 0$ since it is a decreasing function on $t \geq 0$. Thus

$$|x_+(t)| \leq De^{-\mu t}|x_0| \tag{2.30}$$

for $t \geq 0$ with $D = \frac{e^{\mu \tau / 2}}{(K - \mu)\tau} + \frac{1}{2}$. Similarly $|x_-(t)| \leq De^{-\mu t}|x_0|$ for $t \leq 0$. This result could be optimised over μ if desired.

(iii) If $|f(s)| \leq \varepsilon e^{\mu|s|}$ then $Lx = f$ is equivalent to $L_{-\mu}\tilde{x} = \tilde{f}$ with $\tilde{x} = e^{-\mu\Psi}x$ and $\tilde{f} = e^{-\mu\Psi}f$, where $L_{-\mu}$ is as defined in (2.15) but using the opposite sign of μ and Ψ is as defined in (2.14) except now we allow its value of τ to differ from that in the definition of the norm $|\cdot|_1$ in (2.8). Then $||L_{-\mu}^{-1}||^{-1} \geq K - \mu$ for $\mu \in [0, K)$, so

$$|\tilde{x}| \leq \frac{|\tilde{f}|}{K - \mu}. \tag{2.31}$$

This gives

$$|x(t)e^{-\mu\Psi(t)}| = |\tilde{x}(t)| \leq \frac{|\tilde{f}|}{K - \mu} \leq \frac{\varepsilon}{K - \mu}. \tag{2.32}$$

This holds true for all $\tau > 0$ so we can take τ to 0 to obtain the result.

(iv) If f is a bounded function with $f(s) = 0$ for all $s \in (-T, T)$ then again (2.31) with $\tau \to 0$ gives

$$|x(t)| \leq \frac{e^{-\mu(T-|t|)}|f|}{K - \mu}. \tag{2.33}$$

The minimum over $\mu \in [0, K)$ is achieved at $\mu = K - \frac{1}{|t|-T}$ which is in $[0, K)$ for $|t| \leq T - 1/K$, giving the optimised result.

$\blacksquare$

Theorem 2.3.3 *If* $0 \leq \alpha < K \leq ||L^{-1}||^{-1}$, $|f(s)| \leq F$, $|f(s)| \leq \varepsilon e^{\alpha|s|}$ *for* $s \in (-T, T)$, $x = L^{-1}[f]$, $|t| \leq T - 1/K$, *then*

$$|x(t)| \leq \frac{\varepsilon}{K - \alpha} e^{\alpha|t|} + (T - |t|)e^{1-K(T-|t|)}F. \tag{2.34}$$

Proof: Consider

$$f_1(t) = \begin{cases} f(t) & \text{for } |t| < T \\ (t + T + 1)f(-T) & \text{for } -T - 1 < t < -T \\ (T + 1 - t)f(T) & \text{for } T < t < T + 1 \\ 0 & \text{for } |t| > T + 1 \end{cases}$$

and

$$f_2(t) = \begin{cases} 0 & \text{for } |t| < T \\ f(t) - (t + T + 1)f(-T) & \text{for } -T - 1 < t < -T \\ f(t) - (T + 1 - t)f(T) & \text{for } T < t < T + 1 \\ f(t) & \text{for } |t| > T + 1. \end{cases}$$

Note that $f = f_1 + f_2$, so we have

$$|x(t)| \leq |L^{-1}[f_1](t)| + |L^{-1}[f_2](t)| \tag{2.35}$$

By Theorem 2.3.2 (iii) and (iv), we have $|L^{-1}[f_1](t)| \leq \frac{\varepsilon e^{\alpha|t|}}{K-\alpha}$ and $|L^{-1}[f_2](t)| \leq (T - |t|)e^{1-K(T-|t|)}F$ for $|t| \leq T - 1/K$. Adding the two gives the result. $\blacksquare$

The use of this result is to suppose that ε is small and that we can take $T = \frac{1}{\gamma} \log \frac{F}{\varepsilon}$ for some $\gamma \in (\alpha, K)$. Then roughly speaking the first term of (2.34) dominates for $|t|/T < \frac{K-\gamma}{K-\alpha}$. T goes to infinity as $\varepsilon \to 0$. We put this into Corollary 2.3.1.

Corollary 2.3.1 *Let* $T = \frac{1}{\gamma} \log \frac{F}{\varepsilon}$ *then for* $|t|/T < \frac{K-\gamma}{K-\alpha}$ *we have*

$$|x(t)| \leq \frac{\varepsilon + O(\varepsilon)}{K - \alpha} e^{\alpha|t|}.$$

Hence $|x(t)| \leq \frac{\varepsilon + O(\varepsilon)}{K - \alpha} e^{\alpha |t|}$, uniformly on any bounded interval of t.

Proof: Consider the ratio $\rho = y e^{1-y} x$ of the second term of (2.34) to the first where $y = (K - \alpha)(T - |t|)$ and $x = \frac{F}{\varepsilon e^{\alpha T}}$. So $\rho \leq 1$ when $y \geq g(x)$ where g is the inverse function to e^{y-1}/y on $y \geq 1$.

We will show that g is bounded above by the function $\bar{g}(x) = \log(2ex \log(ex))$. Consider the equation $x = e^{y-1}/y$ which, after some manipulation, gives $\log(2ex(\log xe)) = y + \log(2(1 - \frac{\log y}{y}))$. But $\frac{\log y}{y}$ has maximum at $y = e^1$ with largest value e^{-1}, so $2(1 - \frac{\log y}{y}) \geq 1$ giving us $\bar{g} \geq g$.

So $y \geq \bar{g}(x)$ implies the second term (2.34) is at most the first. Now $\log x = \log \frac{F}{\varepsilon} - \alpha T = (\gamma - \alpha)T$ if we take $T = \frac{1}{\gamma} \log \frac{F}{\varepsilon}$ with $\gamma \in (\alpha, K)$. Thus the second term is at most the first when $y \geq \log x + \log(2e(1 + \log x))$ i.e $(K - \alpha)(T - |t|) \geq (\gamma - \alpha)T + \log(2e(1 + (\gamma - \alpha)T))$ which gives

$$
\begin{aligned}
|t| \leq &T - \frac{1}{K - \alpha}((\gamma - \alpha)T + \log(2e(1 + (\gamma - \alpha)T))) \\
\leq &\frac{K - \gamma}{K - \alpha}T - \frac{1}{K - \alpha} \log(2e(1 + (\gamma - \alpha)T)).
\end{aligned}
\tag{2.36}
$$

Similarly, for any $p > 0$, we obtain $\rho \leq p$ if $y \geq g(x/p)$, which is true if

$$
\begin{aligned}
|t| \leq &\frac{K - \gamma}{K - \alpha}T - \frac{1}{K - \alpha} \log(\frac{2e}{p}(1 + (\gamma - \alpha)T) + \log(1/p)). \\
\leq &\frac{K - \gamma}{K - \alpha}T.
\end{aligned}
\tag{2.37}
$$

∎

2.3.3   Continuity of the splitting

Let $\mathcal{F}$ be a uniformly hyperbolic set, then it can be useful to know how the projections $P_\pm(t)$ vary across the members of the set. With some Lipschitz conditions on how the set is generated it can be shown that the projections vary Hölder continuously. This is stated more precisely in the following theorem.

Definition 2.3.4 *Let $\mathcal{A}$ be a matrix function evaluated on the time–extended state space. Take $\mathcal{F}$ to be the set of those matrix functions that are given by $A(t) = \mathcal{A}(y(t), t)$ where $y(\cdot)$ is an orbit of some vector field $\dot{y} = u(y, t)$. We say $\mathcal{F}$ is generated by $\mathcal{A}$ and u.*

Theorem 2.3.4 *Assume $\mathcal{A}$ (bounded) and u are Lipschitz and let $\mathcal{F}$ be a uniformly hyperbolic set generated by $\mathcal{A}$ and u, then the projections $P_\pm(t)$ vary Hölder continuously with the initial condition y_0 at time $t = 0$.*

The difficulty here is that the trajectories from nearby y_0 at $t = 0$ may separate arbitrarily far and the bound

$$|\Delta A| \leq \text{Var}(\mathcal{A}) = \sup_{y_1,y_2,t} |\mathcal{A}(y_1, t) - \mathcal{A}(y_2, t)| \qquad (2.38)$$

is in general insufficient to apply the perturbation Lemma 2.2.1 and in any case is insensitive to $|\Delta y_0|$. Thus we will need to work harder.

Before we state the proof, we note one simple consequence of the continuity of $P_\pm$ in the finite-dimensional case – their ranks are constant on connected components, which can be easily argued by contradiction: Let P and P' be projections based at y_0 and y_0' respectively where $|y_0 - y_0'|$ is arbitrarily small. Assume P' has greater rank than P, then by counting dimensions $\mathcal{N}(P) \cap \mathcal{R}(P')$ is non–trivial. Thus it contains a non-zero v that satisfies $Pv = 0$ and $P'v = v$, so $|P - P'| \geq 1$, which contradicts continuity.

Proof: Unless stated otherwise, all integrals are definite integrals over $\mathbb{R}$. First, we note the difference between the inverses of two invertible linear operators is given by

$$L_1^{-1} - L_0^{-1} = L_1^{-1}(L_0 - L_1)L_0^{-1}. \qquad (2.39)$$

In our case $L_0 - L_1 = \Delta A = A_1 - A_0$, so if we denote $\Delta G(t, u) := G_1(t, u) - G_0(t, u)$, we have

$$\begin{aligned}
\int \Delta G(t, u) f(u) du &= (L_1^{-1} - L_0^{-1})[f](t) \\
&= \int G_1(t, s) \Delta A(s) \left(\int G_0(s, u) f(u) du \right) ds \\
&= \int \left(\int G_1(t, s) \Delta A(s) G_0(s, u) ds \right) f(u) du
\end{aligned}$$

$$(2.40)$$

which gives

$$\Delta G(t, u) = \int G_1(t, s) \Delta A(s) G_0(s, u) ds.$$

Thus we have

$$\Delta P_+(t) = \Delta G(t+, t) = \int G_1(t+, s) \Delta A(s) G_0(s, t) ds. \qquad (2.41)$$

Now $|\Delta A| \leq V = Var(\mathcal{A}) \leq 2|\mathcal{A}|$ gives a crude estimate but for s near 0 we can do better. Specifically, if $\lambda = \text{Lip}_y u$ and $\alpha = \text{Lip}_y \mathcal{A}$ then we get the Gronwall's

estimate $|\Delta y(t)| \le e^{\lambda |t|}|\Delta y_0|$, so $|\Delta A(t)| \le \alpha e^{\lambda |t|}|\Delta y_0|$.

Using the estimate of $|G(t,s)| \le De^{-\mu |t-s|}$ of Theorem 2.3.2 (ii) we obtain

$$|\Delta P_+(t)| \le \int D^2 e^{-2\mu |t-s|}\min\{\alpha e^{\lambda |s|}|\Delta y_0|, V\}ds. \qquad (2.42)$$

Supposing $|\Delta y_0| \le V/\alpha$, let $s^* \ge 0$ be the value such that $\alpha e^{\lambda s^*}|\Delta y_0| = V$, so $e^{\lambda s^*} = \frac{V}{\alpha |\Delta y_0|}$. Taking $|\Delta y_0|$ small enough so that $-s^* < t$ and assuming without loss of generality that $t < 0$,

$$|\Delta P_+(t)| \le \int_{-\infty}^{-s^*} D^2 V e^{-2\mu |s-t|}ds + \int_{-s^*}^{t} + \int_{t}^{0} + \int_{0}^{s^*} D^2 e^{-2\mu |s-t|}\alpha e^{\lambda |s|}|\Delta y_0|ds$$

$$+ \int_{s^*}^{\infty} D^2 V e^{-2\mu |s-t|}ds. \qquad (2.43)$$

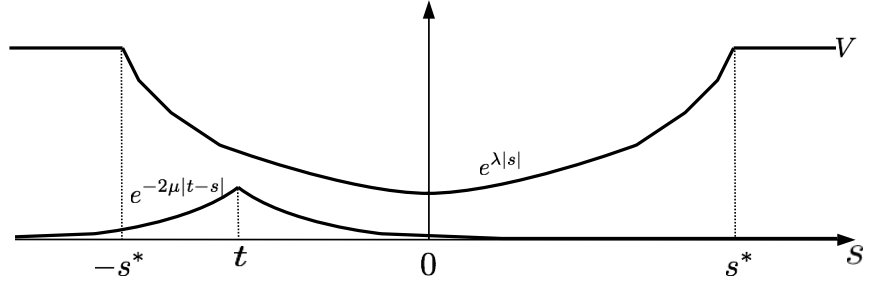See Figure 2.4 for a sketch of the exponential bounds and the five regions of

Figure 2.4: A sketch of $e^{-2\mu |t-s|}$ and $\min\{e^{\lambda |s|}, V\}$ with t fixed and s varying. Note the five integration regions of (2.43) are $[-\infty, -s^*], [-s^*, t], [t, 0], [0, s^*]$ and $[s^*, \infty]$.

integration. Putting $\xi = \alpha|\Delta y(0)|/V \leq 1$, each integral evaluates as follows

$$\begin{aligned}
1^{st} \text{ integral } &\leq \int_{-\infty}^{-s^*} VD^2 e^{2\mu(s-t)} ds \\
&\leq \frac{VD^2}{2\mu} e^{2\mu(s^*-t)} \\
&\leq \frac{VD^2}{2\mu} e^{2\mu|t|} \xi^{2\mu/\lambda},
\end{aligned}$$

$$\begin{aligned}
2^{nd} \text{ integral } &\leq \int_{-s^*}^{t} VD^2 \xi e^{(2\mu-\lambda)s - \lambda t} ds \\
&\leq \frac{VD^2}{2\mu - \lambda} \xi \left(e^{\lambda|t|} - \xi^{2\mu/\lambda} e^{\frac{2\mu}{\lambda}|t|} \xi^{-1} \right) \\
&\leq \frac{VD^2}{2\mu - \lambda} e^{\lambda|t|} \left(\xi - \xi^{2\mu/\lambda} e^{(2\mu-\lambda)|t|} \right),
\end{aligned}$$

Note that if $\lambda = 2\mu$ this term is interpreted as $\frac{VD^2}{\lambda} e^{-2\mu t} \xi \log \xi^{-1}$.

$$\begin{aligned}
3^{rd} \text{ integral } &\leq \int_{t}^{0} VD^2 \xi e^{-2\mu(s-t)} e^{-\lambda t} ds \\
&\leq \frac{VD^2}{-2\mu - \lambda} \xi \left(e^{2\mu t} - e^{-\lambda t} \right),
\end{aligned}$$

$$\begin{aligned}
4^{th} \text{ integral } &\leq \int_{0}^{s^*} VD^2 e^{-2\mu(s-t)} e^{\lambda t} ds \\
&\leq \frac{VD^2}{2\mu - \lambda} e^{-2\mu|t|} \left(\xi - \xi^{2\mu/\lambda} \right) \\
&\leq \frac{VD^2}{2\mu - \lambda} e^{-2\mu|t|} \left(\xi - \xi^{2\mu/\lambda} e^{4\mu|t|} \right),
\end{aligned}$$

$$\begin{aligned}
5^{th} \text{ integral } &\leq \int_{s^*}^{\infty} VD^2 e^{-2\mu(s-t)} ds \\
&\leq \frac{VD^2}{2\mu} e^{-2\mu|t|} \xi^{2\mu/\lambda}.
\end{aligned}$$

Thus for small enough $|\Delta y_0|$ we have $|\Delta P_+(t)| = O(|\Delta y_0|^\delta)$ for some $0 < \delta$ (although not uniformly over t) hence P_+ is Hölder continuous with respect to y_0. Note that if $2\mu > \lambda$ then P_+ is Lipschitz with respect to y_0. We can see this

as follows:

$$1^{st} + 5^{th} \text{ integral } \leq \frac{VD^2}{\mu}e^{2\mu|t|}\xi^{2\mu/\lambda}$$

$$2^{nd} + 4^{th} \text{ integral } \leq \frac{VD^2}{2\mu - \lambda}\left(e^{\lambda|t|} + e^{-2\mu|t|}\right)\xi - \frac{2VD^2}{2\mu - \lambda}e^{2\mu|t|}\xi^{2\mu/\lambda}. \quad (2.44)$$

So the sum of all four integral is bounded by

$$
\begin{aligned}
1^{st} + 5^{th} + 2^{nd} + 4^{th} \leq &\frac{VD^2}{2\mu - \lambda}\left(e^{\lambda|t|} + e^{-2\mu|t|}\right)\xi + \left(\frac{VD^2}{\mu} - \frac{2VD^2}{2\mu - \lambda}\right)e^{2\mu|t|}\xi^{2\mu/\lambda} \\
\leq &\frac{VD^2}{2\mu - \lambda}\left(e^{\lambda|t|} + e^{-2\mu|t|}\right)\xi - \frac{\lambda VD^2}{2\mu - \lambda}e^{2\mu|t|}\xi^{2\mu/\lambda} \\
\leq &\frac{VD^2}{2\mu - \lambda}\left(e^{\lambda|t|} + e^{-2\mu|t|}\right)\xi. \quad (2.45)
\end{aligned}
$$

Adding the bound for the 3rd integral we have $|\Delta P_+(t)| = O(\xi) = O(|\Delta y_0|)$ hence P_+ is Lipschitz with respect to y_0.
The same applies to P_-. ∎

At a later stage we will consider a perturbed set $\tilde{\mathcal{F}}$ generated by $\mathcal{A}$ and $\tilde{u}$, a perturbation of u. It will be useful to know that the Green's function resulting from a concatenation of truncated orbits of the perturbed and unperturbed systems also varies Hölder continuously. The specific choice will be given on the next page. For now, take a trajectory $\tilde{y}(\cdot)$ of the perturbed system $\dot{y} = \tilde{u}(y, t)$ and consider the unperturbed trajectory $y(\cdot)$ that passes through $(\tilde{y}(\sigma), \sigma)$ for some σ. First we calculate a time S that $|\Delta A(t)| = |\mathcal{A}(\tilde{y}(t), t) - \mathcal{A}(y(t), t)| \leq \eta$ remains true for $|t - \sigma| \leq S$ for some η (we will truncate $\tilde{y}$ at $\sigma \pm S$). Now the difference $\Delta y(t)$ between the perturbed and unperturbed trajectory starting at $(\tilde{y}(\sigma), \sigma)$ evolves by

$$\Delta \dot{y} = \tilde{u}(\tilde{y}, t) - u(y, t) = \Delta u(\tilde{y}, t) + (u(\tilde{y}, t) - u(y, t)) \quad (2.46)$$

starting from $\Delta y(\sigma) = 0$. The second term is at most $\lambda \Delta y(t)$ where λ is the Lipschitz constant of u, so we have the Gronwall's estimate

$$
\begin{aligned}
|\Delta y(t)| &\leq \int_\sigma^t ds e^{\lambda|s-\sigma|}|\Delta u(\tilde{y}(s), s)| \\
&\leq \frac{e^{\lambda|t-\sigma|} - 1}{\lambda}|\Delta u| \\
&\leq \frac{e^{\lambda|t-\sigma|}}{\lambda}|\Delta u|. \quad (2.47)
\end{aligned}
$$

26

Taking Lipschitz constant α for $\mathcal{A}$ we obtain

$$|\Delta A(t)| \leq \alpha |\Delta y(t)| \leq \frac{\alpha}{\lambda} e^{\lambda |t - \sigma|} |\Delta u|. \tag{2.48}$$

Thus $|\Delta A(t)| \leq \eta$ for all $|t - \sigma| \leq S$ if

$$e^{-\lambda S} = \frac{\alpha}{\lambda} \frac{|\Delta u|}{\eta}. \tag{2.49}$$

The choice of η determines how big the perturbation $|\Delta u|$ can be.

We are now ready to define, for any σ, a concatenated path as follows

$$y^{\sigma}(t) = \begin{cases} \tilde{y}(t) & \text{for } |t - \sigma| \leq S \\ y(t) & \text{for } |t - \sigma| \geq S + \varepsilon_0 \\ y_-^{\sigma}(t) & \text{for } \sigma - S - \varepsilon_0 < t < \sigma - S \\ y_+^{\sigma}(t) & \text{for } \sigma + S < t < \sigma + S + \varepsilon_0 \end{cases}$$

where y is the unperturbed trajectory passing through $(\tilde{y}(\sigma), \sigma)$,
$y_-^{\sigma}(t) = \tau_-^{\sigma}(t) \tilde{y}(\sigma - S) + (1 - \tau_-^{\sigma}(t)) y(\sigma - S - \varepsilon_0)$ and
$y_+^{\sigma}(t) = \tau_+^{\sigma}(t) \tilde{y}(\sigma + S) + (1 - \tau_+^{\sigma}(t)) y(\sigma + S + \varepsilon_0)$ with $\tau_-^{\sigma} : t \mapsto \frac{t - (\sigma - S - \varepsilon_0)}{\varepsilon_0}$ and
$\tau_+^{\sigma} : t \mapsto \frac{t - (\sigma + S)}{\varepsilon_0}$. So y^{σ} is essentially a concatenation of truncation of $\tilde{y}$ and y
with y_-^{σ} and y_+^{σ} (see Figure 2.5). Note that ε_0 can be chosen to be as small as
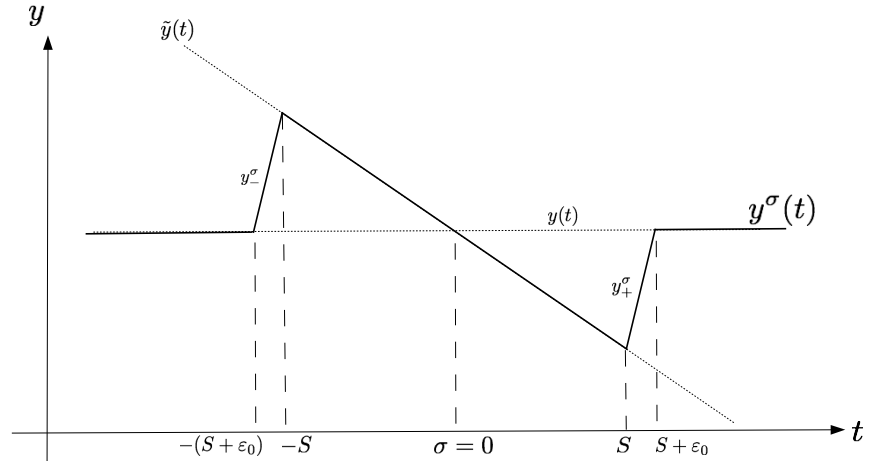we wish.

Figure 2.5: A sketch of $y^{\sigma}(t)$ for the case $\sigma = 0$ which is a concatenation of $y(t)$ for $t \in [-\infty, -(S + \varepsilon_0)]$, $y_-^{\sigma}(t)$ for $t \in [-(S + \varepsilon_0), -S]$, $\tilde{y}(t)$ and $t \in [-S, S]$, $y_+^{\sigma}(t)$ for $t \in [S, (S + \varepsilon_0)]$ and $y(t)$ for $t \in [(S + \varepsilon_0), \infty]$

27

Corollary 2.3.2 *Assume $L : x \mapsto \dot{x} - \mathcal{A}(y(t), t)x$ has bound $\|L^{-1}\|^{-1} \geq K$ and let $\eta < K/2$. Fix $\varepsilon_0 \leq \eta/(\alpha|u|)$ where $\alpha = \mathrm{Lip}_y \mathcal{A}$ and consider the following set of operators parametrised by σ*

$$L_\sigma : C^1 \to C^0$$

$$x \mapsto \dot{x} - A_\sigma(t)x \tag{2.50}$$

with $A_\sigma(t) = \mathcal{A}(y^\sigma(t), t)$. Then L_σ is invertible and the Green's function G_σ is continuous with respect to σ.

Proof: Unless stated otherwise, all integrals are definite integrals over $\mathbb{R}$. L_σ is invertible since it can be shown to be just a small perturbation of L. Firstly, we show that $|\Delta A(t)| := |\mathcal{A}(y^\sigma(t), t) - \mathcal{A}(y(t), t)| \leq 2\eta$ for all t.
It is clear that $|\Delta A(t)| = 0$ for $|t - \sigma| \geq S + \varepsilon_0$ and from how S was calculated we see that $|\Delta A(t)| \leq \eta$ for $|t - \sigma| \leq S$.

Now for $\sigma - S - \varepsilon_0 < t < \sigma - S$ we have

$$
\begin{aligned}
|\Delta A(t)| &\leq \alpha |y_-(t) - y(t)| = \alpha |\tau_-^\sigma(t)(\tilde{y}(\sigma - S) - y(\sigma - S - \varepsilon_0))| \\
&\leq \alpha |\tilde{y}(\sigma - S) - y(\sigma - S - \varepsilon_0))| \\
&\leq \alpha |\tilde{y}(\sigma - S) - y(\sigma - S))| + \alpha |y(\sigma - S) - y(\sigma - S - \varepsilon_0)| \\
&\leq \alpha \frac{e^{-\lambda S}}{\lambda} |\Delta u| + \alpha |u| \varepsilon_0 \leq \eta + \eta \\
&\leq 2\eta. \tag{2.51}
\end{aligned}
$$

Similarly for $\sigma + S < t < \sigma + S + \varepsilon_0$ we have $|\Delta A(t)| \leq 2\eta$. Note that ε_0 can be chosen very small so that better bounds can be obtained, i.e. $|\Delta A| \leq (1 + \varepsilon)\eta$ for some small ε.

So L_σ is a perturbation of L with $\|\Delta L\| = |\Delta A| \leq 2\eta$. By Lemma 2.2.1, if $2\eta < K$ then L_σ is invertible with bound

$$\|L_\sigma^{-1}\|^{-1} \geq K - 2\eta. \tag{2.52}$$

To show the Green's function G_σ is continuous with respect to σ we prove the projections $P_\pm^\sigma$ are continuous with respect to σ. Let us assume without loss of generality $\sigma' < \sigma = 0$. Now consider $y^{\sigma'}$ which is a concatenation of truncations of $\tilde{y}$ and y' with $y_+^{\sigma'}$ and $y_-^{\sigma'}$ where $y'(\cdot)$ is a solution of the unperturbed system passing through $(\tilde{y}(\sigma'), \sigma')$, see Figure 2.6) for a sketch of y^σ and $y^{\sigma'}$. Taking
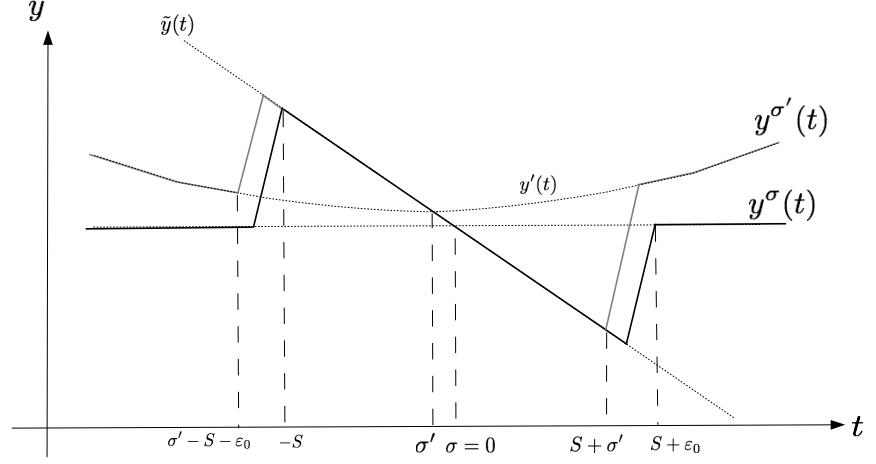
28

Figure 2.6: A sketch of $y^{\sigma'}$ and y^{σ}

$|\Delta A_\sigma| = |A_\sigma - A_{\sigma'}|$ then just as in expression (2.41) we have

$$\Delta P_+^\sigma(t) = \int G_\sigma(t+,s)\Delta A_\sigma(s)G_{\sigma'}(s,t)ds. \tag{2.53}$$

We see that $\Delta A_\sigma(s) = \Delta A(s) := \mathcal{A}(y(s),s) - \mathcal{A}(y'(s),s)$ for $s < \sigma' - S - \varepsilon_0$ and $s > S + \varepsilon_0$ and $\Delta A_\sigma(s) = 0$ for $-S < s < S + \sigma'$. Using the estimate of $|G_x(t,s)| \le De^{-\mu|t-s|}$ of Theorem 2.3.2 (ii) where $x = \sigma, \sigma'$ and $\mu \in [0, K - 2\eta)$ we have the following bound

$$|\Delta P_+^\sigma(t)| \le \int D^2 e^{-2\mu|t-s|}|\Delta A(s)|ds + \int_{\sigma'-S-\varepsilon_0}^{-S} + \int_{S+\varepsilon_0}^{S+\sigma'} D^2 e^{-2\mu|t-s|}|\Delta A_\sigma(s)|ds. \tag{2.54}$$

We show that each integral is $O(|\Delta\sigma|^\delta) = O(|\sigma'|^\delta)$ for some $0 < \delta$ which implies Hölder continuity. From the bound in (2.42) we saw the 1st integral is $O(|\Delta y_0|^\delta)$. But $|\Delta y_0| = |y(0) - y'(0)| \le |y(0) - \tilde{y}(\sigma')| + |\tilde{y}(\sigma') - y'(0)| \le |\tilde{u}||\sigma'| + |u||\sigma'|$ hence $O(|\Delta y_0|^\delta) = O(|\Delta\sigma|^\delta)$. Now let us treat the 2nd integral (by symmetry the 3rd is the same), which can be further split into 3 integrals

$$2^{nd} \text{ integral} \le \int_{\sigma'-S-\varepsilon_0}^{-S-\varepsilon_0} + \int_{-S-\varepsilon_0}^{\sigma'-S} + \int_{\sigma'-S}^{-S} D^2 e^{-2\mu|t-s|}|\Delta A_\sigma(s)|ds. \tag{2.55}$$

Now the first and third integral of (2.55) are $O(|\sigma'|)$ as they are integrals of bounded functions over a range of length $|\sigma'|$. For the second integral of (2.55)

29

we first show $|\Delta A_\sigma(s)| = O(|\sigma'|)$ for $s \in [-S - \varepsilon_0, \sigma' - S]$ as follows

$$
\begin{aligned}
|\Delta A_\sigma(s)| \leq & \alpha |y_-^\sigma(s) - y_-^{\sigma'}(s)| \\
\leq & \alpha \Big| \tau_-^\sigma(s) \tilde{y}(-S) - \tau_-^{\sigma'}(s) \tilde{y}(\sigma' - S) \\
& + (1 - \tau_-^\sigma(s)) y(-S - \varepsilon_0) - (1 - \tau_-^{\sigma'}(s)) y'(\sigma' - S - \varepsilon_0) \Big| \\
\leq & \alpha \Big| \frac{\sigma'}{\varepsilon_0} \Big(\tilde{y}(\sigma' - S) - y'(\sigma' - S - \varepsilon_0) \Big) + \tau_-^\sigma(s) \Big(\tilde{y}(-S) - \tilde{y}(\sigma' - S) \Big) \\
& + (1 - \tau_-^\sigma(s)) \Big(y(-S - \varepsilon_0) - y'(\sigma' - S - \varepsilon_0) \Big) \Big| \\
\leq & \frac{\alpha}{\varepsilon_0} |\tilde{y}(\sigma' - S) - y'(\sigma' - S - \varepsilon_0)||\sigma'| + \alpha |\tilde{y}(-S) - \tilde{y}(\sigma' - S)| \\
& + \alpha |y(-S - \varepsilon_0) - y'(\sigma' - S - \varepsilon_0)|.
\end{aligned}
\tag{2.56}
$$

We can see the first term is $O(|\sigma'|)$ and the second term is bounded by $\alpha |\sigma'||\tilde{u}|$ hence is also $O(|\sigma'|)$. Now for the third term

$$
\begin{aligned}
3^{rd} \text{ term } \leq & \alpha |y(-S - \varepsilon_0) - y'(-S - \varepsilon_0) + y'(-S - \varepsilon_0) - y'(\sigma' - S - \varepsilon_0)| \\
\leq & \alpha \frac{y(0) - y'(0)}{\lambda} e^{\lambda|S + \varepsilon_0|} + \alpha |\sigma'||u| \\
\leq & \alpha \frac{(|u| + |u'|)|\sigma'|}{\lambda} e^{\lambda|S + \varepsilon_0|} + \alpha |\sigma'||u|,
\end{aligned}
\tag{2.57}
$$

hence it is also $O(|\sigma'|)$. Thus the second integral of (2.55) is $O(|\sigma'|)$ as it is an integral of an $O(|\sigma'|)$ function over a finite range. So the second integral of (2.54) is $O(|\sigma'|)$. From this we can conclude that $|\Delta P_+^\sigma(t)| = O(|\sigma'|^\delta)$ for some $0 < \delta$ although not uniformly over t. This implies P_+^σ and hence G_σ, varies Hölder continuously with respect to σ. ∎

2.3.4 Set of uniformly hyperbolic systems and pseudo–orbits

Given a uniformly hyperbolic set $\mathcal{F}$ that is generated by $\mathcal{A}$ and u, it is useful to know if the set $\tilde{\mathcal{F}}$ generated by perturbing u remains uniformly hyperbolic. This proves to be true for small enough perturbations as we shall see in the following theorem.

Theorem 2.3.5 *Let $\mathcal{A}$ (bounded) and u be Lipschitz and let $\mathcal{F}$ be a uniformly hyperbolic set with bound K that is generated by $\mathcal{A}$ and u. Let $\tilde{u}$ be a perturbation. If $|\Delta u| = |\tilde{u} - u|_0$ is small enough, the set $\tilde{\mathcal{F}}$ generated by $\mathcal{A}$ and $\tilde{u}$ remains uniformly hyperbolic with bound $\tilde{K}$ slightly smaller than K.*

In other words, given the assumptions of the above theorem there is a $\tilde{K}$ such that for all orbits $\tilde{y}(\cdot)$ of $\dot{y} = \tilde{u}(\tilde{y}, t)$, the linear operator $\tilde{L}$ associated to $\tilde{A}(t) = \mathcal{A}(\tilde{y}(t), t)$ is invertible and it satisfies the bound $||\tilde{L}^{-1}||^{-1} \geq \tilde{K}$.

There are various approaches to show the invertibility of $\tilde{L}$. A nice one which is similar to (Pal00), involves constructing approximate right and left inverses T and U in the sense that $||I - \tilde{L}T|| = \varepsilon_T < 1, ||I - U\tilde{L}|| = \varepsilon_U < 1$, so that $\tilde{L}T$ and $U\tilde{L}$ are invertible with norms at most $1/(1 - \varepsilon_T)$ and $1/(1 - \varepsilon_U)$. Then $T(\tilde{L}T)^{-1}$ is a true right inverse to $\tilde{L}$ and $(U\tilde{L})^{-1}U$ is a true left inverse, so $\tilde{L}$ is invertible. Finally, one should show that T or U is bounded and then $||\tilde{L}^{-1}|| \leq ||T||/(1 - \varepsilon_T)$ or $\leq ||U||/(1 - \varepsilon_U)$.

Even with this approach there are various possible choices for the approximate inverses. The difficulty is in constructing the left inverse since $U\tilde{L}$ is a mapping from C^1 to C^1 so the derivative has to be estimated too. We will give a construction where $T = U$.

Proof: Take

$$T[f](t) = \int ds \frac{1}{2a} \int_{t-a}^{t+a} d\sigma \, G_\sigma(t, s) f(s) \qquad (2.58)$$

where G_σ is the Green's function for $L_\sigma x(t) = \dot{x}(t) - A_\sigma(t) x(t)$ with $A_\sigma(t) = \mathcal{A}(y^\sigma(t), t)$ and $y^\sigma(t)$ is a concatenation of paths as given in (2.3.3), and a is some duration of order τ. Note that it makes sense to integrate G_σ over σ because by corollary 2.3.2 it depends continuously on σ.

Bounding $||T||$
We treat T as an operator from C^0 to C^1 and wish to bound it. For each σ, $\int ds \, G_\sigma(t, s) f(s) \leq |f|/(K - 2\eta)$ because, as we saw in corollary 2.3.2, A was changed by at most 2η along an unperturbed trajectory. Thus averaging over an interval of σ produces $|T[f](t)| \leq |f|/(K - 2\eta)$.

Now we bound the derivative. To take care of the jump in $G_\sigma(t, s)$ at $s = t$, we write $T[f](t) = (\int_{-\infty}^{t} + \int_{t}^{\infty}) ds \frac{1}{2a} \int_{t-a}^{t+a} d\sigma \, G_\sigma(t, s) f(s)$ and now differentiate with respect to t to obtain

$$\tau \partial_t (T[f])(t) = \frac{\tau}{2a} \int (G_{t+a}(t, s) - G_{t-a}(t, s)) f(s) ds$$
$$+ \frac{\tau}{2a} \int d\sigma \left(\int A_\sigma(t) G_\sigma(t, s) f(s) ds + f(t) \right). \qquad (2.59)$$

The second term is just the average over σ of $\tau \partial_t (L_\sigma^{-1}[f])(t)$ so is bounded by $|f|/(K - 2\eta)$ (because $||L_\sigma^{-1}|| \leq 1/(K - 2\eta)$ as an operator from C^0 to C^1.

31

Note interchanges of order of integration and differentiation under the integral sign and with respect to limits are all valid.

To bound the first integral in (2.59), we use the same idea as in the proof of continuity of the splitting

$$\int \Delta G(t,s)f(s)ds = \int dr\, G_{t+a}(t,r)\Delta A(r)\int ds\, G_{t-a}(r,s)f(s). \qquad (2.60)$$

Now $|\int ds\, G_{t-a}(r,s)f(s)| \leq |f|/(K-2\eta)$, $|\Delta A| \leq V$ and $\Delta A(r) = 0$ for $|r-t| \leq S-a$ where $S = \frac{-1}{\lambda}\log(\frac{\alpha|\Delta u|}{\lambda\eta})$ as in (2.49), so applying Theorem 2.3.2(iv) we obtain

$$|\int \Delta G(t,s)f(s)| \leq \varepsilon|f|/(K-2\eta) \qquad (2.61)$$

where

$$\varepsilon = (S-a)e^{1-(K-2\eta)(S-a)}V \qquad (2.62)$$

provided $(K-2\eta)(S-a) \geq 1$, which is true if Δu is small enough.

Combining the bounds for the two terms of (2.59), we obtain

$$\tau|\partial_t(T[f])(t)| \leq (1 + \frac{\tau}{2a}\varepsilon)|f|/(K-2\eta). \qquad (2.63)$$

So we obtain

$$||T|| \leq (1 + \frac{\tau}{2a}\varepsilon)/(K-2\eta), \qquad (2.64)$$

which is only slightly larger than K^{-1}. To optimise the result, it is useful to choose η to depend on $|\Delta u|$ in such a way as to make the corrections in the numerator and denominator of roughly equal relative size. This is achieved approximately by taking $\eta \propto |\Delta u|^{K/(K+\lambda)}$. More specifically (2.62) says $\varepsilon \approx Ve^{-KS}$ (on a logarithmic scale of approximation), so $\varepsilon\frac{\tau}{2a} = \eta/K$ if $\eta \approx KV\frac{\tau}{2a}e^{-KS}$. But (2.49) says $\eta = \frac{\alpha}{\lambda}|\Delta u|e^{\lambda S}$ so eliminating S between these two equations yields

$$\eta \approx \left(\frac{KV\tau}{2a}\right)^{\frac{\lambda}{K+\lambda}}\left(\frac{\alpha}{\lambda}|\Delta u|\right)^{\frac{K}{K+\lambda}}. \qquad (2.65)$$

Estimating $I - \tilde{L}T$

This is an operator from C^0 to C^0.

$$(I - \tilde{L}T)[f](t) = f(t) - (\partial_t - \tilde{A}(t))(\int_{-\infty}^{t} + \int_{t}^{\infty})ds \, \frac{1}{2a} \int_{t-a}^{t+a} d\sigma \, G_\sigma(t,s)f(s).$$

(2.66)

This evaluates to

$$-\frac{1}{2a} \int ds \, \Delta G(t,s)f(s) + \frac{1}{2a} \int d\sigma \int ds \, \Delta A_\sigma(t)G_\sigma(t,s)f(s).$$

(2.67)

But $|\Delta A_\sigma(t)| = |\tilde{A}(t) - A_\sigma(t)| = 0$ for $|t - \sigma| \leq S$, so taking $|\Delta u|$ small enough that $S > a$, we have only the first term, which we bounded in (2.61), so

$$||I - \tilde{L}T|| \leq \frac{\varepsilon}{2a(K - 2\eta)}.$$

(2.68)

So if $\varepsilon < 2aK$, T is an approximate right inverse of $\tilde{L}$ for η small enough and $(\tilde{L}T)^{-1}$ exists. Then $T(\tilde{L}T)^{-1}$ is a true right inverse of $\tilde{L}$.

Estimating $I - T\tilde{L}$

This is an operator from C^1 to C^1 so we have to bound both its value acting on any C^1 function x and the value of its derivative.

$$(I - T\tilde{L})[x](t) = x(t) - \frac{1}{2a} \int_{t-a}^{t+a} d\sigma (\int_{-\infty}^{t} + \int_{t}^{\infty})ds \, G_\sigma(t,s)(\partial_s - \tilde{A}(s))x(s).$$

(2.69)

Integrating by parts and using $\partial_s G_\sigma(t,s) = -G_\sigma(t,s)A_\sigma(s) - I\delta(t - s)$ (where the use of Dirac δ–function is a convenient encoding of the jump condition (2.25)) transforms this to

$$\frac{1}{2a} \int d\sigma \int ds \, G_\sigma(t,s)\Delta A_\sigma(s)x(s),$$

(2.70)

and $\Delta A_\sigma(s) = 0$ for $|s - \sigma| \leq S$, hence for $|s - t| \leq S - a$, so it can be bounded by $\varepsilon|x|$ where ε is given by (2.62).

Next we bound the derivative of (2.70).

$$\partial_t \frac{1}{2a} \int_{t-a}^{t+a} d\sigma (\int_{-\infty}^{t} + \int_{t}^{\infty}) ds \, G_\sigma(t,s) \Delta A_\sigma(s) x(s) =$$

$$\frac{1}{2a} \int (G_{t+a}(t,s) \Delta A_{t+a}(s) - G_{t-a}(t,s) \Delta A_{t-a}(s)) x(s) ds$$

$$+ \frac{1}{2a} \int (G_\sigma(t,t-) - G_\sigma(t,t+)) \Delta A_\sigma(t) x(t) d\sigma$$

$$+ \frac{1}{2a} \int \int A_\sigma(t) G_\sigma(t,s) \Delta A_\sigma(s) x(s) \, ds d\sigma. \tag{2.71}$$

The second term is zero because $\Delta A_\sigma(t) = 0$ for $\sigma \in (t-a, t+a)$. The third term has $\Delta A_\sigma(s) = 0$ for $|s - t| \leq S - a$, so is bounded by $\varepsilon |A||x|$. Similarly, each term of the first integral is bounded by $\frac{\varepsilon}{2a}|x|$. Thus

$$\tau |\partial_t (I - T\tilde{L})[x](t)| \leq (\frac{\tau}{a} + \tau |A|) \varepsilon |x|. \tag{2.72}$$

Finally we can choose $\tau < a$ and $\tau |A| \leq 1$, so we obtain

$$||I - T\tilde{L}|| \leq 2\varepsilon. \tag{2.73}$$

So if $\varepsilon < 1/2$, T is an approximate right inverse of $\tilde{L}$ and $(T\tilde{L})^{-1}$ exists. Then $(T\tilde{L})^{-1}T$ a true left inverse of $\tilde{L}$.

Obtaining $\tilde{K}$

Thus if $\varepsilon = V(S-a)e^{1-(K-2\eta)(S-a)} < \min(\frac{1}{2}, 2aK)$ we have both $||I - \tilde{L}T||$ and $||I - T\tilde{L}|| < 1$, so $\tilde{L}$ is invertible. From (2.64) and (2.73) we have the bound

$$||\tilde{L}^{-1}||^{-1} \geq \frac{(1 - 2\varepsilon)(K - 2\eta)}{1 + \varepsilon/2} = \tilde{K}. \tag{2.74}$$

Choosing $\eta \propto |\Delta u|^{K/(K+\lambda)}$ we obtain

$$||\tilde{L}^{-1}||^{-1} \geq K - O(|\Delta u|^{K/(K+\lambda)}) \tag{2.75}$$

which says that $\tilde{K}$ is slightly smaller than K for Δu small. $\blacksquare$

Constructing the Green's function $\tilde{G}$

Now that we know the pseudo–orbit $\tilde{y}$ is uniformly hyperbolic, one can construct its true Green's function $\tilde{G}$ using the unperturbed set $\mathcal{F}$. For each time s, consider $y(\cdot)$ that solves the unperturbed equation $\dot{y} = u(y,t)$ starting at $y(s) = \tilde{y}(s)$ and let $E_\pm(\cdot)$ be the exponential dichotomy splitting along $y(\cdot)$. Let $\tilde{X}$ be the principal matrix solution of $\dot{x} = \tilde{A}(t)x$, take the subspace $\tilde{E}_-(t) = \lim_{s \to -\infty} \tilde{X}(t,s) E_-(s)$, which exists because the forwards dynamics applied to subspaces is contracting near the unperturbed E_- subspace, and

similarly $\tilde{E}_+(t) = \lim_{s \to +\infty} \tilde{X}(t, s) E_+(s)$. Then construct complementary projections $\tilde{P}_\pm(t)$ to have these as ranges and let $\tilde{G}(t, s) = \tilde{X}(t, s) \tilde{P}_+(s)$ for $t > s$, $-\tilde{X}(t, s) \tilde{P}_-(s)$ for $t < s$.

Chapter 3

Invariant manifolds and normal hyperbolicity

3.1 Normal hyperbolicity and invariant manifolds

The concept of normal hyperbolicity applies to the context of nonlinear systems that have some invariant manifold, $\mathcal{M}$, in which any tangential contraction in forward or backward time is weaker than any transverse contraction in the same direction of time. The definition is a local statement at $\mathcal{M}$, thus the linearised dynamic at $\mathcal{M}$ is central to the study. As such, when considering continuous–time dynamics normal hyperbolicity theory can employ the results from Chapter 2 on uniform hyperbolicity. In particular, the transverse linearised dynamic along the set of trajectories on $\mathcal{M}$ generates a uniformly hyperbolic set. Thus the theory on C^1 perturbation of the nonlinear system can make use of the result on pseudo–orbits in section 2.3.4 of Chapter 2. In the context of non–autonomous systems, $\mathcal{M}$ is non–compact as it is defined on the time–extended space.

In (Fen71), the unperturbed invariant manifold $\mathcal{M}$ is assumed compact and if it has a boundary it is taken to be "invariant overflowing" which means the backward orbits remain in the manifold and the vector field through any point on the boundary is strictly outward pointing. Under certain conditions on the generalised Lyapunov type numbers for the flow, $\mathcal{M}$ persists under any small perturbation of the system. The perturbed invariant manifold $\bar{\mathcal{M}}$ arises from the fixed point of a graph transform G which acts on a space of Lipschitz graphs from a reference manifold (e.g. unperturbed $\mathcal{M}$) to a transverse bundle. If there is no transverse expansion, G is the standard graph transform

which loosely speaking, takes each point on a candidate graph, computes their pre–image along the tangential direction on the candidate graph, then with this pre–image, flow forward in the transverse direction to obtain a point which is taken to be the point on the iterated graph. If there is transverse expansion, G is defined by solving an implicit zero equation introduced by the expansion, and separately solving a standard graph transform equation.

The graph transform method is also used in (HPS77) in discrete–time setting where the non–compact case was also dealt with (Theorem (6.1) in (HPS77)). The definition of normal hyperbolicity in (HPS77) is given by spectral gap conditions that reflect the dominance of the transverse contraction or expansion rates over those in the tangential direction– which is another way of expressing the generalised Lyapunov type numbers in (Fen71). If the unperturbed discrete map f has no transverse expansion the treatment is identical to (Fen71). However, if there were transverse expansion, the local unstable manifold $W^u_{\bar{f}}(\bar{\mathcal{M}})$ of the perturbed invariant manifold $\bar{\mathcal{M}}$ under the perturbed map $\bar{f}$ is given by the fixed point of the standard graph transform G^s defined as in (Fen71). G^s has contraction rate roughly equal to the ratio of the transverse contraction rate and the tangential contraction rate of f. Similarly $W^s_{\bar{f}}(\bar{\mathcal{M}})$ is constructed by applying the previous step to $\bar{f}^{-1}$ with a graph transform G^u which has contraction rate roughly equal to the ratio of the transverse expansion rate and the tangential expansion rate of f. Then $\bar{\mathcal{M}}$ is found by taking the intersection $W^s_{\bar{f}}(\bar{\mathcal{M}}) \cap W^s_{\bar{f}}(\bar{\mathcal{M}})$.

We introduce the definition of normal hyperbolicity in our context and show that the standard definition implies it. We note that the definition given here is more general in the sense that it allows the hyperbolic rates to vary with time. We will give a Theorem 3.2.2 based on Dan Henry (Hen81) that give the invariant manifold under certain conditions and assumptions. This is a path–wise approach which is advantageous as it avoids the graph transform. The proof of the C^1 property and the normal hyperbolicity of this invariant manifold is for future development. A second approach outlined here is given in Conjecture 1 which is a hybrid of path–wise and graph transform approach. A brief description of the standard graph transform approach for computing the invariant manifold will also be given in Theorem 3.2.3. A comparison between these approaches and recent work by (BOV97, GV04, BHV03) will be given at the end of the chapter.

Attention will be restricted to non–autonomous systems of the form

$$\dot{\theta} = \Theta(\theta, r, t)$$
$$\dot{r} = R(\theta, r, t)$$
$$\dot{t} = 1 \tag{3.1}$$

with $r \in \mathbb{R}^n$ and $\theta \in M$ where M is some compact submanifold without boundary. In the application to a non–autonomous oscillator, $M = \mathbb{R}/T\mathbb{Z}$, which represents a limit cycle with period T. This product structure $M \times \mathbb{R}^n \times \mathbb{R}$ is not a great restriction, as the normal bundle to a submanifold can always be trivialised by adding some artificial extra dimensions to the fibres cf. (Eld12) section 2.5, 2.6 and references within.

3.2 Computing the invariant manifold

We wish to show that under certain conditions the non–autonomous system (3.1) has a normally hyperbolic invariant submanifold.

Let us consider the space of Lipschitz graphs whose Lipschitz constant with respect to θ is at most $l > 0$

$$\mathcal{G} = \{\rho : M \times \mathbb{R} \to U \mid \mathrm{Lip}_\theta \, \rho \le l\} \tag{3.2}$$

where $U = \{r \in \mathbb{R}^n \mid |r| \le \xi\}$.

Note that we use the term "graph" for an element of $\rho \in \mathcal{G}$ interchangeably with the graph of ρ given by $\mathrm{graph}(\rho) := \{(\theta, \rho(\theta, t), t) \in M \times U \times \mathbb{R} : (\theta, t) \in M \times \mathbb{R}\}$.

A graph transform type approach requires the consideration of $\mathcal{G}$ which the graph transform acts on – this is considered in Conjecture 1. However, a path–wise approach will be given based on (Hen81) in Theorem 3.2.2 which does not use a graph transform.

3.2.1 Two operators

We will consider two operators that are key to our study of invariant manifold. The notation here is that the partial derivative of a vector field X with respect to x is written as X_x and the sup norm over the defining domain is simply written as $|X_x|$.

Definition 3.2.1 (Pseudo–orbit) *For $\rho \in \mathcal{G}$ and $(\theta_0, t_0) \in M \times \mathbb{R}$ define the corresponding pseudo orbit $\theta_{\rho,\theta_0,t_0} : \mathbb{R} \to M$ as the solution to $\dot{\theta} = \Theta(\theta, \rho(\theta, t), t)$ starting at $\theta(t_0) = \theta_0$.*

To simplify notation we drop the subscripts in $\theta_{\rho,\theta_0,t_0}(t)$.

Definition 3.2.2 (Operator L) *For $\rho \in \mathcal{G}$ and $(\theta_0, t_0) \in M \times \mathbb{R}$, consider the corresponding pseudo–orbit $\theta(\cdot)$. Then for any C^0 function $r : \mathbb{R} \to U$ we define the operator $L_r : C^1(\mathbb{R}, \mathbb{R}^n) \to C^0(\mathbb{R}, \mathbb{R}^n)$ by*

$$L_r[x](t) = \dot{x}(t) - R_r x(t). \tag{3.3}$$

with R_r evaluated on $p(t) = (\theta(t), r(t), t)$.

Note that the subscript in L_r refers to the function $r(\cdot)$.

Definition 3.2.3 (Operator J) *Consider the definition of the operator L above. Given in addition a C^0 function $\bar{\sigma} : \mathbb{R} \to L(TM, \mathbb{R}^n)$ we define $J_{\bar{\sigma}} : W^{1,\infty}(\mathbb{R}, L(TM, \mathbb{R}^n)) \to W^{0,\infty}(\mathbb{R}, L(TM, \mathbb{R}^n))$ by*

$$J_{\bar{\sigma}}[\sigma](t) = \dot{\sigma} - R_r \sigma + \sigma(\Theta_\theta + \Theta_r \bar{\sigma}), \tag{3.4}$$

with $R_r, \Theta_\theta, \Theta_r$ evaluated on $p(t)$ and where $W^{1,\infty}$ is the space of bounded Lipschitz functions and $W^{0,\infty}$ the space of L^∞ functions.

We enlarge the natural $J_{\bar{\sigma}} : C^1 \to C^0$ setting here to cater for some forcing functions that will not be continuous e.g. arising from the discontinuity in the Green's function for L at $s = t$, or from our allowing Lipschitz graphs not just C^1 graphs. By Rademacher's theorem, see (ACP10), any function $\sigma \in W^{1,\infty}$ is differentiable almost everywhere. Thus we can equip $W^{1,\infty}$ with the norm $|\sigma|_{1,\infty} = \max\{|\sigma|_0, \tau|\dot{\sigma}|_\infty\}$ where $|\cdot|_\infty$ is the L^∞ norm and τ chosen so that $\tau|R_r|, \tau|\Theta_r|, \tau|\Theta_\theta| \leq 1$.

Note that $J_{\bar{\sigma}}$ is related to the slope dynamic and in particular the Ricatti equation

$$\dot{\sigma} = R_\theta + R_r \sigma - \sigma(\Theta_\theta + \Theta_r \sigma), \tag{3.5}$$

which can be obtained by setting $\delta r = \sigma \delta \theta$ for some matrix function σ and the linearised equations of r and θ in (3.1).

Since each pair of operators $(L_r, J_{\bar{\sigma}})$ is essentially defined by a $\theta_0 \in M$ let us make the following definition:

39

Definition 3.2.4 (Set of pairs of operators) *For any $\rho \in \mathcal{G}$, let us fix $t_0 \in \mathbb{R}$ and define the set of pairs of operators $\mathcal{F}_\rho := \{(L_r, J_{\bar{\sigma}}) : \theta_0 \in M\}$ where each pair $(L_r, J_{\bar{\sigma}})$ is defined given (θ_0, t_0) as above.*

Definition 3.2.5 (Uniformly Hyperbolic set) *$\mathcal{F}_\rho$ is a uniformly hyperbolic set with bounds K_0 and κ_0 if each L_r and $J_{\bar{\sigma}}$ are invertible with $||L_r^{-1}||^{-1} \geq K_0$ and $||J_{\bar{\sigma}}^{-1}||^{-1} \geq \kappa_0$.*

3.2.2 Definition of Normal Hyperbolicity

We give a definition of Normal Hyperbolicity using the two operators defined above and show that the standard definition due to (HPS77) implies it.

Let $F(t; p)$ be the flow of the non–autonomous system (3.1) starting at $p \in M \times \mathbb{R}^n \times \mathbb{R}$ with end time t.

Definition 3.2.6 (Invariant graph) *Consider $\rho \in \mathcal{G}$ with $\mathcal{M} = graph(\rho) \cong M \times \mathbb{R}$. Then ρ is an invariant graph under the non–autonomous system (3.1) if $F(t; \mathcal{M}) = \mathcal{M}$.*

If $\rho \in \mathcal{G}$ is invariant then for each $(\theta_0, t_0) \in M \times \mathbb{R}$, letting θ be the pseudo–orbit, we take $r(t) = \rho(\theta(t), t)$ and $\bar{\sigma}(t) = \rho_\theta(\theta(t), t)$ in the definition of $\mathcal{F}_\rho$.

Definition 3.2.7 (Normal Hyperbolicity with two operators) *An invariant graph $\rho \in \mathcal{G}$ under the non–autonomous system (3.1) is normally hyperbolic iff $\mathcal{F}_\rho$ (using $\bar{\sigma} = \rho_\theta$) is uniformly hyperbolic.*

Compare this with the standard definition found in (HPS77):

Definition 3.2.8 (Standard definition of Normal Hyperbolicity) *An invariant graph $\rho \in \mathcal{G}$ under the non–autonomous system (3.1) is normally hyperbolic iff the tangent bundle of $M \times \mathbb{R}^n \times \mathbb{R}$ restricted to $\mathcal{M}$, splits into three Hölder continuous subbundles*

$$T_{\mathcal{M}}(M \times \mathbb{R}^n \times \mathbb{R}) = V_+ \oplus T\mathcal{M} \oplus V_- \tag{3.6}$$

which are invariant by the linearised flow of F, denoted by DF, such that for all $p_0 = (\theta_0, r_0, t_0) \in \mathcal{M}$, $t > t_0$, $k \in \{0, 1\}$,

$$a) \quad ||DF(t; p_0)_{|V_+(p_0)}|| \leq C\delta^{|t-t_0|}[m(DF(t; p_0)_{|T_{p_0}\mathcal{M}})]^k \tag{3.7}$$

and for all $t < t_0$, $k \in \{0, 1\}$,

$$b) \quad ||DF(t; p_0)_{|V_-(p_0)}|| \leq C\delta^{|t-t_0|}[m(DF(t; p_0)_{|T_{p_0}\mathcal{M}})]^k. \tag{3.8}$$

for some constants $0 < \delta < 1$ and $0 < C < \infty$.

Recall that the "minimum norm" $\mathrm{m}(A)$ of a linear transformation A is defined as $\mathrm{m}(A) = \inf\{|Ax| : x = 1\}$. Note here that $V_\pm$ are conventionally called the stable and unstable subbundles respectively. We use the "$\pm$" to say forward and backward contracting in time respectively. This definition of normal hyperbolicity is defined for discrete system in (HPS77) and is termed *eventually relatively 1-normally hyperbolic* (since $k \leq 1$), however the invariant manifold we are working on is non–compact and the continuity of the subbundles are Hölder continuous.

We will show the standard Definition 3.2.8 of Normal Hyperbolicity implies that given in Definition 3.2.7. However Definition 3.2.7 of Normal Hyperbolicity allows the rates to vary with time thus it is more general in this respect.

Lemma 3.2.1 *If $\rho \in \mathcal{G}$ is Normally Hyperbolic invariant according to Definition 3.2.8 then ρ is Normally Hyperbolic according to Definition 3.2.7.*

Proof: For any $p_0 = (\theta_0, r_0, t_0) \in \mathcal{M}$ let us write $p_t = F(t; p_0)$. We wish to show the invertibility of the two operators
$L : x \mapsto \dot{x} - R_r(p_t)x$ and $J : \sigma \mapsto \dot{\sigma} - R_r(p_t)\sigma + \sigma(\Theta_\theta(p_t) + \Theta_r(p_t)\bar{\sigma})$ with $\bar{\sigma} = \rho_\theta$.

Consider the vertical subbundle $E = \mathbb{R}^n$ to the tangent bundle of $M \times \mathbb{R}^n \times \mathbb{R}$ and write $V = V_+ \oplus V_-$. Define a projection along $T\mathcal{M}$ by $\pi : V \to E; v \mapsto x$ where x is uniquely written as $x = v + \eta$ with $v \in V = V_+ \oplus V_-$ and $\eta \in T\mathcal{M}$. Thus there is a splitting $E_\pm = \pi V_\pm$ with $E = E_- \oplus E_+$. Note that π is invertible since v and η are uniquely determined by x. Also, define a projection $\Pi : T\mathcal{M} \to T\mathcal{M}$ by $\delta\theta \mapsto (\delta\theta, \rho_\theta\delta\theta, 0)$ and write $R = \mathcal{R}(\Pi) \subset T\mathcal{M}$, the range of Π.

Invertibility of L
Given any impulse $y \in E$ at time t_0 we wish to construct a unique bounded solution for $L[x] = y\delta_{t_0}$ where δ is the Dirac–delta function at time t_0. Now y is uniquely given by $y = x_+ - x_-$ with $x_\pm \in E_\pm$ and there are $v_\pm \in V_\pm$ such that $x_\pm = \pi v_\pm$. Letting $v_\pm(t) = DF(t; p_0)_{|V_\pm} v_\pm$ we see that by a) and b) in Definition 3.2.8 with $k = 0$, $v_\pm(t) \to 0$ exponentially at rate $\ln \delta$ as $t \to \pm\infty$. So $x_\pm(t) = \pi v_\pm(t)$ also decay exponentially with the same rate too. Let $x(t) = \pm x_\pm(t)$ for $t > t_0$ and $t < t_0$ respectively then $Lx = y\delta_{t_0}$, thus L is invertible.

Invertibility of J
Recall that the operator J is related to the linearised equation of the non–

autonomous system (3.1),

$$\delta\dot{r} = R_r(p_t)\delta r + R_\theta(p_t)\delta\theta$$
$$\delta\dot{\theta} = \Theta_\theta(p_t)\delta\theta + \Theta_r(p_t)\delta r \tag{3.9}$$

where the linearised tangential dynamic is given by $\delta\dot{\theta} = (\Theta_\theta + \Theta_r\bar{\sigma})\delta\theta$ with $\bar{\sigma} = \rho_\theta$.

Given any impulse slope $h \in L(TM, E)$ at time t_0, we wish to construct a unique bounded solution for $J[\sigma](t) = h\delta_{t_0}$. We split $h = h_+ - h_-$ where $h_\pm \in L(TM, E_\pm)$. Then associate $h_\pm$ with $\tilde{\sigma}_\pm \in L(R, V_\pm)$ by taking $\tilde{\sigma}_\pm = \pi^{-1}h_\pm\Pi^{-1}$. Take $\tilde{\sigma}_\pm(t) = DF(t; p_0)_{|V_\pm}\tilde{\sigma}_\pm DF(t_0; p_t)_{|R}$ where $p_t = F(t; p_0)$. Then by a) and b) in Definition 3.2.8 with $k = 1$, $\tilde{\sigma}_\pm(t) \to 0$ exponentially at rate $\ln\delta$ as $t \to \pm\infty$. Now obtain $\sigma_\pm(t) = \pi\sigma_\pm(t)\Pi$ and note that $\sigma_\pm(t)$ also decay exponentially with the same rate too. Let $\sigma(t) = \pm\sigma_\pm(t)$ for $t > t_0$ and $t < t_0$ respectively then $J[\sigma](t) = h\delta_{t_0}$, thus J is invertible. ∎

3.2.3   Assumptions and Conditions

Here we will give the assumptions and conditions for the existence of invariant manifold. First we give a definition of the modulus of continuity of a function which gives information about the regularity of the function. See (Leb09) and (dlVP52) for background references.

Definition 3.2.9 $\omega : \mathbb{R} \to \mathbb{R}$ *is a module of continuity for a function* $g : U \subset X \to Y$ *from a subset of a Banach space into another if it satisfies* $|g(x_1) - g(x_2)| \leq \omega(|x_1 - x_2|)$ *for all* $x_1, x_2 \in U$ *and* $\omega(s) \to 0$ *as* $s \to 0$. *If* ω *is bounded then* g *is said to have a bounded module of continuity.*

Unless stated otherwise, we make the following assumptions of the map R and Θ of (3.1).

Assumption 1 *Take* $\theta \in M$, $r \in U$, $t \in \mathbb{R}$. *The following functions* $R_r(\theta, \cdot, t)_{|U}, R_r(\cdot, r, t)_{|M}$ *and* $\Theta_\theta(\theta, \cdot, t)_{|U}, \Theta_\theta(\cdot, r, t)_{|M}$ *have bounded modules of continuity* $\omega_{\theta,t}(\cdot) \leq |\omega_{\theta,t}|$; $\omega_{r,t}(\cdot) \leq |\omega_{r,t}|$; $\alpha_{\theta,t}(\cdot) \leq |\alpha_{\theta,t}|$ *and* $\alpha_{r,t}(\cdot) \leq |\alpha_{r,t}|$

with uniform bounds

$$\varepsilon_r := \sup_{\theta,t} |\omega_{\theta,t}|;$$

$$\varepsilon_\theta := \sup_{r,t} |\omega_{r,t}|;$$

$$\delta_r := \sup_{\theta,t} |\alpha_{\theta,t}|;$$

$$\delta_\theta := \sup_{r,t} |\alpha_{r,t}| \tag{3.10}$$

respectively. Furthermore, assume $R_r(\theta,\cdot,t)$ has Lipschitz constant $L_{\theta,t}$ and $l_r = \sup_{\theta,t} L_{\theta,t}$ is bounded. Let $\tau > 0$ be such that $\sup_{p \in \Omega} \tau |R_r(p)| \le 1$.

Assumption 2 *We make the following assumption on Θ. There is an $V > 0$ such that for any $t_0 \in \mathbb{R}$, $r : \mathbb{R} \to U$ and any $\theta_i : \mathbb{R} \to M$ where $i = 1,2$ with $\theta_1(t_0) = \theta_2(t_0)$, we have $\sup_t |\Phi(t_0,t)||\Phi(t,t_0)| \le V < \infty$ where Φ is the principal matrix solution of the system $\delta\dot\theta = [\Theta_\theta]\delta\theta$ starting at $\delta\theta(t_0) = 0$, where $[\Theta_\theta](t) = \int_0^1 d\lambda \Theta_\theta(\theta_\lambda(t), r, t)$ with $\theta_\lambda = \lambda\theta_1 + (1-\lambda)\theta_2$.*

Conditions 1 *Consider the zero graph $\rho_0 \equiv 0$ and let us assume the following conditions*

C1.1: *For all trajectories $(\theta(t), 0, t) \in \rho_0$, taking $r(t) = 0$ and $\bar\sigma = 0$, we have $||L_0^{-1}||^{-1} \ge K_0$ and $||J_0^{-1}||^{-1} \ge \kappa_0$ for some $K_0, \kappa_0 > 0$.*

C1.2: *There is a small enough $\eta > 0$ such that $|R_{|\rho_0}| \le \eta/\tau \le \frac{(K_0 - \varepsilon_r)^2}{2l_r}$.*

C1.3: $K_0 - (\varepsilon_r + \varepsilon_\theta + \tau^{-1}) > 0$.

C1.4: $\kappa = \kappa_0 - (\varepsilon_r + \varepsilon_\theta + \delta_\theta + \delta_r) > 0$.

C1.5: $2|R_\theta||\Theta_r|V < \kappa^2$.

Assumption 3 *Given Condition 1 is satisfied. Take Φ and $r : \mathbb{R} \to U$ and t_0 as in Assumptions 2. There is a $\gamma \in (\gamma_-, \gamma_+)$ where $\gamma_\pm = \frac{1}{2}\kappa \pm \sqrt{\frac{1}{2}\kappa^2 - A}$ with $A = |R_\theta||\Theta_r|V$ such that $||r||_{t_0} := \sup_t |\Phi(t_0,t)|e^{-\gamma|t-t_0|}|r(t)| < \infty$ exists.*

To briefly summarise, Assumption 1, 2 and 3 refers to the system vector fields R and Θ while Condition 1 refer to a candidate manifold ρ_0. Note that *C1.2* essentially says that ρ_0 is nearly invariant and *C1.1* says that ρ_0 defines a uniformly hyperbolic set. *C1.3* and *C1.4* are satisfied if U is a small enough neighborhood and ρ_0 is sufficiently close to being invariant. *C1.5* is satisfied if the coordinate system is chosen well enough.

Given these conditions we wish to show that there is an invariant C^1 graph

ρ nearby, which is normally hyperbolic. In particular, its derivative ρ_θ is the self-consistent solution of

$$\rho_\theta = J_{\bar\sigma}^{-1}[R_\theta] \tag{3.11}$$

using $\bar\sigma = \rho_\theta$, which is true if the map $\sigma \mapsto J_\sigma^{-1}[R_\theta]$ is a contraction with fixed point ρ_θ. Condition 1 will be used to find the invariant manifold ρ by Theorem 3.2.2, however its C^1 property will not be shown here and can be considered for future work.

3.2.4   Continuation

Let us begin with showing a continuation result which is very important for Theorem 3.2.2 that gives the invariant manifold.

Lemma 3.2.2 (Continuation) *Let $F : X \to Y$ be a C^1 map between Banach spaces with module of continuity ω for the derivative DF. Suppose $|F(0)| \leq \eta$ and $||DF^{-1}|| \leq K^{-1}$. Let $\Omega(h) = \int_0^h \omega(s)ds$ and $h()$ be the inverse function to $\omega(h)$. Let $q(h) = Kh - \Omega(h)$. If $\eta \leq q(h(K))$ then F has a locally unique zero x and $|x| \leq \varepsilon(\eta)$, where ε is the inverse function to q on $[0, h(K)]$.*

Proof: Consider the homotopy $F_\lambda(x) = F(x) - (1 - \lambda)F(0)$ for $\lambda \in [0, 1]$. $F_0(0) = 0$ and $DF_\lambda = DF$ so is invertible at $x = 0$. By the Implicit Function Theorem it has a C^1 continuation x_λ with $F_\lambda(x_\lambda) = 0$ as long as $DF_\lambda(x_\lambda)$ remains invertible. By the chain rule

$$\frac{dx}{d\lambda} = DF_\lambda(x)^{-1}\frac{dF_\lambda}{d\lambda} = -DF(x)^{-1}F(0). \tag{3.12}$$

But from a Taylor expansion and using the module of continuity of DF at x we have $||DF(x)^{-1}|| \leq \frac{1}{||DF(0)^{-1}||^{-1} - \omega(|x|)}$ as long as the denominator remains positive. So

$$|\frac{dx}{d\lambda}| \leq \frac{\eta}{K - \omega(|x|)}. \tag{3.13}$$

It follows by integration with respect to λ that

$$q(|x|) = K|x| - \Omega(|x|) \leq \eta\lambda, \tag{3.14}$$

where $\Omega(\xi) = \int_0^\xi \omega(s)ds$, as long as $\omega(|x|)$ remains less than K, i.e. as long as $\eta \leq q(h(K))$. In particular, under the hypothesis the continuation can be

completed to $\lambda = 1$, giving a zero of F with the stated bound (q is invertible because it is a strictly increasing function). ∎

If DF is Lipschitz with Lipschitz constant l, then we can take the module of continuity to be $\omega(|x|) = l|x|$, then the above Lemma says that for $\eta \leq q(h(K)) = \frac{K^2}{2l}$, F has a unique zero, x, that satisfies

$$|x| \leq \varepsilon(\eta) = \frac{2\eta}{K + \sqrt{K^2 - 2l\eta}}. \tag{3.15}$$

Let us first use this to determine a locally unique r trajectory given a θ one.

Corollary 3.2.1 *Assume Conditions 1, then for any fix $\theta(\cdot)$ satisfying $\dot{\theta} = \Theta(\theta, 0, t)$ the equation given by*

$$\dot{r} = R(\theta(t), r, t) \tag{3.16}$$

has a unique solution $\tilde{r}$ with $|\tilde{r}|_1 \leq \varepsilon(\eta) = \frac{2\eta/\tau}{K + \sqrt{K^2 - 2l_r\eta/\tau}}$ with $K = K_0 - \varepsilon_r$. Furthermore the linear operator $L_{\tilde{r}}$ is invertible with bound $||L_{\tilde{r}}^{-1}||^{-1} \geq K$.

Proof: We consider $F : r \mapsto \dot{r} - R(\theta(t), r, t)$ where $r : \mathbb{R} \to U$ is C^1 and show that it has derivative $DF(r) = L_r : x \mapsto \dot{x} - R_r(\theta(t), r(t), t)x$, in particular

$$\lim_{|r_2 - r_1|_{C^1} \to 0} \frac{|F(r_2) - F(r_1) - L_{r_1}[r_2 - r_1]|_{C^0}}{|r_2 - r_1|_{C^1}} = 0. \tag{3.17}$$

Now we see

$$|F(r_2) - F(r_1) - L_{r_1}[r_2 - r_1]|_{C^0} = |R_r(r_1)(r_2 - r_1) - (R(r_1) - R(r_2))|_{C^0}$$

$$\leq |R_r(r_1) - \int_0^1 R_r(r_\lambda)d\lambda|_{C^0}|r_2 - r_1|_{C^0} \tag{3.18}$$

where $r_\lambda = (1-\lambda)r_1 + \lambda r_2$. Note that for presentation purpose we have excluded the dependence on θ and time t in the functions R and R_r. But $R_r(r_\lambda) = R_r(r_1) + \lambda O(r_2 - r_1)$ for small $|r_2 - r_1|_{C^0}$ so

$$\int_0^1 R_r(r_\lambda)d\lambda = R_r(r_1) + O(|r_2 - r_1|_{C^0}). \tag{3.19}$$

45

Since $|r_2 - r_1|_{C^0} \leq |r_2 - r_1|_{C^1}$ we have

$$\frac{|F(r_2) - F(r_1) - L_{r_1}[r_2 - r_1]|_{C^0}}{|r_2 - r_1|_{C^1}} \leq O(|r_2 - r_1|_{C^0})$$

$$\leq O(|r_2 - r_1|_{C^1}) \qquad (3.20)$$

hence $DF(r) = L_r$. By Condition 1 L_r is a small perturbation of L_0 with $||L_r - L_0|| = |R_r(\theta(\cdot), 0, \cdot) - R_r(\theta(\cdot), r(\cdot), \cdot)| \leq \varepsilon_r$, so by Lemma 2.2.1 it is invertible and satisfies $||L_r^{-1}||^{-1} \geq K = K_0 - \varepsilon_r$ for all r. Note that DF has Lipschitz constant l_r and $q(h(K)) = \frac{K^2}{2l_r}$ where q and h are as in Lemma 3.2.2. Now $|F(0)| = |R(\theta(t), 0, t)| \leq \eta/\tau$ so by Lemma 3.2.2 F has a locally unique zero $\tilde{r}$ and by (3.14) we have

$$|\tilde{r}|_1 \leq \frac{2\eta/\tau}{K + \sqrt{K^2 - 2l_r\eta/\tau}} =: \varepsilon(\eta). \qquad (3.21)$$

Moreover since $L_{\tilde{r}}$ is a perturbation of L_0, it is invertible with bound $||L_{\tilde{r}}^{-1}||^{-1} \geq K$. ■

For computational purposes it would be useful to estimate $\tilde{r}$ by using a Newton method which is stated as a theorem below.

Theorem 3.2.1 (Newton Map Theorem) *Assume Conditions 1 and fix any $\theta(\cdot)$. Let $L_0 : x \mapsto \dot{x} - R_r(\theta(t), 0, t)x$ and $F : r \mapsto \dot{r} - R(\theta(t), r, t)$ be as in the proof of Corollary 3.2.1. Now consider the Newton map $N : \mathcal{B}_\eta(0) \to \mathcal{B}_\eta(0)$ defined by*

$$N[r](t) = r(t) - L_0^{-1}[F(r)](t) \qquad (3.22)$$

where $\mathcal{B}_\eta(0) \subset C^1$ is an η – ball centered at $r \equiv 0$. Then N is a well defined contraction. N has a locally unique fixed point with bound given in (3.21).

Proof: To show N is a contraction it is sufficient to show that $||DN(r)|| = ||I - L_0^{-1}L_r|| < 1$ for $r \in \mathcal{B}_\eta(0)$. Note that DN exists since DF exists as seen in the proof of Corollary 3.2.1. Let us first prove that L_0^{-1} is an approximate left inverse of L_r. Letting G be the Green's function of L_0^{-1} we can obtain

$$x(t) - L_0^{-1}L_r[x](t) = \int_{-\infty}^{\infty} G(t,s)[\dot{x}(s) - R_r(\theta(s), r(s), s)x(s)]ds$$

$$= \int_{-\infty}^{\infty} G(t,s)\Delta R_r(s)x(s)ds \qquad (3.23)$$

where $\Delta R_r(s) = R_r(\theta(s), r(s), s) - R_r(\theta(s), 0, s)$. But by Assumption 1 $|\Delta R_r| \leq \varepsilon_r$ so using the bound $||L_0^{-1}||^{-1} \geq K_0$ from Condition 1 we have

$$||I - L_0^{-1} L_r|| \leq \frac{\varepsilon_r}{K_0}. \tag{3.24}$$

By Condition 1 we have $\varepsilon_r / K_0 < 1$ hence N is a contraction.

To show N is well defined note that $|F(0)| \leq \eta/\tau$ so we have

$$|N[0]| = |L_0^{-1}[F(0)]|$$
$$\leq \eta/(\tau K_0).$$

Now for $r \in \mathcal{B}_\eta(0)$ we have

$$|N[r]| \leq |N[r] - N[0]| + |N[0]|$$
$$\leq ||DN(r)|||r| + |N[0]|$$
$$\leq \frac{\varepsilon_r \eta}{K_0} + \frac{\eta \tau^{-1}}{K_0}$$
$$\leq \left(\frac{\varepsilon_r + \tau^{-1}}{K_0}\right)\eta. \tag{3.25}$$

By Condition 1, $(\varepsilon_r + \tau^{-1})/K_0 \leq 1$ so we have $N[r] \in \mathcal{B}_\eta(0)$. Thus N maps $\mathcal{B}_\eta(0)$ to itself and since it is a contraction, N has a unique fixed point $\tilde{r}$ which is also the zero of F where $\tilde{r}$ has bound given in (3.21).

$\blacksquare$

The expression for N has an $\dot{r}$ term within the definition of F which may not be advantageous in numerical implementations. Thus it is desirable to find an equivalent expression without this term. By using integration by parts and $\partial_2 G(t, s) = -G(t, s)A(s) - I\delta(t - s)$, where $A(s) = R_r(\theta(s), 0, s)$, we can obtain

$$N[r](t) = \int G(t, s)[R(\theta(s), r(s), s) - R_r(\theta(s), 0, s)r(s)]ds. \tag{3.26}$$

3.2.5 Path–wise approach to computing invariant manifold

Let us go on to show that the non–autonomous system (3.1) has an invariant manifold given Conditions 1. This will be given in Theorem 3.2.2 based on the approach of (Hen81) Chapter 9 which has the advantage of avoiding the graph transform and the invariant manifold is obtained path–wise. However, in contrast to (Hen81), the approach here uses the operators defined in (3.3, 3.4) in place of the consideration of spectral gap. To show that the invariant

manifold obtained here is normally hyperbolic according to Definition 3.2.7, it is required that the manifold is at least Lipschitz with respect to θ_0 so that the operator (3.4) is defined. The Lipschitz property is not shown here. Let us state the following lemmas that leads to the theorem for the invariant manifold.

Lemma 3.2.3 *Assume Condition 1 then the operator $J : \sigma \mapsto \dot{\sigma} - [R_r]\sigma + \sigma[\Theta_\theta]$ is invertible with $||J^{-1}||^{-1} \geq \kappa_0 - (\varepsilon_\theta + \varepsilon_r + \delta_\theta + \delta_r)$ and given any $h \in W^{0,\infty}$ we have*

$$\sigma(t) = J^{-1}[h](t) = \int_{-\infty}^{\infty} G(t,s)[h(s)]\Phi(s,t)ds. \qquad (3.27)$$

Proof: The operator J is a small perturbation of J_0 with

$$||J - J_0|| \leq |R_r(\theta(\cdot), 0, \cdot) - [R_r](\cdot)| + |\Theta_r(\theta(\cdot), 0, \cdot) - [\Theta_r](\cdot)|$$
$$\leq \varepsilon_r + \varepsilon_\theta + \delta_r + \delta_\theta. \qquad (3.28)$$

By Condition 1 we have $\varepsilon_r + \varepsilon_\theta + \delta_r + \delta_\theta < \kappa_0$ so by Lemma 2.2.1, J is invertible with $||J^{-1}||^{-1} \geq \kappa := \kappa_0 - (\varepsilon_r + \varepsilon_\theta + \delta_r + \delta_\theta)$ and by differentiating with respect to time the unique response $\sigma = J^{-1}[h]$ can be verified to be given by

$$\sigma(t) = \int_{-\infty}^{\infty} G(t,s)h(s)\Phi(s,t)ds \qquad (3.29)$$

∎

Lemma 3.2.4 *Take the operator $J : \sigma \mapsto \dot{\sigma} - [R_r]\sigma + \sigma[\Theta_\theta]$. Given any $|h(s)| \leq \varepsilon e^{\gamma|s|}$ for some $\gamma \in [0, \kappa)$ then $|\sigma(t)| \leq \frac{\varepsilon e^{\mu|t|}}{\kappa - \gamma}$.*

Proof: The proof is identical to the proof of Theorem 2.3.2 (iii). ∎

Theorem 3.2.2 *Assume Condition 1 and fix (θ_0, t_0). Given any $r \in \mathcal{B}_\varepsilon := \{r \in C^1 : |r|_1 \leq \varepsilon(\eta)\}$ where ε is defined in (3.21), obtain $\theta(\cdot)$ by solving $\dot{\theta} = \Theta(\theta, r(t), t)$ starting at (θ_0, t_0). Then by Corollary 3.2.1 there is a unique $\tilde{r} \in \mathcal{B}_\varepsilon$ which satisfies $\dot{\tilde{r}} = R(\theta(t), \tilde{r}(t), t)$. Define $\tilde{T} : \mathcal{B}_\varepsilon \to \mathcal{B}_\varepsilon$ by $r \mapsto \tilde{r}$ then $\tilde{T}$ is a contraction in the $|| \cdot ||_{t_0}$ norm defined in Assumption 3.*

Proof: Take any $r_i \in \mathcal{B}_\varepsilon$ and $\tilde{r}_i = \tilde{T}(r_i)$ where $i = 1, 2$. Then $\Delta \tilde{r} = \tilde{r}_1 - \tilde{r}_2$ satisfies

$$\Delta \dot{\tilde{r}} = R(\theta_1(t), \tilde{r}_1(t), t) - R(\theta_2(t), \tilde{r}_2(t), t)$$
$$= [R_\theta]\Delta\theta + [R_r]\Delta\tilde{r} \qquad (3.30)$$

48

where $[R_\theta](t) = \int_0^1 d\lambda R_\theta(\theta_\lambda(t), r_1(t), t)$ and $[R_r](t) = \int_0^1 d\lambda R_r(\theta_2(t), r_\lambda(t), t)$ and $\Delta\theta = \theta_1 - \theta_2$ satisfies

$$\Delta\dot\theta = \Theta(\theta_1(t), r_1(t), t) - \Theta(\theta_2(t), r_2(t), t)$$
$$= [\Theta_\theta]\Delta\theta + [\Theta_r]\Delta r$$

where $[\Theta_\theta](t) = \int_0^1 d\lambda \Theta_\theta(\theta_\lambda(t), r_1(t), t)$, $[\Theta_r](t) = \int_0^1 d\lambda \Theta_r(\theta_2(t), r_\lambda(t), t)$, $\Delta r = r_1 - r_2$ and $x_\lambda(t) = \lambda x_1(t) + (1 - \lambda)x_2(t)$.

Let G be the Greens function for the operator $L : x \mapsto \dot x - [R_r]x$ which exists since L is just a small perturbation of L_0 with $||L - L_0|| \le K_0 - (\varepsilon_\theta + \varepsilon_r)$. Similarly let Φ be the principal matrix solution of $\delta\dot\theta = [\Theta_\theta]\delta\theta$ starting at $\delta\theta(t_0) = 0$. Then we have

$$\Delta\theta(s) = \int_{t_0}^s du \Phi(s, u)[\Theta_r](u)\Delta r(u)$$
$$= \Phi(s, t)\Phi(t, t_0) \int_{t_0}^s du e^{\gamma|u-t_0|}[\Phi(t_0, u)[\Theta_r](u)\Delta r(u)e^{-\gamma|u-t_0|}] \quad (3.31)$$

for any $\gamma \in (\gamma_-, \gamma_+)$ as in Assumptions 3. So we have

$$\Delta\tilde r(t) = \int_{-\infty}^\infty ds G(t, s)[R_\theta](s)\Delta\theta(s)$$
$$= \int_{t_0}^\infty ds G(t, s)[R_\theta](s)\Phi(s, t)\Phi(t, t_0) \int_{t_0}^s du \, e^{\gamma|u-t_0|}[\Phi(t_0, u)[\Theta_r](u)\Delta r(u)e^{-\gamma|u-t_0|}]$$
$$+ \int_{-\infty}^{t_0} ds G(t, s)[R_\theta](s)\Phi(s, t)\Phi(t, t_0) \int_s^{t_0} du \, e^{\gamma|u-t_0|}[\Phi(t_0, u)[\Theta_r](u)\Delta r(u)e^{-\gamma|u-t_0|}]$$
$$(3.32)$$

Since $\int_{t_0}^s du \, e^{\gamma|u-t_0|} = \int_s^{t_0} du \, e^{\gamma|u-t_0|} \le \frac{e^{\gamma|s-t_0|}}{\gamma}$ we have by Lemma 3.2.4

$$|\Phi(t_0, t)||\Delta\tilde r(t)| \le |\Phi(t_0, t)| \left| \int_{-\infty}^\infty ds G(t, s)h(s)\Phi(s, t)\Phi(t, t_0) \right| ||\Delta r||_{t_0}$$
$$\le \frac{|R_\theta||\Theta_r|e^{\gamma|t-t_0|}}{\gamma(\kappa - \gamma)} |\Phi(t_0, t)||\Phi(t, t_0)|||\Delta r||_{t_0}. \quad (3.33)$$

with $|h(s)| \le \frac{|R_\theta||\Theta_r|}{\gamma} e^{\gamma|s-t_0|}$. Thus we have

$$||\Delta\tilde r||_{t_0} \le \frac{|R_\theta||\Theta_r|V}{\gamma(\kappa - \gamma)} ||\Delta r||_{t_0}. \quad (3.34)$$

By the choice of γ we have $\frac{|R_\theta||\Theta_r|V}{\gamma(\kappa-\gamma)} < 1$ hence $\tilde T$ is a contraction.

∎

Given (θ_0, t_0) let r be the fixed point of $\tilde{T}$ as in Theorem 3.2.2. Let $\theta(\cdot)$ be the solution of $\dot{\theta} = \Theta(\theta, r(t), t)$ starting from $\theta(t_0) = \theta_0$. Then $r(\cdot)$ and $\theta(\cdot)$ solves the non–autonomous system (3.1) such that $\theta(t_0) = \theta_0$. We define $\tilde{\rho}(\theta_0, t_0) = r(t_0)$ which is the invariant manifold we seek.

Note that since $|R_\theta||\Theta_r|$ can be made arbitrarily small by appropriate choice of coordinate system, the contraction rate of $\tilde{T}$ can be very small.

The application in mind of Theorem 3.2.2 is in a perturbation framework. For example, take a normally hyperbolic autonomous system with an appropriate time extended coordinate system such that the system is given by

$$\dot{r} = \bar{R}(\theta, r, t)$$
$$\dot{\theta} = \bar{\Theta}(\theta, r, t) \tag{3.35}$$

and possesses a normally hyperbolic invariant manifold given by $\rho_0 \equiv 0$ and Assumptions 1, 2, 3 and Conditions 1 are satisfied by $\bar{R}$ and $\bar{\Theta}$. The application to perturbation is stated in the following corollary.

Corollary 3.2.2 *Let R and Θ be an $\varepsilon\ C^1$ small perturbation of $\bar{R}$ and $\bar{\Theta}$ respectively and assume that Θ satisfies Assumptions 2 with the same F as that for $\bar{\Theta}$. Then the perturbed non–autonomous system defined by R and Θ satisfies Assumptions 1 and Conditions 1. If Θ also satisfies Assumptions 3 then by Theorem 3.2.2 the perturbed system possesses an invariant manifold.*

Proof: Let the quantities and functions of Assumptions 1, 2, 3 and Conditions 1 related to $\bar{R}$ and $\bar{\Theta}$ be marked by an overline, while those of R and Θ with no overline.

Since R and Θ are $\varepsilon - C^1$ close to $\bar{R}$ and $\bar{\Theta}$ we have

$$\max\{|R_r - \bar{R}_r|, |R_\theta - \bar{R}_\theta|, |\Theta_r - \bar{\Theta}_r|, |\Theta_\theta - \Theta_\theta|\} \leq \varepsilon.$$

Thus, ignoring the other variables for simpliticity, we have $|R_r(r) - R_r(r')| \leq |R_r(r) - \bar{R}_r(r')| + 2\varepsilon$ which implies that $\varepsilon_r \leq \bar{\varepsilon}_r + 2\varepsilon$. Similar argument applies to the other quantities in Assumptions 1.

For Conditions 1 *C1.1*, we see that the operator $L_0 : x \mapsto \dot{x} - R_r x$ is a perturbation of $\bar{L}_0 : x \mapsto \dot{x} - \bar{R}_r x$ with $||L_0 - \bar{L}_0|| \leq \varepsilon$. Similarly, $||J_0 - \bar{J}_0|| \leq 2\varepsilon$ hence if ε is small enough, L_0^{-1} and J_0^{-1} exists with $||L_0^{-1}||^{-1} \leq K_0 = \bar{K}_0 - \varepsilon$ and $||J_0^{-1}||^{-1} \leq \kappa_0 = \bar{\kappa}_0 - 2\varepsilon$.

For Conditions 1 *C1.2*, since R is $\varepsilon - C^1$ close to $\bar{R}$ we have $|R_{|\rho_0} - \bar{R}_{|\rho_0}| \leq \varepsilon$. By invariance we have $\bar{R}_{|\rho_0} = 0$ so if ε is small enough there is an η such that $|R_{|\rho_0}| \leq \eta/\tau \leq \frac{K_0}{2l_r}$. It is clear that if ε is small enough, *C1.3*, *C1.4* and *C1.5* are satisfied.

Thus the perturbed system has an invariant manifold. ∎

If the perturbed manifold is shown to be C^1 smooth then, since the state space in the center direction can be extended to include ε, it can be easily shown that the perturbed manifold also depends C^1 on ε.

The contrast with standard perturbation theory for normally hyperbolic system (HPS77, Fen71) is that Corollary 3.2.2 has further restrictions on the class of perturbation given by Assumptions 2 and 3.

Invariant manifolds for model equations will be computed in later chapters. However due to time constraint, the method based on Theorem 3.2.2 will not be implemented.

3.2.6 Hybrid approach to computing invariant manifold

A hybrid approach involving path–wise consideration at each graph transform to obtain the invariant graph for the non–autonomous system (3.1) is given here. This will be given as a conjecture and an outline of a possible proof will be given. This method for computing invariant manifolds will be tested on model systems in subsequent chapters.

The following lemma is a small alteration to Newton Map Theorem 3.2.1 where the Newton step here is based at each candidate graph ρ rather than a fixed graph ρ_0. This Newton step will be implemented in later chapters. We state it without proof as it is very similar to that of Theorem 3.2.1.

Lemma 3.2.5 *Given Conditions 1 consider $\rho \in \mathcal{G}$ and (θ_0, t_0) and take θ which solves $\dot{\theta} = \Theta(\theta, \rho, t)$ starting at $\theta(t_0) = \theta_0$. Let $L_\rho : x \mapsto \dot{x} - R_r(\theta(t), \rho, t)x$ and $F : r \mapsto \dot{r} - R(\theta(t), r, t)$ be as in the proof of Corollary 3.2.1. Now consider the Newton map $N : \mathcal{B}_\eta(0) \to \mathcal{B}_\eta(0)$ defined by*

$$N[r](t) = r(t) - L_\rho^{-1}[F(r)](t) \tag{3.36}$$

where $\mathcal{B}_\eta(0) \subset C^1$ is an η – ball centered at $r \equiv 0$. Then N is a well defined contraction. N has a locally unique fixed point with bound given in (3.21).

As in (3.26) a practical expression for N can be given as follows

$$N[r](t) = \int G(t,s)[R(\theta(s), r(s), s) - R_r(\theta(s), \rho(\theta(s), s), s)r(s)]ds. \quad (3.37)$$

See Chapter 5 where this expression is used in the pseudo–codes.

Conjecture 1 *Assume Conditions 1 and consider the map*

$$T : \mathcal{G} \to \mathcal{G}$$
$$\rho \mapsto \tilde{\rho} \quad (3.38)$$

defined by

$$(T\rho)(\theta_0, t_0) = \tilde{\rho}(\theta_0, t_0) = \tilde{r}(t_0) \quad (3.39)$$

where $\tilde{r}$ is the Newton fixed point given ρ, θ_0, t_0 as in Theorem 3.2.1. T is a well defined contraction and its fixed point ρ^* is a C^1 invariant normally hyperbolic submanifold of the non–autonomous system (3.1).
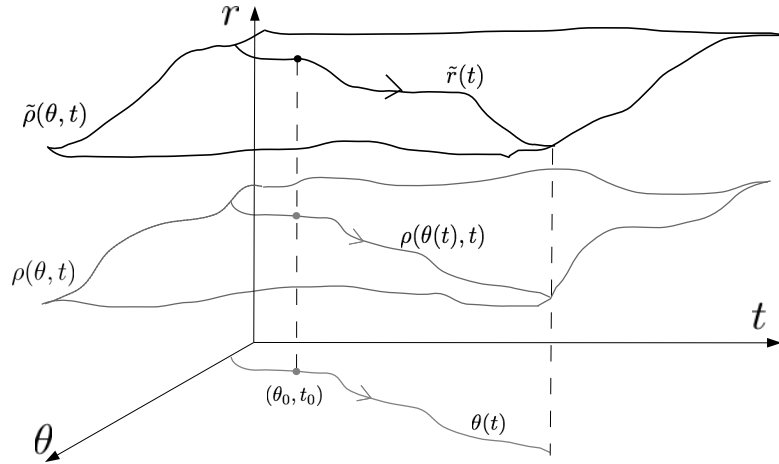
For an illustration of T see Figure 3.1.

Figure 3.1: A sketch of $T\rho = \tilde{\rho}$ and the Newton fixed point $\tilde{r}$ depending on ρ, θ_0, t_0.

Outline of possible proof: Let us give brief ideas of the tasks involved.

Well defined

To show that T is well defined we need to show $\mathrm{Lip}_\theta \tilde\rho \leq l$, which is a question of how $\tilde r$ depends on θ_0 (and t_0 but let us deal with θ_0 here). Now $\tilde r$ is a zero of an implicit function problem, $F(\tilde r) = \dot{\tilde r} - R(\theta, \tilde r, t) = 0$, so we can apply the chain rule to deduce how it varies with respect to differentiable changes in the function R resulting from changes in the path θ, i.e. $0 = D_r F \delta\tilde r + D_\theta F \delta\theta = \delta\dot{\tilde r} - R_r \delta\tilde r - R_\theta \delta\theta$. We are interested principally in the value at t_0, so

$$\delta\tilde r(t_0) = L_{\tilde r}^{-1}[R_\theta \delta\theta](t_0). \tag{3.40}$$

Now $\delta\theta$ is the solution of

$$\delta\dot\theta = (\Theta_\theta + \Theta_r \rho_\theta)\delta\theta \tag{3.41}$$

starting from $\delta\theta(t_0) = 0$. There are two problems and one is that ρ_θ may not be defined everywhere along the path since it is only assumed Lipschitz. The other is that $\delta\theta$ may be unbounded. If we ignore both these problems, we would obtain that $\tilde r(t_0)$ depends C^1 on θ_0 with derivative

$$\delta\tilde r(t_0) = \int G(t_0, s) R_\theta(s) \Phi(s, t_0) ds\; \delta\theta_0 \tag{3.42}$$

where Φ is the matrix solution of (3.41) from the identity. Now if we take the time derivative of (3.42) at a general t, using $\partial_t \Phi(s, t) = -\Phi(s, t)[\Theta_\theta + \Theta_r \rho_\theta](t)$ we would obtain

$$\begin{aligned}
\delta\dot r(t) &= [G(t, t+) - G(t, t-)]R_\theta(t)\Phi(t, t)\delta\theta_0 \\
&\quad + \int [\partial_t G(t, s) R_\theta(s)\Phi(s, t) + G(t, s)R_\theta\; \partial_t \Phi(s, t)]ds\delta\theta_0 \\
&= R_\theta(t)\delta\theta_0 + R_r(t)\delta\tilde r(t) - \delta\tilde r(t)[\Theta_\theta + \Theta_r \rho_\theta](t) \tag{3.43}
\end{aligned}$$

which implies $\delta\tilde r(t_0) = J_{\rho_\theta}^{-1}[R_\theta](t_0)\delta\theta_0$. Thus if $|R_\theta|$ is small enough we have $\mathrm{Lip}_\theta \tilde\rho \leq ||J_{\rho_\theta}^{-1}|||R_\theta| \leq l$.

Contraction

In order to show that T is a contraction we need to show that there is a constant $c < 1$ such that

$$|T\rho - T\rho'| \leq c|\tilde\rho - \tilde\rho'|. \tag{3.44}$$

This is a question of how $\tilde{r}$ varies with changes in ρ. Now a change $\delta\rho$ implies that $\delta\theta$ is subjected to the forced equation

$$\dot{\delta\theta} = (\Theta_\theta + \Theta_r \rho_\theta)\delta\theta + \Theta_r \delta\rho \qquad (3.45)$$

from $\delta\theta(t_0) = 0$ and has solution given by $\delta\theta(t) = \int_{t_0}^{t} ds \Phi(t,s)\Theta_r(s)\delta\rho(s)$. Thus we have,

$$\begin{aligned}
\delta\tilde{r}(t) &= L_{\tilde{r}}^{-1}[R_\theta \delta\theta](t) \\
&= \int G(t,u)R_\theta(u) \int_t^u ds\ \Phi(u,s)\Theta_r(s)\delta\rho(s). \qquad (3.46)
\end{aligned}$$

Ignoring the two problems mentioned above, by taking the time derivative

$$\begin{aligned}
\delta\dot{r}(t) &= \left[G(t,t+)R_\theta(t) \int_t^{t+} ds\ \Phi(t+,s)\Theta_r(s)\delta\rho(s) \right. \\
&\qquad\qquad \left. - G(t,t-)R_\theta(t) \int_t^{t-} ds\ \Phi(t-,s)\Theta_r(s)\delta\rho(s) \right] \\
&\quad + \int \partial_t G(t,u)R_\theta(u) \int_t^u ds\ \Phi(u,s)\Theta_r(s)\delta\rho(s) \\
&\quad + \int G(t,u)R_\theta(u)\ \partial_t \int_t^u ds\ \Phi(u,s)\Theta_r(s)\delta\rho(s) \\
&= R_\theta(t)\Theta_r(t)\delta\rho(t) + R_r(t)\delta\tilde{r}(t) - \int ds\ G(t,u)R_\theta(u)\Phi(u,t)\Theta_r(t)\delta\rho(t) \\
&= R_\theta(t)\Theta_r(t)\delta\rho(t) + R_r(t)\delta\tilde{r}(t) - J_{\rho_\theta}^{-1}[R_\theta](t)\Theta_r(t)\delta\rho(t), \qquad (3.47)
\end{aligned}$$

we can deduce

$$\delta r(t_0) = L_{\tilde{r}}^{-1}\left[R_\theta \Theta_r \delta\rho - J_{\rho_\theta}^{-1}[R_\theta]\Theta_r \delta\rho \right](t_0). \qquad (3.48)$$

Thus we have

$$|\delta\tilde{r}| \leq ||L_{\tilde{r}}^{-1}||\big(1 + ||J_{\rho_\theta}^{-1}||\big)|R_\theta||\Theta_r||\delta\rho| \qquad (3.49)$$

which implies the Lipschitz constant of T is in the order of $|R_\theta||\Theta_r|$ which can be made very small by choosing an appropriate coordinate system. ∎

The sketch proof indicates that the invariant manifold can be estimated accurately through only a few iterations of T if the coordinate system is chosen appropriately.

3.2.7 Graph transform approach to computing invariant manifold

The Graph Transform method for computing invariant submanifolds was developed in (HPS77) for discrete time systems and (Fen71) for continuous time systems. Let us briefly describe the method in the context for our non–autonomous system after discretisation. Later we will numerically compare the Graph Transform method and our method developed here.

We discretise the non-autonomous system (3.1) by taking the time–T map $f : M \times \mathbb{R}^n \times \mathbb{R} \to M \times \mathbb{R}^n \times \mathbb{R}$ which is a C^1 diffeomorphism.

Invariant manifolds for contracting and expanding systems

Let us first outline the Graph Transform method for contracting systems due to (HPS77), i.e. the case where $E_- \equiv 0$ and $E_+ \equiv \mathbb{R}^n$. Here we consider the time–T map f defined by the flow of the non–autonomous system (3.1).

We assume the non–autonomous system (3.1) is a small C^1 perturbation of some normally hyperbolic system which has $\rho_0 \equiv 0$ as its invariant normally hyperbolic submanifold. It may be possible to simply assume Condition 1 however it is not clear that our definition of normal hyperbolicity here implies the standard definition as in (HPS77).

Let us spell out the graph transform as follows. Given a $\rho \in \mathcal{G}$ and (θ_0, t_0) we have $\theta(t)$ as in the previous subsection. Then take $\hat{r}(t_0)$ to be the value after time T in the forward integral of $\dot{r} = R(\theta(t), \rho(\theta(t), t), t)$ starting from $\rho(\theta(t_0 - T), t_0 - T)$ at time $t_0 - T$. See figure 3.2.7.

Theorem 3.2.3 (Graph Transform) *Assume we have Conditions 1 and consider the map*

$$\hat{T} : \mathcal{G} \to \mathcal{G}$$
$$\rho \mapsto \hat{\rho} \tag{3.50}$$

defined by

$$(\hat{T}\rho)(\theta_0, t_0) = \hat{\rho}(\theta_0, t_0) = \hat{r}(t_0). \tag{3.51}$$

Then $\hat{T}$ is a well defined contraction and its fixed point $\bar{\rho}$ is a C^1 normally hyperbolic invariant manifold of f.

Proof: It is found in the proof of persistence of normal hyperbolicity for a small perturbation of the diffeomorphism, see proof of Theorem 4.1 (and 6.1 for

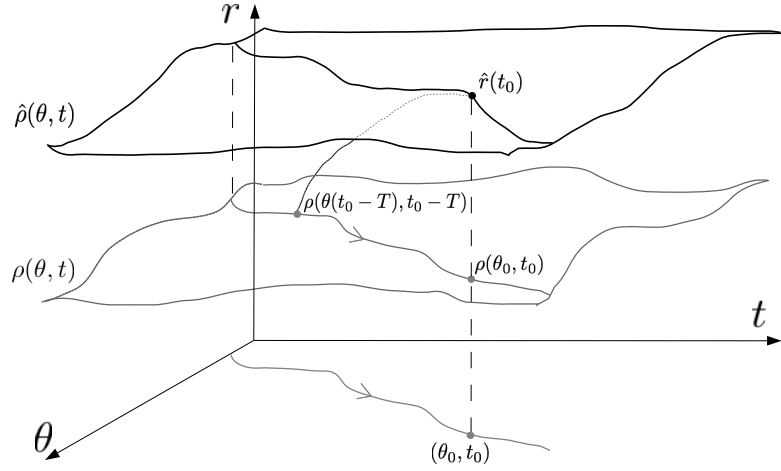non–compact case) part (a) and (f) in (HPS77). ∎

Figure 3.2: A sketch of $\hat{T}\rho = \hat{\rho}$ and $\hat{r}(t_0)$.

We recall that the contraction rate of $\hat{T}$, in the sup norm, is roughly equal to the ratio of the normal contraction rate of f (which depends on the time T) and the tangential contraction rate.

For expanding systems where $E_+ \equiv 0$ and $E_- \equiv \mathbb{R}^n$, one can treat the system in backward time, i.e. work with f^{-1} by taking the time–T map so then its backward contracting space is equal to $0 = E_+$. Thus we are in the contracting regime which means we can apply Theorem 3.2.7 to compute the invariant manifold.

Invariant manifold for general systems

We now briefly outline how to compute the invariant manifold, $\bar{\rho}$, for the general case where there are both contraction and expansion, i.e. neither E_- or E_+ are trivial. Given the existence of splittings E_+^0 and E_-^0 at $\rho_0 \equiv 0$, we consider the space of graphs $\mathcal{G}_+$ whose elements are of the form $\rho_+ : M_+ \times \mathbb{R} \to E_-^0$ where $M_+ = M \times E_+^0$. See Figure 3.2.7. Then, not including technicalities, we are in the contracting regime and so we can obtain a fixed point $\bar{\rho}_+$. Similarly, by considering $\mathcal{G}_-$ whose elements are of the form $\rho_- : M_- \to E_+^0$ where $M_- = M \times E_+^0$ this brings us to the expanding regime. So we can obtain a fixed point

$\bar{\rho}_-$ as above. Then the invariant manifold is given by

$$\bar{\rho} = \bar{\rho}_+ \cap \bar{\rho}_-. \tag{3.52}$$

The manifolds $\bar{\rho}_+$ and $\bar{\rho}_-$ are conventionally called the stable and unstable manifold of $\bar{\rho}$ and are notated by $W^s(\bar{\rho})$ and $W^u(\bar{\rho})$, respectively.
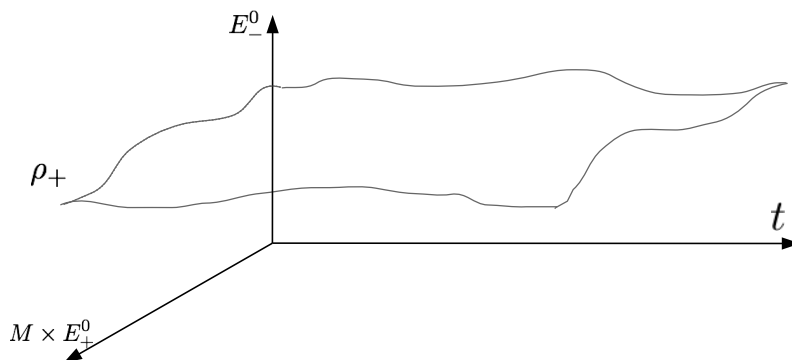
Figure 3.3: A sketch of ρ_+.

3.2.8 Comparisons of methods that compute invariant manifolds

The method presented in Theorem 3.2.2, Conjecture 1 and the standard Graph Transform of Theorem 3.2.3 are suitable for systems which have a collapse of dynamics on the invariant manifold. The contraction rate of the methods developed here depends on the coordinate and can be made arbitrarily small by choosing an appropriate coordinate system so that $|R_\theta||\Theta_r|$ is small. In contrast, the Graph Transform method has a contraction rate that can be made arbitrarily small by choosing large T for the time–T map. However, for general

systems where both contraction and expansion in the transverse direction exists, the method outlined for the Graph Transform involves taking intersection at the end. In contrast, the methods developed here does not need this extra step.

In (BOV97, BHV03), methods were developed to compute normally hyperbolic invariant manifold based on the Graph Transform of (HPS77). In (BOV97), for the case where there is no normal expansion, a global Newton operator which is a contraction on an appropriate ball of function space, was used to compute the invariant manifold. For the case where there is no normal contraction, the same Newton operator was used. With these special cases, they obtained a "hybrid" method to compute the invariant manifold for the general case where both the normal contraction and expansion exists. The assumption made in (BOV97, BHV03) is that the invariant manifold is compact. In contrast, the method developed here does not assume compactness. In addition, the method here does not need a combination of two steps as in the "hybrid" method for general systems.

A method based on solving a system of quasi–linear PDEs was developed to compute invariant manifolds in (GV04). The system of PDE comes from the property that the vector field evaluated on any point of the invariant manifold is orthogonal to the normal of the manifold at that point. In contrast to our method here, this approach was used to compute the stable and unstable manifold of a fixed saddle point.

Chapter 4

Synchronisation of non–autonomous oscillators

Synchronisation of non–autonomous systems plays an important role in the sciences and engineering since most systems in real life are influenced by external factors. See (MM10) and references within for some study of this phenomenon.

Here we will develop the theory for the synchronising of one oscillator to a time–dependent forcing. We will give the definition of synchronisation for many oscillators and outline how one can study synchronisation in the many oscillators scenario. Note that although synchronisation is the focus of the thesis, oscillator systems need not always be synchronised.

Take any m independent attracting normally hyperbolic oscillators, with equation of the form

$$
\begin{aligned}
\dot{\theta} &= \omega \\
\dot{r} &= g(\theta, r)
\end{aligned}
$$

(4.1)

where $\theta = [\theta_i]_{i=1}^m \in S^m$, $r = [r_i]_{i=1}^m \in U \subset (\mathbb{R}^{n_i})^m$, $\omega = [\omega_i]_{i=1}^m$ and $g(\theta, r) = [g_i(\theta_i, r_i)]_{i=1}^m$. When they are coupled and forced by a small external signal $f = (f_1, f_2)$ we write the equation as

$$
\begin{aligned}
\dot{\theta} &= \Theta(\theta, r, t, f_1) \\
\dot{r} &= R(\theta, r, t, f_2)
\end{aligned}
$$

(4.2)

Note that f is a function of the (θ, r, t)–space (or in the simplest cases only of time) so f can be omitted in the equation above but serves as a functional

59

parameter. The cross product of the limit cycles in the uncoupled system in the time extended space is a normally hyperbolic manifold which we assume to be $\rho_0 = \{r = 0\}$. However, if the oscillators are weakly coupled and weakly forced and their interaction depends on time, the invariant manifold theory in Chapter 3 applies and an invariant manifold, ρ, exists and is C^1 close to ρ_0. Thus, all the oscillators remain "oscillating" and it is of interest to find conditions for when they synchronise which corresponds to the collapse of dynamic on ρ. Since we are only interested in the dynamic on ρ we restrict our attention to the higher dimensional time–dependent coupled phase equations

$$\dot{\theta} = \omega + h(\theta, t) \tag{4.3}$$

where the vectors $h = [h_i]_{i=1}^m$. The variable θ_i and parameter ω_i corresponds to the state and intrinsic frequency of oscillator i. We note that h depends on ρ, but we exclude this notation for simplicity and view the time term as a contribution of this dependency.

We will also consider the "reliability" of the unforced coupled system (4.2). Vaguely speaking, a system is "reliable" if independent of its initial state, repeated presentation of a forcing produces essentially the same response after an initial period, i.e. the response to a signal is reproducible. We will discuss conditions for reliability in oscillator systems as studied in (LSBY09) where the oscillators are taken to be phase oscillators. See below for a definition of reliability for the m unforced coupled system (4.1) which is more general than that given by (LSBY09) where the only the phase of the oscillators are considered. However, we are only considering a particular forcing rather than a class of forcings as in (LSBY09)

Definition 4.0.10 (Reliability) *Take the coupled m normally hyperbolic oscillators system given by (4.2) with no forcing, i.e. $f = 0$. Consider a forcing f and let $\Psi(t; p_0, f)$ be the flow of the forced system (4.2) in the time extended space starting at $p_0 = (\theta_0, r_0, t_0) \in S^m \times U \times \mathbb{R}$ with end time t. Then the coupled system is reliable if for almost all $p_0, p_0' \in S^m \times U$ we have, for all $t > t_0$*

$$|\Psi(t; p_0, f) - \Psi(t; p_0', f)| \leq De^{-\lambda|t-t_0|} \tag{4.4}$$

for some $0 \leq D < \infty$ and $\lambda > 0$.

Note that we use the norm defined by $|(\theta, r, t)| = \max_{1 \leq i \leq m}\{|\theta_i|, |r_i|\}$. We remark that the definition above gives exponential convergence to the common output which can be a desired property in applications.

4.1 One oscillator

Here we study the one oscillator system which may give ideas for the study of the many oscillator system.

4.1.1 Synchronisation of a forced oscillator

We define synchronisation for the system 4.3 where $m = 1$ as follows

Definition 4.1.1 (Synchronisation to a forcing)
For the time–dependent system (4.3), synchronisation occurs when it possesses an attracting uniformly hyperbolic trajectory $\theta^*(\cdot)$.

The definition above is analogous to "phase locking" (PRK01) for weak periodic forcing where synchronisation is said to occur if a stable fixed point exists for the phase difference equation. However, our definition is more general as it applies to weak aperiodic forcings and as far as I know our definition is original.

Note that we are dealing with C^1 systems hence their invariant manifolds, ρ, are also C^1. We shall see that the synchronised trajectory $\theta^*(\cdot)$ is also C^1. See Figure 4.1 for a sketch of θ^*.
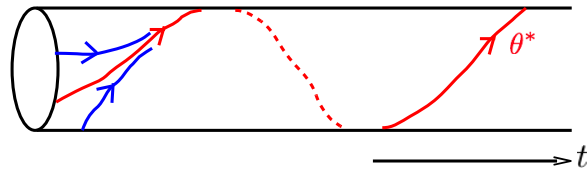

Figure 4.1: A sketch of an attracting normally hyperbolic trajectory θ^* (shown in red) on the invariant cylinder.

We now give sufficient conditions for synchronisation to occur for the time–dependent system (4.3).

Conditions 2 (Synchronisation conditions) *Take the time–dependent system (4.3) and consider the following conditions*

S1: *Existence of an invariant strip $[\theta_-(t), \theta_+(t)]$ i.e. there are differentiable paths $\theta_-(\cdot)$ and $\theta_+(\cdot)$ such that $|\theta_+ - \theta_-| > \varepsilon$ for some $\varepsilon > 0$. In addition*

the following holds: $\omega + h(\theta_-(t), t) > \dot{\theta}_-(t)$ and $\omega + h(\theta_+(t), t) < \dot{\theta}_+(t)$.

S2: *Contraction in the invariant strip, i.e. $h_\theta(\theta, t) \leq -k < 0$ for all $\theta \in [\theta_-, \theta_+]$.*

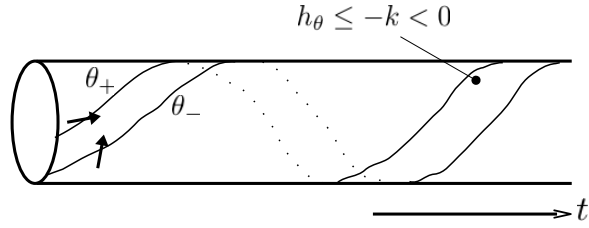See Figure 4.2 for a sketch of these conditions.

Figure 4.2: A sketch of an invariant strip on the invariant cylinder.

Theorem 4.1.1 *If the time–dependent system (4.3) has Conditions 2, then synchronisation occurs.*

Proof: We wish to show that there is a continuously differentiable attracting normally hyperbolic trajectory $\theta^*(\cdot)$. Consider the space $C^1(\mathbb{R}, \mathbb{R})$ whose elements are paths $\theta(\cdot)$ that lies in the invariant strip, i.e. $\theta(t) \in [\theta_-(t), \theta_+(t)]$. Let $\varphi(t; \theta_0, s)$ be the flow of the system (4.3) starting from θ_0 at time s. Fix a time $\tau > 0$ and take the operator $\mathcal{H} : C^1 \to C^1$ defined by

$$(\mathcal{H}\theta)(t) = \varphi(t; \theta(t - \tau), t - \tau). \tag{4.5}$$

See Figure 4.3 for a sketch of how $\mathcal{H}$ is defined. It is clear that $\theta \in [\theta_-, \theta_+]$ implies $\mathcal{H}(\theta) \in [\theta_-, \theta_+]$ and $\frac{\partial \mathcal{H}(\theta)}{\partial t} = \frac{\partial \varphi}{\partial \theta} \cdot \dot{\theta}$ which is continuous, so $\mathcal{H}$ is well defined. We wish to show that $\mathcal{H}$ is a contraction. Note that for $\theta_1, \theta_2 \in C^1$ we have

$$\begin{aligned} \Delta\dot{\varphi} &= h_\theta(\theta_1, t)\Delta\varphi \\ &\leq -k\Delta\varphi \end{aligned} \tag{4.6}$$

where $\Delta\varphi(t) = \varphi(t; \theta_2(t - \tau), t - \tau) - \varphi(t; \theta_1(t - \tau), t - \tau)$ which gives us the Gronwall's inequality

$$\Delta\varphi(t) \leq e^{-k\tau}\Delta\varphi(t - \tau). \tag{4.7}$$

But $(\mathcal{H}\theta_2)(t) - (\mathcal{H}\theta_1)(t) = \Delta\varphi(t) \leq e^{-k\tau}(\theta_2(t-\tau) - \theta_1(t-\tau))$ for all t, so we have

$$|\mathcal{H}(\theta_2) - \mathcal{H}(\theta_1)| \leq e^{-k\tau}|\theta_2 - \theta_1|. \tag{4.8}$$

Hence $\mathcal{H}$ is a contraction with rate $e^{-k\tau} < 1$. Thus it has a fixed point $\theta^*(\cdot)$ which solves the time–dependent system (4.3). Moreover, by **S2** of Conditions 2 the linearised system $\dot{\delta\theta} = h_\theta(\theta^*(t), t)\delta\theta$ is uniformly hyperbolic. So $\theta^*(\cdot)$ is an attracting normally hyperbolic trajectory. ∎
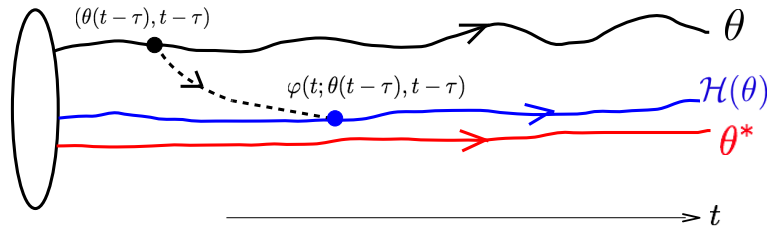
Figure 4.3: A sketch of how $\mathcal{H}$ is defined.

Given that synchronisation can be detected by Conditions 2, the robust region where synchronisation persists, can be computed by applying Lemma 3.2.2. See (BM03) for more details.

4.1.2 Reliability of one oscillator systems

We discuss here the conditions for reliability of one oscillator system, in particular we consider the type of forcing in which the system is reliable. Consider the forced one oscillator system (4.2) which we recall below

$$\dot{\theta} = \Theta(\theta, r, t, f_1)$$
$$\dot{r} = R(\theta, r, t, f_2) \tag{4.9}$$

with $f = (f_1, f_2)$ where $\theta \in S^1$ (center variable) and $r \in U \subset \mathbb{R}^n$ (transverse variable). Given that the unforced oscillator has an attracting normally hyperbolic invariant cylinder $\rho_0 = \{r = 0\}$, by the theory of Chapter 3, if f is small enough, the forced system (4.9) also have an attracting normally hyperbolic invariant cylinder which we denote by ρ. Thus for any initial points $p_0 \in S^1 \times U \times \mathbb{R}$ the flow $\Psi(t; p_0, f)$ in Definition 4.0.10 tends to ρ exponentially in the transverse direction as $t \to \infty$. Let us give the following corollary that gives conditions for reliability.

Corollary 4.1.1 *If the forcing f produces only one uniformly attracting hyperbolic trajectory $\xi^*(t) = (\theta^*(t), r^*(t), t)$ on the cylinder ρ as in Definition 4.1.1, then for almost all $p_0 \in S^1 \times U \times \mathbb{R}$ we have $\Psi(t; p_0, f) \to \xi^*(t)$ exponentially in the tangential direction.*

Thus under Corollary 4.1.1 the forced system is reliable under f. However, it is clear that if there were more than one uniformly hyperbolic attracting trajectories on ρ the system under f is not reliable. Thus the definition of synchronisation is more general than that of reliability in this context.

4.2 Many oscillators

4.2.1 Synchronisation of many oscillators

For $m > 1$, define a cylinder in the time extended space $S^m \times$ time by the graph of a function $\zeta : S^1 \times$ time $\to S^{m-1}$, thus the cylinder is 2 dimensional. We define synchronisation as follows

Definition 4.2.1 (Synchronisation of many oscillators)
Synchronisation occurs when the time–dependent coupled equation (4.3) possesses an attracting normally hyperbolic invariant cylinder ζ^*.

A similar definition of synchronisation is found in (MM10) where a "diagonal–like" submanifold at each instance of time t is defined which is equivalent to a time t slice of the cylinder in our context.
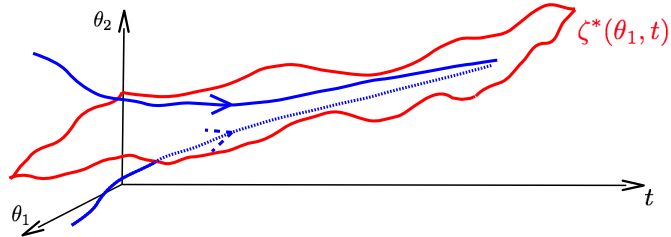

Figure 4.4: A sketch of an attracting normally hyperbolic invariant cylinder ζ^* (shown in red) on graph of $\rho \cong S^1 \times S^1 \times$ time.

See Figure 4.4 for a sketch of ζ^* for when $m = 2$. Further work to find sufficient conditions for synchronisation to occur in this case would be valuable. The idea of an invariant region in the case of one oscillator provides an inspiration for this, although this may not be feasible for $m \geq 3$. However, (MM10) developed an alternative approach that utilises a dissipation condition "**H**". This

has an equivalent form that is amenable to their analysis for linearly coupled systems of many oscillators. Their assumption of linear coupling is not a necessity for the existence ζ^*, thus their approach may be used for nonlinear coupling.

Let us outline another approach which tackles the problem at network level by treating synchronisation as a percolation process. This will require us to find conditions for synchronisation of two oscillators and extend the theory of the robust region to this scenario. However, one can adopt the approach of (MM10) for two nonlinearly coupled oscillators which may be a natural next step for their approach.

The idea here is that the oscillator in the network pairs up with another that has similar characteristics. For example, their frequency difference could be sufficiently small in which case they would form an active connection. While they are doing this other oscillators within the network are also pairing up and forming active connections. Then we can apply the theory from the case of two oscillators and find that the paired oscillators synchronise to form essentially one oscillator. Thus the network renormalises with fewer oscillators than before. Then new pairing begins and the aggregation process repeats until we obtain clusters of oscillators. The other possibility is that the process may keep on going until one super cluster is formed where the entire network is in synchrony with some outliers. Thus the network synchronises by percolation. This approach may be more applicable in a realistic network since it is highly plausible that some oscillator may fail to synchronise with the cluster. See Figure 4.5 for a schematic of this process.

4.2.2 Reliability of m oscillator systems

We saw in the beginning of the chapter that if the coupling and forcing f is small enough in the m oscillator system (4.2) there is an attracting normally hyperbolic invariant manifold ρ. So given any point $p_0 \in S^m \times U \times \mathbb{R}$ the flow $\Psi(t; p_0, f)$ in Definition 4.0.10 will tend to ρ exponentially in the transverse direction – which is necessary for reliability. If the forcing f is such that the coupled oscillators synchronises with an attracting normally hyperbolic invariant cylinder ζ^* on ρ, we are essentially in the one oscillator scenario found in Section 4.1.2. In particular, Corollary 4.1.1 gives conditions for reliability in this context. Note then that reliability in the m oscillator system is a stronger property than synchronisation in Definition 4.2.1 as it requires further collapse of dynamics on the invariant cylinder ζ^*.
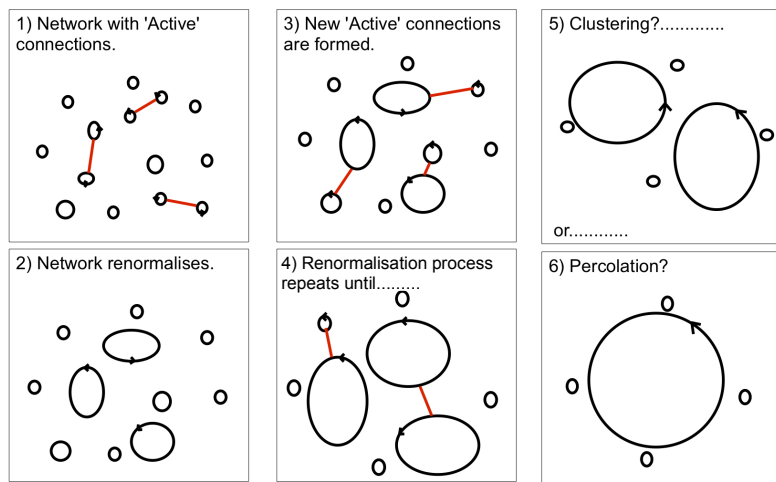
Figure 4.5: A diagram showing synchronisation as an aggregation process. 1) The oscillators in the network form "active" pairs. 2) Each active pair synchronises to become essentially one oscillator thus the network renormalises. 3) Further active pairing takes place. 4) Further network renormalisation takes place. 5) The aggregation process could stop and clustering could take place or 6) The entire network synchronises with some outliers.

Chapter 5

Applications

Normally hyperbolic invariant manifold theory has many applications in the sciences and appears in many physical systems. For a list see (WHM94). It can be used in dimension reduction for large systems where the dynamics on the invariant manifold is the desired reduced system. Due to the persistence property it can be used to describe many physical systems that are robust to small changes in parameters of the governing equations.

Here, we will apply it to attracting normally hyperbolic oscillators that are aperiodically forced. The aim is to obtain a perturbation result where the unforced system is the idealised unperturbed system. This result will be used here to compute the perturbed normally hyperbolic invariant manifold of a simple 2–D model and in a physiological model presented in Chapter 6.

Pseudo–codes for the methods to compute invariant manifolds will be given. In particular the method based on Conjecture 1 and the Graph Transform of Theorem 3.2.3 will be implemented.

5.1   Aperiodic oscillators

The unperturbed oscillator has an invariant cylinder in the time–extended space, which persists under time–dependent forcing. We wish to numerically compute the perturbed cylinder and find forcing which causes further collapsing of dynamics on it.

Consider a normally hyperbolic limit cycle γ in the (θ, r, t)–coordinate given

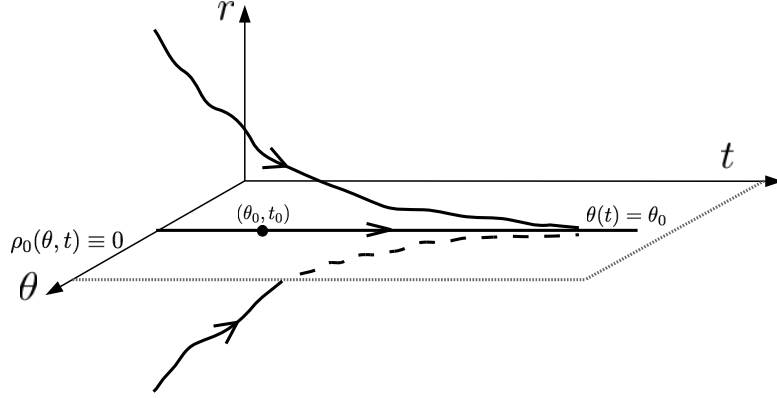Figure 5.1: A trajectory on the attracting cylinder $\rho_0 \equiv 0$.

by the following unperturbed equation

$$\dot{r} = g(\theta, r, t)$$
$$\dot{\theta} = \omega \qquad (5.1)$$

with angular frequency $\omega \in \mathbb{R}$, $r \in \mathbb{R}^n$ and $\theta \in \mathbb{R}/2\pi\mathbb{Z}$. Without loss of generality we assume $\omega = 0$ because we can take a coordinate change by taking $\theta \to \theta - \omega t$ to obtain a system with frequency 0 in the new coordinate. Note that g is θ–periodic and $g(\theta, 0, t) = 0$. We assume the coordinate system is chosen such that $|g_\theta|$ is small on $\{r = 0\}$.

In the time extended space $\mathbb{R}/2\pi\mathbb{Z} \times \mathbb{R}^n \times \mathbb{R}$, γ is the invariant cylinder given by the zero graph $\rho_0(\theta, t) \equiv 0$, see Figure 5.1. By the assumption of normal hyperbolicity, given ρ_0 and any θ_0, t_0 we have $\theta(t) = \theta_0$ and $L : x \mapsto \dot{x} - g_r(\theta(t), 0, t)x$ is invertible with $||L^{-1}||^{-1} \geq K$ for some $K > 0$ and its Green's function satisfies $|G(t, s)| \leq De^{-\mu|t-s|}$ for some $\mu > 0$ and $D > 1$.

The constant μ and D can be related to the Floquet exponents and multipliers of the limit cycle. For example, if γ is attracting, then for $g_r(\theta, 0, t)$ independent of time or is time periodic, we can take μ to be the smallest absolute Floquet exponent of the linearised r equation $\dot{x} = g_r(\theta_0, 0, t)x$. Note that the property of normal hyperbolicity for a limit cycle can be given in terms of the constants μ and D, e.g. Floquet exponents and multipliers. In which case K can be easily determined by using the fact that L^{-1} has kernel G.

5.1.1 Perturbed system

We wish to consider a small perturbation of (5.1) given by

$$\dot{r} = g(r, \theta, t) + \varepsilon \bar{R}(r, \theta, t)$$
$$\dot{\theta} = \varepsilon \bar{\Theta}(r, \theta, t) \tag{5.2}$$

and apply Chapter 3 to show that it has an attracting normally hyperbolic invariant graph $\bar{\rho}$ for non large ε. Let us write $R = g + \varepsilon \bar{R}$ and $\Theta = \varepsilon \bar{\Theta}$ and state this in the following theorem.

Theorem 5.1.1 *The perturbed equation (5.2) has a normally hyperbolic invariant manifold if ε is small enough.*

Proof: We are required to check that $\rho_0 \equiv 0$ satisfies **C1** and **C2** of Condition 1 under the perturbed equation.

Check **C1**:
(i) $|R| \leq \varepsilon|\bar{R}|$; (ii)$|R_\theta| = |g_\theta + \varepsilon \bar{R}_\theta|$ and (iii)$|R_\theta||\Theta_r| \leq (|g_\theta + \varepsilon \bar{R}_\theta|)\varepsilon|\bar{\Theta}_r|$ are small if ε is small enough.

Check **C2**:
Given ρ_0 and θ_0, t_0 we have $\theta(t)$ which solves $\dot{\theta} = \Theta(\theta, 0, t)$ from θ_0 at t_0. Then $L_0 : x \mapsto \dot{x} - R_r(\theta(t), 0, t)x$ is a small perturbation of $L : x \mapsto \dot{x} - g_r(\theta(t), 0, t)x$ with $|\Delta L| \leq \varepsilon|\bar{R}_r|$. By lemma 2.2.1 in Chapter 2, if ε is small such that $\varepsilon < K/|\bar{R}_r|$, then L_0 is invertible since L is invertible.

Now $J_0 : \sigma \mapsto \dot{\sigma} - R_r(\theta, 0, t)\sigma + \sigma\Theta_\theta(\theta, 0, t)$ is just a small perturbation of L with $|L_0 - J_0| \leq \varepsilon|\bar{\Theta}_\theta|$. So by lemma 2.2.1 in Chapter 2, J_0 is also invertible if $\varepsilon < K/|\bar{\Theta}_\theta|$. $\blacksquare$

Note that the perturbation can be more general than just additive.

5.1.2 Pseudo–codes for physical systems

Here we will develop numerical methods to estimate invariant manifolds on Conjecture 1 (operator T) and the Graph Transform method of Theorem 3.2.3 (operator $\hat{T}$). In particular we consider applications to attracting systems hence there is no expansion in the transverse direction. Later, we will investigate a particular case where $r \in \mathbb{R}$ for the system given by (5.2). For presentation purposes in this section we write $R(\theta, r, t) = g(\theta, r, t) + \varepsilon \bar{R}(\theta, r, t)$ and $\Theta(\theta, r, t) = \varepsilon \bar{\Theta}(\theta, r, t)$.

It is desirable to compute the invariant cylinder $\bar{\rho}$ which simple integration in forward time may not suffice as there could be attracting trajectories on the cylinder. With the parameter ε and functions g, $\bar{R}$ and $\bar{\Theta}$ fixed, I will give pseudo–codes that computes the T–iterate of a given input surface ρ restricted to a fixed area $[t_{min}, t_{max}] \times [\theta_{min}, \theta_{max}]$. The output will be an array of co-ordinates of the form $(x, y, z) = (t, \theta, r)$ which will give a surface representing the cylinder $T\rho$ in the lift with $r = (T\rho)(\theta, t)$. The next iterate of ρ can then be computed by feeding the array for $T\rho$ back into the algorithm. This could have been automated but due to time constraint it was not carried out. However, a separate simple code (not presented here) was used to calculate the sup norm differences between two surfaces to estimate the contraction rate of T. The parameter ε which represents the forcing in the system, was chosen by trial and error such that the algorithm converges. The case that the code does not converge may indicate that the forcing was too big for an invariant surface to exist. In subsequent examples we found that the sup norm difference between two iterates of the given starting surface was very small which indicates that $T\rho$ is a good estimate for $\bar{\rho}$.

Algorithm 1: Green's function

> **Inputs:** $\{\theta(t), t \in [t_{\min}, t_{\max}]$ and $\rho \in \mathcal{G}.\}$
>> **for** $(t_{\min} - s^* < s < t_{\max})$
>>> **comment:** $s^* > 0$ is large enough to ensure $G(t, t - s^*)$
>>> is very small.
>>> $x(t) = $ forward integrate $\dot{x} = R_r(\theta(u), \rho(\theta(u), u), u)x$
>>> starting from $x(s) = 1$ for a time length of s^*;
>>> **store:** $G(t, s) = x(t)$ for $t \in (\max\{t_{\min}, s\}, \min\{s + s^*, t_{\max}\})$;
>> **return:** G;

See Figure 5.2 for the domain of the Green's function G. See Figure 5.3 and 5.4 for the C++ header file for Algorithm 1.
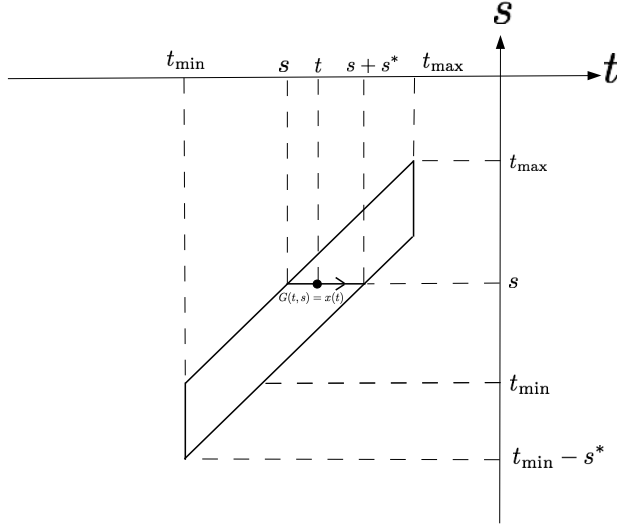
Figure 5.2: G has the indicated trapezium as its domain.

Algorithm2: Newton fixed point.

    Inputs: $\{\theta(t), t \in [t_{\min}, t_{\max}]$ and $\rho \in \mathcal{G}.\}$

        $G =$**Algorithm 1:** Green's function$\{\theta(t), t \in [t_{\min}, t_{\max}]$ and $\rho \in \mathcal{G}\}$;

      $r(s) =\rho(\theta(s), s) \quad s \in [t_{\min}, t_{\max}]$;

    while $(error > \varepsilon)$

        comment: ε is some pre–assigned accuracy for the Newton

        fixed point.

        $f(s) = R(\theta(s), r(s), s) - R_r(\theta(s), \rho(\theta(s), s), s)\ r(s) \quad s \in [t_{\min}, t_{\max}]$;

        for $(t_{\min} < t < t_{\max}) \quad \tilde{r}(t) =$ Trapezium rule: $\displaystyle\int_{t-s^*}^{t} G(t,s)f(s)ds$;

        $error = |r - \tilde{r}|$;

        $r =\tilde{r}$;

    return $\tilde{r}$;

Note that the overhead is mainly in computing G and not the **while** loop, which inexpensively evaluates the Green's function, G, and f to update r, possibly multiple times. See Figure 5.5 - 5.8 for the C++ header file for Algorithm 2. To practically estimate the invariant manifold we must decide on a finite domain

of ρ.

Algorithm 3: Invariant manifold.

  Inputs: $\{\rho(\theta,t) \in \mathcal{G}, \quad t \in [t_{\min}, t_{max}], \quad \theta \in [\theta_{\min}, \theta_{\max}]\}$

  comment: can initialise $\rho \equiv 0$.

    for $(t_{\min} < t_0 < t_{\max}; \quad \theta_{\min} < \theta_0 < \theta_{\max})$

     $\theta(t) =$ backward integrate $\dot{\theta} = \Theta(\theta, \rho(\theta,t), t)$

     starting from $\theta(t_0) = \theta_0$ until it reach boundary of ρ at time t_b;

     $\tilde{r}(t) =$ **Algorithm 2:** Newton fixed point$\{\theta(t), t \in [t_b, t_0], \rho \in \mathcal{G}\}$;

     store: $\tilde{\rho}(\theta(t), t) = \tilde{r}(t)$;

  Output: $\tilde{\rho}$;

To compute the next iterate of ρ we can repeat **Algorithm 3** with the updated input or we can modify the algorithm to automate this if desired. Note that for greater efficiency, $\theta(t)$ does not need to be computed to the boundary of ρ as the value of $\tilde{\rho}$ may have already been computed near the boundary from previous θ traces within the **for** loop. In addition, the method is amenable to parallel computing as the ranges in the for loop can be split into several regions hence split the task up. See figure 5.9 - 5.14 for the header file of Algorithm 3. To estimate the invariant manifold using the Graph Transform method we can replace **Algorithm 2** with **Algorithm 2.1** (below) in **Algorithm 3**.

Algorithm 2.1: Graph Transform method.

  Inputs: $\{\theta(t), t \in [t_{\min}, t_{\max}] \text{ and } \rho \in \mathcal{G}.\}$

    for $(t_{\min} < t < t_{\max})$

$$r(t) = \rho(\theta(t-T), t-T) + \int_{t-T}^{t} R(\theta(s), \rho(\theta(s), s), s)ds;$$

    comment: T is the time defining the time T–map.

  return r;

Note that when comparing the contraction rates of the Graph Transform method and our method we should take $T = s^*$ for a fair comparison. We refer the algorithm based on the Newton fixed point theorem by Algorithm A and the algorithm based on the Graph Transform by Algorithm B. The computations below and in following chapter were performed on a MacBook Pro laptop with Intel Core i7 2GHz processor.

5.1.3 Discretisation details

In the following computations, we restrict the surface to a grid area given by $[t_{min}, t_{max}] \times [\theta_{min}, \theta_{max}] \subset \mathbb{R} \times M$ and the grid is separated into small cells denoted by $\Delta t \times \Delta \theta$ each of size specified in the tables below.

For Algorithm A, recall that s^* is the length in time where the Greens function is truncated for each $t \in [t_{min}, t_{max}]$ i.e. $G(t, s)$ for $s < t - s^*$ is not included in the computation, see the pseudo–code for Algorithm 1. The discrete time step to compute $x(t)$ in Algorithm 1 for the Greens function is denoted by dt while the discrete time step to compute $\theta(t)$ in Algorithm 3 is denoted by δt. The Newton error of Algorithm 2 are specified in the tables below along with s^*, dt and δt.

For Algorithm B, s^* is the length in time that we integrate the system forward in time to create a time–s^* map. The discrete time step to compute $r(t)$ in Algorithm 2.1 is also denoted by dt while the discrete time step to compute $\theta(t)$ is denoted by δt. All these quantities will be detailed in the tables below.

```
#ifndef FUNCTION2D_H
#define FUNCTION2D_H

#include "function.h"
#include "simple_types.h"
#include <vector>
#include <ostream>

/*
  A function defined on a parallelogram.
 */
class function2d {
public:
  // A trivial constructor that produces a function with four sample
  // points at the corners of the unit square, all initialised to zero.
  function2d ();

  function2d (point2d start, point2d hor, point2d vert,
              unsigned int hor_samples, unsigned int vert_samples);

  function2d (const rect &domain,
              unsigned int hor_samples, unsigned int vert_samples);

  void set_sample(unsigned int i, unsigned int j, double x);

  double get_sample (unsigned int i, unsigned int j) const
    { return samples[i][j]; }

  void print_heightfield (std::ostream &os) const;

  double evaluate (double x, double y) const;

  double evaluate_green (double x, double y) const;

  bool in_domain (double x, double y) const;

  //protected:
  point2d start, vert, hor;
  double vert_samples, hor_samples;
  rect bbox;
```

Figure 5.3: C++ header file for Algorithm 1 (i).

```cpp
  // Stored in rows so that array[i][j] selects i'th row and j'th
  // column because array[i][j] is parsed as (array[i])[j]
  std::vector<std::vector<double> > samples;
};

/*
  vector_field takes s and returns a double (s can range between
  trange.first-slength and trange.second).
 */
function2d green_function (interval trange, double slength,
                           two_doubles_to_double vector_field,
                           double cell_size, void* user_data);

/*
   Returns the integral of G(t,s)*f(s) over range with t fixed.
 */
double inner_product (const function2d &G, const function &f,
                      const interval &range, const interval &false_range,
                      double t, double false_t);

double trapez_rule (const function2d &G, const function &f,
                    const interval &range, const interval &false_range,
                    double t, double false_t);


#endif
```

Figure 5.4: C++ header file for Algorithm 1 (ii).

```cpp
#ifndef FUNCTION_H
#define FUNCTION_H

#include "simple_types.h"
#include <vector>
#include <ostream>
#include <utility>

// double_to_double is a pointer to a function taking a double and
// returning one.
typedef double (*double_to_double)(double);

// two_doubles_to_double is a pointer to a function that takes two
// doubles (x,t) and returns one. It takes one extra argument, a const
// void* which gets filled in with a user supplied pointer.
typedef double (*two_doubles_to_double)(double,double,const void*);

// A pair of doubles makes an interval
typedef std::pair<double,double> interval;

class function
{
public:
  // Constructor that takes an initializer
  function (double_to_double f, double min, double max, int N);

  // A constructor that doesn't do anything except reserve the memory.
  function (double min, double max, int N);

  // Steals the contents of samples!
  function (std::vector<double> &samples, double min, double max);

  // Dump the function to a stream to see that it works!
  void print (std::ostream &os) const;

  // How we do stuff like squaring: Applies txform to each
  // sample. The transform is newf = txform(x,oldf)
  void transform (two_doubles_to_double txform, void* user_data);
```

Figure 5.5: C++ header file for Algorithm 2 (i).

```cpp
// Turn f into f^2.
void square ();

// Find the domain of the function
interval domain () const;

// Get the length of the function's domain
double domain_length () const { return max - min; }

// Return how many samples there are of the function in the given
// interval.
unsigned int samples_in_interval (interval i) const;

// Return a copy of this function, restricted to the intersection
// between our domain and i.
function restriction (interval i) const;

// Evaluate the function somewhere in its domain, using linear
// interpolation. If called outside of the domain, return zero
// (throwing an error would be cleverer)
double evaluate (double x) const;

void set_sample (int i, double x);

// Arithmetic with functions (is harder!) (again, this would be cool
// with operator overloading, and it'd be nice to have more
// operators)
function subtract (const function &f) const;

// Return the maximum modulus of the function
double sup_norm () const;

// Return a vector of point2d's which is the graph of the function
std::vector<point2d> graph () const;

// From a sample index, return the corresponding argument, x.
double arg_from_index (unsigned int i) const;
```

Figure 5.6: C++ header file for Algorithm 2 (ii).

```cpp
  // For a sample argument, return the corresponding index, i (as a
  // double, since we might land between samples, and I don't want to
  // decide which way to round here).
  double index_from_arg (double x) const;

  void set_sample (unsigned int i, double x) { samples[i] = x; }
  double get_sample (unsigned int i) const { return samples[i]; }
  unsigned int samples_number () const { return samples.size(); }

  static function identity (double min, double max, unsigned int n);


  //s: added smoothing
  // Return a function which is a numerical derivative using spline
  // based method with bandwidth h.
  function derivative (double h) const;

  // Return a smoothed version of this function using splines with
  // bandwidth h.
  function spline_smoothed (double h) const;

protected:
  double min, max;
  std::vector<double> samples;


  function fast_subtract (const function& f) const;
};

interval intersect_intervals (const interval &a, const interval &b);

// Euler integration
function euler_b (two_doubles_to_double f, double min, double max,
                 unsigned int N, double start_val, const void* user_data);
function euler (two_doubles_to_double f, double min, double max,
               unsigned int N, double start_val, const void* user_data);

double euler_value (two_doubles_to_double f, double min, double max,
                    int N, double start_val, const void* user_data);

#endif
```

Figure 5.7: C++ header file for Algorithm 2 (iii).

```cpp
#ifndef SIMPLE_TYPES_H
#define SIMPLE_TYPES_H

#include <ostream>

/*
  2D point
 */
class point2d {
public:
  point2d(double _x, double _y) : x(_x), y(_y) {}

  point2d subtract (const point2d &other) const
    { return point2d(x - other.x, y - other.y); }
  point2d add (const point2d &other) const
    { return point2d(x + other.x, y + other.y); }

  double norm2 () const;
  double norm () const;

  double dist_to_numbers (double _x, double _y) const;

  void print (std::ostream &os) const;

  double x, y;
};

double dot_product (const point2d &v, const point2d &w);

/* Rectangle */
class rect {
public:
  rect (double x, double y, double w, double h)
    : x(x), y(y), w(w), h(h) {}

  double x, y, w, h;
};


#endif
```

Figure 5.8: C++ header file for Algorithm 2 (iv).

```cpp
#ifndef SURFACE_H
#define SURFACE_H

#include "function2d.h"
#include <pthread.h>
#include <vector>
#include <exception>
#include <ostream>
#include <string>
#include <stdexcept>

typedef std::vector<std::vector<bool> > bitmap;
typedef std::vector<point2d> trace;

enum simulation_constant {
  OMEGA, OMEGA1, OMEGA2, MU, EPSILON, SLENGTH,
  CELLSIZE, THETA_STEPSIZE,
  GREEN_FUNC_SAMPLES, NEWTON_STEPS,

  SIMULATION_CONSTANTS_LENGTH
};

class invalid_config : public std::runtime_error {
public:
  invalid_config (const std::string &str) : std::runtime_error(str) {}
};

class surface {
public:
  surface (double tmin, double tmax,
           double thetamin, double thetamax);

  surface (const surface& s);

  /*
    destructor
  */
  ~surface ();
```

Figure 5.9: C++ header file for Algorithm 3 (i).

```
/*
  Read in a config file and throw away current contents.
*/
void read_config (std::istream &config, bool in_surface_load=false);

/*
  Read in an existing surface.
 */
void read_surface (std::istream &stream);

/*
  Return true if the surface is not defined at this point. Unless
  you know the mutex lock is held, leave acquire_lock true.
*/
bool red_block (double t, double theta,
                bool acquire_lock=true);

/*
  Return whether there's a point for the next rho that we've already
  calculated in the box containing (t, theta). Unless you know the
  mutex lock is held, leave acquire_lock true.
*/
bool occupied (double t, double theta,
               bool acquire_lock=true);

/*
  Return a simulation constant by name
*/
double constant (simulation_constant name) const;

/* Return the height of the surface at the given point */
double height (double t, double theta, bool acquire_lock=true);

point2d revert_to_vw(double theta, double r, double t);

/* Calculate G(t,s) for the given theta */
function2d green_function (const function &theta);

function NewtonMethod(const function &th);

function graph_integrator (const function &theta);
```

Figure 5.10: C++ header file for Algorithm 3 (ii).

```cpp
/* To start the newton step, let r(t) = rho(t,theta(t)). */
function initial_r (const function &theta);

/* Set next_red_blocks and occupancies to reflect a theta that ain't
 * going to work. */
void invalidate_trace (const function &theta, bool acquire_lock=false);

/* Invalidate the bit of a trace that is no use. */
void invalidate_trace_end (const function &theta, double min_valid);

/* Get the next trace to do, and then run Newtons method on it, then
   store the value of the new rho at the calculated points */
void do_next_trace ();

/* Work out the fraction of the surface that's filled with traces so
 * far (out of the non-red stuff). */
double fraction_done ();

/* Work out the fraction of the surface that's been marked as red. */
double fraction_red ();

/* Print a list of red blocks in the format j i to the stream */
void output_red_blocks (std::ostream &os);

/* Print a list of config parameters in the format NAME # to the stream */
void output_config (std::ostream &os) const;

/* Print the new values for rho blocks to the stream in the format
   j i rho(t(j),th(i))
*/
void output_new_rho (std::ostream &os, std::ostream *poutrhostream,
                     std::ostream *pdiffstream, std::ostream *poutvwstream);
```

Figure 5.11: C++ header file for Algorithm 3 (iii).

```
/*
  Constants
*/
double constants[SIMULATION_CONSTANTS_LENGTH];
double constants_mins[SIMULATION_CONSTANTS_LENGTH];
double constants_maxes[SIMULATION_CONSTANTS_LENGTH];
std::string constant_names[SIMULATION_CONSTANTS_LENGTH];

void initialise_default_constants ();
void make_bitmaps (double tmin, double tmax,
                   double thetamin, double thetamax,
                   bool check_block_dims);

void read_red_blocks (std::istream &stream);
void read_rho (std::istream &stream);
void read_polar (std::istream &stream);

/* Calculate the next place to start a theta trace to find an
 * unknown bit of the next rho! Call with mutex held. */
point2d next_theta_start () const;

/* Find the longest possible theta trace starting at (t0,
 * theta0). Call this with the mutex lock held. */
function theta_trace (double t0, double theta0, bool *red_to_left);

function forward_theta_trace (double t0, double theta0, bool *red_to_left);

/* Find the next valid theta trace.  */
function next_theta_trace (bool *red_to_left);

/* Find the next theta trace, then mark it as done so that another
 * thread doesn't do the same work.
 *
 * Set *red_to_left to true if we stop due to undefined rho to our
 * left.
 */
function assign_theta_trace (bool *red_to_left);

/* Store the calculated value of the new rho at a given point. */
void store_trace_values (function &r, function &th);
```

Figure 5.12: C++ header file for Algorithm 3 (iv).

```cpp
void set_block (double t, double theta, bitmap &blocks);
void set_next_red_block (double t, double theta, bool acquire_lock=false);
void set_occupied (double t, double theta,
                   bool take_mutex=true);

/* Check that (t,theta) is in the domain of definition. If it's
   outside of the bounding box by a little bit, clamp it. If it's miles
   out, throw an out_of_range exception */
void fuzzy_clamp (double *t, double *theta) const;

unsigned int count_red ();
unsigned int count_occupied ();

/* Set occupancies for theta. Call with mutex lock held. */
void mark_trace_done (const function &theta);

/* Find the leftmost non-red block. */
unsigned int leftmost_non_red () const;

void initialise_surface_to (double x);
void normalise_samples_sum_and_count();
void interpolate_samples_sum();

/*
  Info needed at the start of a T run.
*/
double tmin, tmax;
double thetamin, thetamax;



unsigned int block_rows, block_cols;

function2d rho;

//s:
coord param;

forcing poisson;
```

Figure 5.13: C++ header file for Algorithm 3 (v).

```cpp
  // A mutex controlling access to the bitmaps: red_blocks,
  // next_red_blocks and occupancies.
  // pthread_mutex_t bitmap_mutex;

  ////////////////// The rest are protected by bitmap_mutex //////////////////

  // red_blocks is points where we don't currently know rho.
  bitmap red_blocks;

  // next_red_blocks is points where (due to theta trajectories
  // falling out) we know we won't know rho next time.
  bitmap next_red_blocks;

  // If a block in occupancies is true, then either we've already
  // calculated the next r in that block or we've convinced ourselves
  // that we can't (see next_red_blocks).
  bitmap occupancies;

  // Here we're going to store samples that we've computed which
  // should count towards the final answer. The last step will be to
  // divide sample_sum pointwise by sample_count to get the new rho,
  // which we'll output.
  std::vector<std::vector<double> > samples_sum;
  std::vector<std::vector<unsigned int> > samples_count;
};

/* This only takes a surface for the constants */
double R (double theta, double r, double t,
          surface &surf);

class enough_traces : public std::exception {};

#endif
```

Figure 5.14: C++ header file for Algorithm 3 (vi).

5.2 A simple 2–D oscillator

We will numerically study a simple 2–D linearly attracting oscillator and its response to various time–dependent forcing. If the forcing is not too large we can apply Theorem 5.1.1 and see that the oscillator remains oscillating in the sense that there is an invariant cylinder in the time–extended space. We will compute the cylinder using our method and the Graph Transform method outlined in Chapter 3. Then by varying the parameters in the forcing, we will investigate the type of dynamics occurring on the cylinder. Let us now give the equation of the oscillator,

$$\dot{r} = -\mu r$$
$$\dot{\varphi} = \Omega \qquad\qquad (5.3)$$

with $\Omega \in \mathbb{R}$, $r \in \mathbb{R}$ and $\varphi \in M = \mathbb{R}/2\pi\mathbb{Z}$. It represents a $2 - D$ normally hyperbolic limit cycle with intrinsic angular frequency $\Omega \in \mathbb{R}$ and attraction rate $\mu > 0$, i.e. the Floquet exponent is $-\mu$. The limit cycle is given by the cylinder $\rho_0 \equiv 0$ in the time–extended space $\mathbb{R}/2\pi\mathbb{Z} \times \mathbb{R} \times \mathbb{R}$.

Let us consider the following forcing on the oscillator

$$\dot{r} = -\mu r + 0.1\varepsilon \sin(0.1(r - \varphi + \omega_1 t)) \qquad\qquad (5.4)$$
$$\dot{\varphi} = \Omega + \varepsilon \cos(\varphi - r - \omega_2 t) \qquad\qquad (5.5)$$

which represents an external forcing of angular frequency $\omega_1 \in \mathbb{R}$ in the r direction and $\omega_2 \in \mathbb{R}$ in the φ direction. The forcing is quasi–periodic if ω_1/ω_2 is irrational, else it is periodic. To allow more interesting dynamics to occur on the invariant surface while ensuring its existence, the amplitude of the forcing in the φ direction is specifically made larger than that in the r direction (by a factor of 10). The factor of 0.1 inside the sinusoid ensures a slower oscillation in the r coordinate which is only for aesthetic purposes when displaying the invariant surface and the dynamic on it which is in the φ direction.

Note that for weak periodic and quasi–periodic forcing the standard normally hyperbolicity theory for compact invariant manifolds can be used to obtain the perturbed invariant manifold. This can be done by extending the forced system to a compact n-torus (with an appropriately n) to obtain an autonomous system which is a perturbation of a normally hyperbolic system. For example, the

system (5.4) is equivalent to the following extended autonomous system

$$
\begin{aligned}
\dot{r} &= -\mu r + 0.1\varepsilon \sin(0.1(r - \varphi + \varphi_1)) \\
\dot{\varphi} &= \Omega + \varepsilon \cos(\varphi - r - \varphi_2) \\
\dot{\varphi}_1 &= \omega_1 \\
\dot{\varphi}_2 &= \omega_2.
\end{aligned}
\tag{5.6}
$$

with $(\varphi_1, \varphi_2) \in \mathbb{T}^2$. When $\varepsilon = 0$, the system (5.6) possess a compact attracting invariant manifold given by $\tilde{M} = \{r = 0\} \cong S^1 \times S^1 \times S^1$. Thus when $\varepsilon > 0$ is small, then since (5.6) is a small perturbation of a normally hyperbolic system, $\tilde{M}$ persists due to the standard theory of normal hyperbolicity for compact manifolds. For the purpose of demonstration we will use our method to compute the perturbed manifold.

For ease of implementation we shall take a coordinate system that is relative to the intrinsic frequency of the oscillator. In particular we take $\theta = \varphi - \Omega t$ so that the forced equation is of the form

$$
\dot{r} = -\mu r + 0.1\varepsilon \sin(0.1(r - \theta + (\omega_1 - \Omega)t)) \tag{5.7}
$$

$$
\dot{\theta} = \varepsilon \cos(\theta - r + (\Omega - \omega_2)t) \tag{5.8}
$$

which will ensure a slower deviation along the θ coordinate for small ε, i.e. the trajectories stay within a given rectangular grid for a longer time.

We will numerically investigate how the dynamics change by varying ω_2 and fix the other parameters as follows

$$
\mu = 1, \quad \varepsilon = 0.1, \quad \Omega = 1, \quad \omega_1 = -1.02. \tag{5.9}
$$

Note that more complicated forcing can be considered. For example, we can allow ε to depend on time to model the fluctuation of the amplitude of the forcing. But we shall restrict ourselves to the simple case here to highlight the main ideas.

5.2.1 Contraction rate of T and $\hat{T}$

To investigate the contraction rates of the two methods we will take $\omega_2 = 1.2$. To estimate the contraction rate of T of Theorem 1 we consider the following initial surfaces $\rho_1 = \{r = 10\}$ and $\rho_2 = \{r = -10\}$ and infer its contraction rate c_T given by

$$|T\rho_1 - T\rho_2| \le c_T |\rho_1 - \rho_2|. \tag{5.10}$$

Similarly for $\hat{T}$ of Theorem 3.2.3 and its contraction rate $c_{\hat{T}}$.

From the numerical results, see the 3–D Figure 5.15 (cross your eyes till the two red dots meet), we have $|T\rho_1 - T\rho_2| = 1.5 \times 10^{-4}$ while $|\rho_1 - \rho_2| = 20$, thus we have an estimate of

$$c_T = 7.5 \times 10^{-6}. \tag{5.11}$$

In the case of $\hat{T}$, from Figure 5.16 we can obtain a similar estimate

$$c_{\hat{T}} = 7.5 \times 10^{-6}. \tag{5.12}$$

See Table 5.1 for a summary of these results where quantitative details used for each of the Algorithms A and B are also included for reference.

	T	$\hat{T}$
Contraction rate	7.5×10^{-5}	7.5×10^{-5}
ρ_1	$\{r = 10\}$	$\{r = 10\}$
ρ_2	$\{r = -10\}$	$\{r = -10\}$
$|\rho_1 - \rho_2|$	20	20
$|T\rho_1 - T\rho_2|$	1.5×10^{-4}	1.5×10^{-4}
grid area $(t \times \theta)$	$[-30, 0] \times [0, 2\pi]$	$[-30, 0] \times [0, 2\pi]$
grid cell $= |\Delta t| \times |\Delta\theta|$	0.02×0.04	0.02×0.04
s^*	10.00001	10.00001
dt	0.005	0.005
δt	0.003	0.003
Newton error	0.05	$-$
Approx. run time for first iterate	35 mins	33 mins

Table 5.1: Results from Algorithm A and B where two surfaces are iterated. Quantitative details of both algorithms are also included.

5.2.2 Iterates of T and $\hat{T}$

We check how close T and $\hat{T}$ estimates the invariant manifold by taking just the first iterate of $\rho_0 \equiv 0$.

From the numerical results, see the 3–D Figure 5.17, we have

$$|T\rho_0 - T^2\rho_0| = 3 \times 10^{-5}, \tag{5.13}$$

which is very good. If we were to estimate the contraction rate by using the iterates we would obtain $c_T = 3 \times 10^{-3}$ (since $||T\rho_0 - \rho_0|| = 0.01$). Similar values were obtained for $\hat{T}$ as shown in Figure 5.18. Note that it is not desirable to use successive iterates to estimate the contraction rate because the difference between successive surfaces are so small that they are of the order of the size of numerical noise as indicated in Figure 5.17 B and Figure 5.18 (Right). The noise could be minimised by using a finer grid or by removing large deviations which due to time constraint was not implemented. Thus the first iterate of ρ_0 is already a good estimate for the invariant manifold.

	T	$\hat{T}$
Contraction rate	3×10^{-3}	3×10^{-3}
ρ_0	$\{r = 0\}$	$\{r = 0\}$
$|\rho_0 - T\rho_0|$	0.01	0.01
$|T\rho_0 - T^2\rho_0|$	3×10^{-5}	3×10^{-5}
grid area $(t \times \theta)$	$[-30, 0] \times [0, 2\pi]$	$[-30, 0] \times [0, 2\pi]$
grid cell $= |\Delta t| \times |\Delta\theta|$	0.008×0.04	0.008×0.039
s^*	10.00001	10.00001
dt	0.003	0.003
δt	0.002	0.002
Newton error	0.05	−
Approx. run time in first iterate	35 mins	33 mins
Approx. run time in second iterate	47 mins	46 mins

Table 5.2: Results from Algorithm A and B where two iterates of a surface was investigated. Quantitative details of both algorithms are also included.

5.2.3 Dynamics on the invariant manifold

We investigated how ω_2 affects the dynamics on the invariant manifold, which, by the previous section, is reasonably estimated by $T\rho_0$ where $\rho_0 \equiv 0$. By varying ω_2 we saw that the dynamic on the invariant manifold can change dramatically. In particular, we saw in Figure 5.19 that there is no collapsing of dynamic when $|\Omega - \omega_2| = 0.2$ but we found that collapsing of dynamic appears for $|\Omega - \omega_2| < 0.1$, see Figure 5.20 for the case where $\omega_2 = 1.01$. This essentially says that the oscillator can be slaved by the forcing if their frequency difference is less than 0.1. See Table 5.3 for a summary of these results.

Frequency difference $|\Omega - \omega_2|$	Dynamics on cylinder
> 0.1	no collapse of dynamics
< 0.1	collapsing of dynamics exist

Table 5.3: Summary of results from varying ω_2

5.2.4 Numerical results

To view in 3–D, hold the figures at arm's length then cross your eyes until the two red dots meet horizontally. Otherwise, ignore the pictures in the right column for 2–D images.

3D effect: cross your eyes until the two red circles meet.
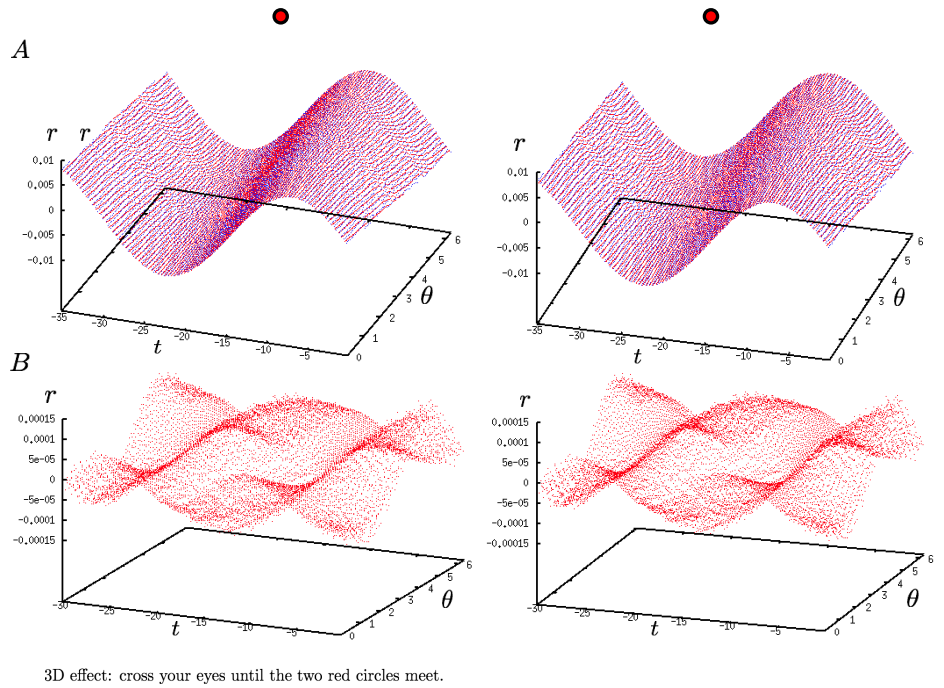
Figure 5.15: A: red – $T\rho_1$, blue – $T\rho_2$. B: Difference between $T\rho_1$ and $T\rho_2$ where $\rho_1 \equiv 10$ and $\rho_2 \equiv -10$.
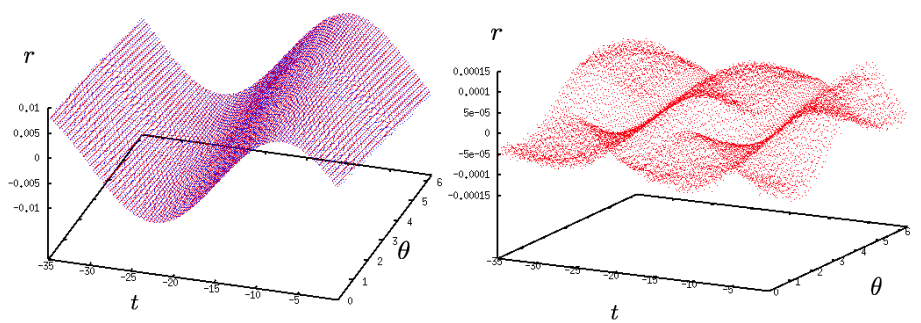

Figure 5.16: Numerical results from implementing the Graph Transform method – $\hat{T}$. Left: red – $\hat{T}\rho_1$, blue – $\hat{T}\rho_2$. Right: Difference between $\hat{T}\rho_1$ and $\hat{T}\rho_2$ where $\rho_1 \equiv 10$ and $\rho_2 \equiv -10$.

3D effect: cross your eyes until the two red circles meet.
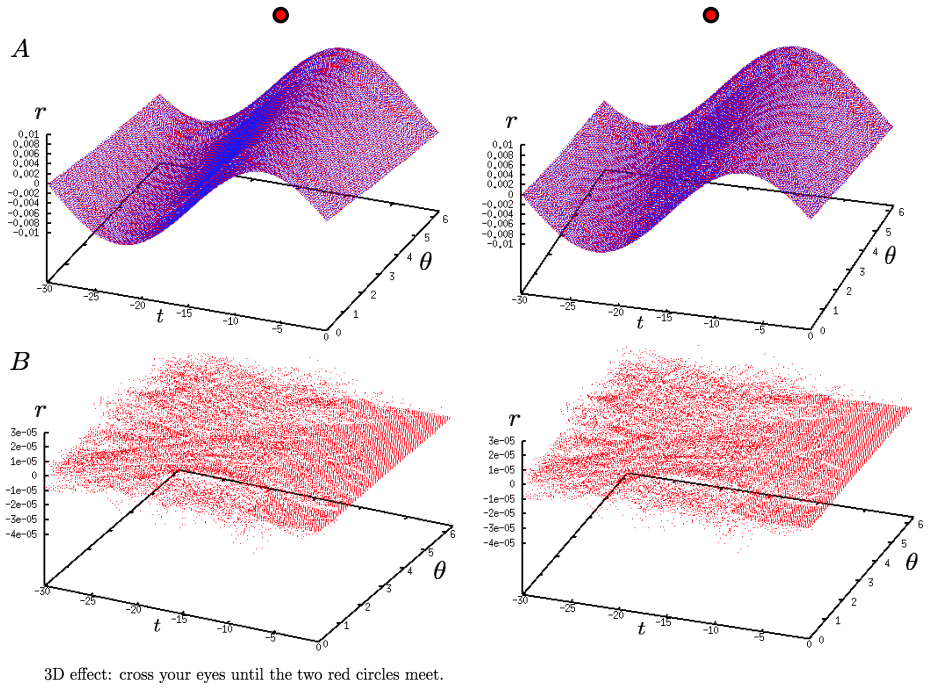
Figure 5.17: A: red – $T\rho_0$, blue – $T^2\rho_0$. B: Difference between $T\rho_0$ and $T^2\rho_0$ where $\rho_0 \equiv 0$.
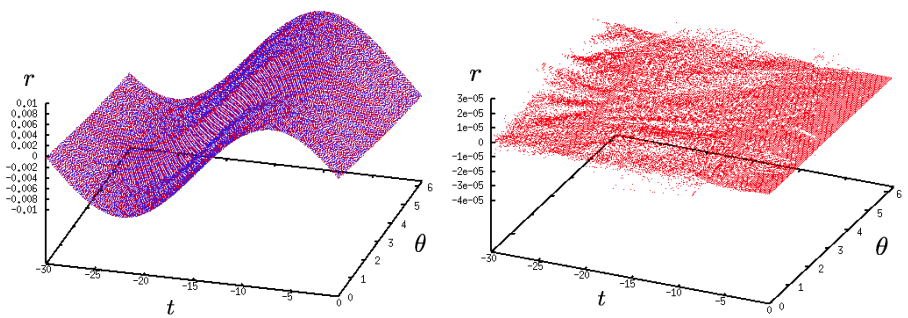
Figure 5.18: Numerical results from implementing the Graph Transform method – $\hat{T}$. Left: red – $\hat{T}\rho_0$, blue – $\hat{T}^2\rho_0$. Right: Difference between $\hat{T}\rho_0$ and $\hat{T}^2\rho_0$ where $\rho_0 \equiv 0$.
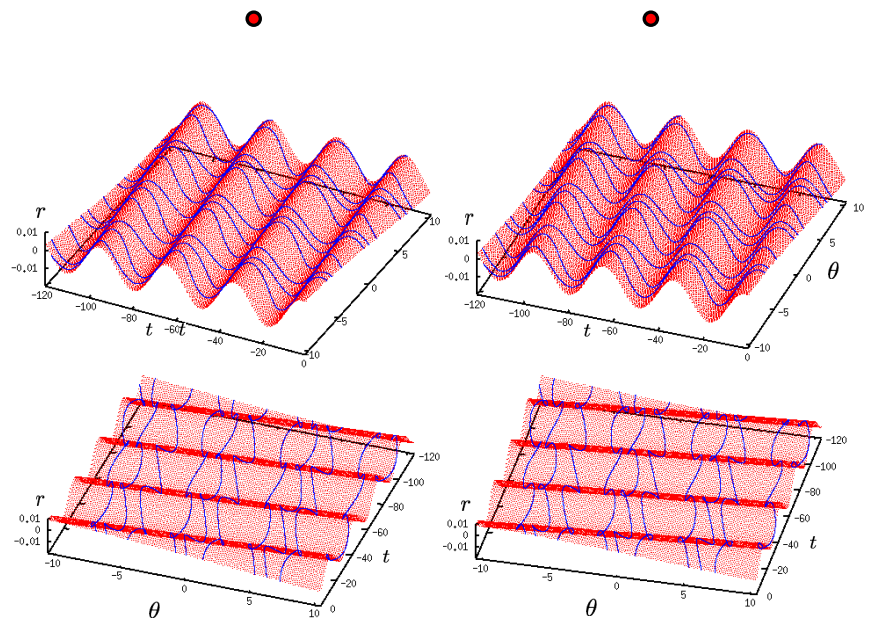
3D effect: cross your eyes until the two dots meet.

Figure 5.19: No synchronisation on the invariant manifold.
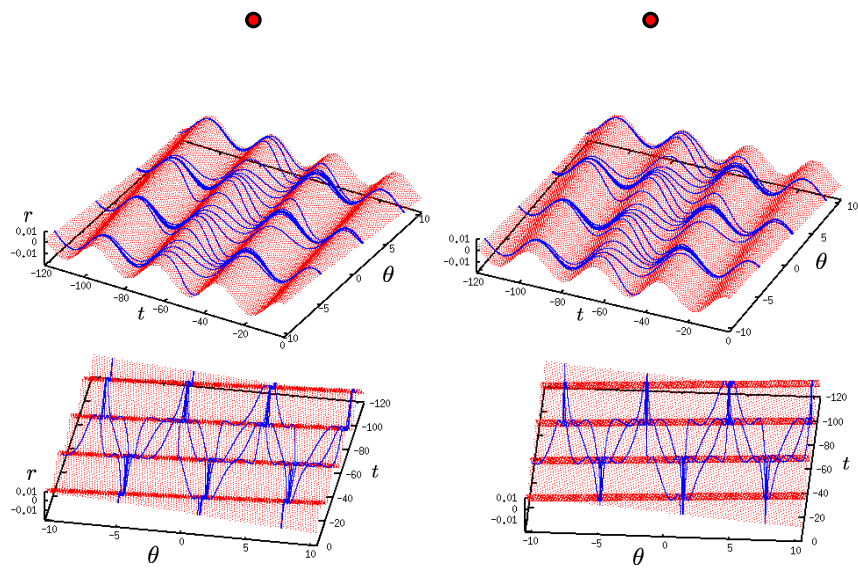
3D effect: cross your eyes until the two dots meet.

Figure 5.20: Synchronisation on the invariant manifold.

Chapter 6

The Morris–Lecar model

The aim of this section is to evaluate the methods developed in the previous chapters in a biophysically realistic model of a single forced oscillator, namely the Morris–Lecar oscillator. The Morris–Lecar model (ML81) was developed to describe the voltage oscillations in giant barnacle muscle fibres. However, there is an equivalent model which is used as a reduced neuronal model that describes the voltage dynamic of a neuron which incorporates a fast sodium and a slow potassium channel. The model is biophysically relevant, exhibits many properties and since it is only 2–D it is a very popular model. As we will see, the model can possess a linearly attracting limit cycle for certain parameter regimes. Thus we can use the method we have developed to explore the response of the oscillator to certain forcing. In particular we will find periodic, two–frequency–periodic and modified Poisson spike train inputs that will enslave the oscillator to demonstrate that synchronisation can take place. However, synchronisation does not always take place and in a physiological setting this might be a desirable property.

6.1   Equations and parameters

The equation we will investigate here can be found in (PKS08)

$$C\frac{dV}{dt} = I_{stim} - \bar{g}_{fast}m_\infty(V)(V - E_{Na}) - \bar{g}_{slow}(V - E_K)w - g_{leak}(V - E_{leak}) + f(t)$$

$$\frac{dw}{dt} = \phi_w \frac{w_\infty(V) - w}{\tau_w(V)} \qquad\qquad (6.1)$$

where

$$m_\infty(V) = \frac{1}{2}\left(1 + \tanh\left(\frac{V - \beta_m}{\gamma_m}\right)\right)$$

$$w_\infty(V) = \frac{1}{2}\left(1 + \tanh\left(\frac{V - \beta_w}{\gamma_w}\right)\right)$$

$$\tau_w(V) = \frac{1}{\cosh(\frac{V - \beta_w}{2\gamma_w})} \tag{6.2}$$

with parameters

$$C = 2\mu F/cm^2$$

$$\phi_w = 0.15$$

$$\bar{g}_{fast} = 20 \; mS/cm^2$$

$$\bar{g}_{slow} = 20 \; mS/cm^2$$

$$g_{leak} = 2 \; mS/cm^2$$

$$E_{Na} = 50 \; mV$$

$$E_K = -100 \; mV$$

$$E_{leak} = -70 \; mV$$

$$\beta_m = -1.2 \; mV$$

$$\gamma_m = 18 \; mV$$

$$\gamma_w = 10 \; mV$$

The fast activation variable V represents the voltage of the neuron cell membrane measured in mV while w represents some slow recovery variable which is dimensionless. We will investigate the effect of various forcing functions $f(t)$. In the absence of the forcing f, varying the parameter β_w gives rise to class 1, 2 and 3 excitability. These classes are based on the type of bifurcation the model undergoes in the $I - V$ plane where the stimulus current I_{stim} is the bifurcation parameter. See (Izh07). In particular, for $\beta_w = 0$ the model undergoes a saddle node on invariant circle bifurcation where there is a pair of fixed points lying on an invariant circle, one stable and the other unstable, for $I_{stim} < 40\mu A/cm^2$. As I_{stim} increases to $40\mu A/cm^2$ the pair of fixed points meet and become one saddle fixed point on the circle which disappears for $I_{stim} > 40\mu A/cm^2$ where a linearly attracting limit cycle is formed. See Figure 2 in (PKS08). This is the simplest nontrivial normally hyperbolic invariant manifold. This gives rise to what is known as "tonic spiking" in physiological terminology. See Figure 6.1

for one spike. For our numerical implementation we will take

$$\beta_w = 0 \; mV$$

$$I_{stim} = 70 \; \mu A/cm^2$$

which gives a limit cycle, denoted by γ, with approximate period $T = 5.59992 \; ms$. Since γ is normally hyperbolic it possesses invariant leaves a.k.a. isochrons
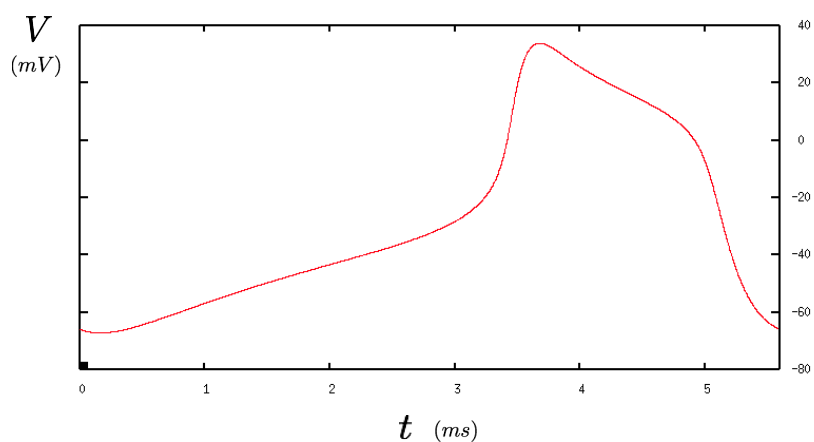

Figure 6.1: Time evolution of voltage for one cycle on γ i.e. a "spike".

(Guc75), (Win80), that foliates a neighbourhood of γ. Specifically, a leaf based at $p \in \gamma$ is given by

$$l(p) = \{x \in \mathbb{R}^2 \; : \; |\varphi(t;p) - \varphi(t;x)| \to 0 \text{ as } t \to \infty\} \tag{6.3}$$

where $\varphi(t;z)$ denotes the trajectory of the (V,w) system (6.1) starting from $z \in \mathbb{R}^2$ at $t_0 = 0$. We can see that $l(\varphi(t;p)) = \varphi(t;l(p))$ which shows invariance. Note that $l(p)$ is transverse to γ at p and l varies as smoothly as equation (6.1).

For simplicity we may write the equation (6.1) as

$$(\dot{V}, \dot{w}) = F(V, w) = (F_1(V, w), F_2(V, w)), \tag{6.4}$$

and may set $x = (V, w)$.

6.2 New coordinate system

We can use the invariant leaves to define a new coordinate system, in particular the linearisation of the leaves at γ gives a transverse bundle to γ which can be easily implemented by using the adjoint method which is presented next. If desired, higher order approximation of isochrons can be obtained (SD09).

6.2.1 Adjoint method

The adjoint method simply solves an adjoint equation for a periodic solution and then taking its orthogonal, gives the linearised isochrons. Let us explain why the adjoint solution relates to the linearised isochrons in this way (BMH04).

Fix a point $p_0 \in \gamma$, then we can define the phase map $\Phi' : \gamma \to \mathbb{R}/T\mathbb{Z}$ by

$\Phi'(p) = \phi = \{$ Time it takes for the trajectory to reach $p \in \gamma$ starting from $p_0 \in \gamma\}$.

But this can be extended to Φ defined on a neighborhood $N(\gamma)$ of γ by taking $\Phi(x) := \Phi'(p)$ for $x \in l(p) \cap N(\gamma)$ which means x and p have the same asymptotic phase. So for each $p \in \gamma$, $l(p)$ is the contours of Φ. More specifically, $l(p) = \Phi^{-1}(c)$ for some constant c. Thus the linearisation of $l(p)$ at $p \in \gamma$ is orthogonal to $\nabla_x \Phi(p)$.

Now if $\gamma(t)$ is a trajectory lying on the limit cycle, γ, then $\nabla_x \Phi(\gamma(t))$ is T periodic and satisfies the following adjoint equation (BMH04),

$$\dot{z}(t) = -[DF(\gamma(t))]^T z(t). \tag{6.5}$$

Note that $\nabla_x \Phi(\gamma(t))$ has a constraint which is given by

$$\nabla_x \Phi(\gamma(t)) \cdot F(\gamma(t)) = 1 \tag{6.6}$$

which arises from the fact that $\dot{\phi} = 1$. So to obtain $\nabla_x \Phi(\gamma(t))$ we simply solve (6.5) for a periodic solution and normalise it by the constraint (6.6) for a fixed $t = 0$, say. However, we are only interested in the orthogonal of $\nabla_x \Phi(\gamma(t))$ so we do not need to impose this constraint. $\nabla_x \Phi(\gamma(t))$ is commonly known as the instantaneous Phase Response Curve or iPRC. For examples, see (BMH04), (Izh07) and (EK84).

The adjoint equation has the opposite stability of γ, so in practice to obtain an approximation of the periodic solution of (6.5) we start with any initial value

then integrate backwards in time and allow a transient length of time to pass. Then take a time length of T of the integrated solution as an approximation to a periodic solution. Taking the orthogonal of this solution gives the linearised isochrons at each point $p \in \gamma$ which we denote by $I(p)$.

See Figure 6.2 for a numerical approximation of γ and some linearised isochrons on it given by $p + I(p)$ where $p \in \gamma$. Note that there is a linearised isochron for every point on γ and the figure only shows a subset of linearised isochrons separated by a constant time length. It can be seen from the figure that the oscillator is faster on the top of γ compared to the bottom left.
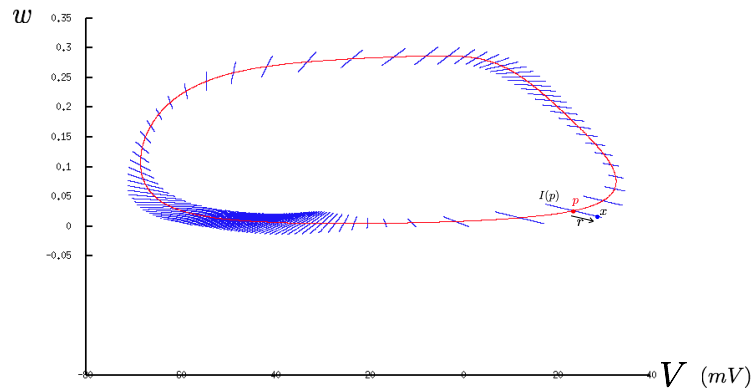
Figure 6.2: The limit cycle γ with some linearised isochrons at γ.

6.2.2 Coordinate change

For ease of numerical implementation, we wish to find a coordinate change using the linearised isochrons, rather than the actual isochrons, such that any perturbation of the time–extended (V, w) system (6.1) can be written in the form of

$$
\begin{aligned}
\dot{r} &= R(\theta, r, t) \\
\dot{\theta} &= \Theta(\theta, r, t) \\
\dot{t} &= 1.
\end{aligned}
$$

Take the phase map Φ' defined above and let us extend it using the linearised isochron, rather than the actual isochron, to $\bar{\Phi} : N(\gamma) \to \mathbb{R}/T\mathbb{Z} \times \mathbb{R}$ defined by $\bar{\Phi}(x) = \Phi'(p)$ where $x \in (p + I(p)) \cap N(\gamma)$. Then let us define $P' : N(\gamma) \to \mathbb{R}/T\mathbb{Z} \times \mathbb{R}$ by

$$P'(x) = (\phi, r) := (\bar{\Phi}(x), x - p) \text{ for } x \in (p + I(p)) \cap N(\gamma). \qquad (6.7)$$

See Figure 6.2 for a sketch of r. However, $\dot{\phi} = 1$ will cause too much deviation in the phase direction, so for ease of implementation, we take a further change of coordinate in the time–extended space $P : N(\gamma) \times \mathbb{R} \to \mathbb{R}/T\mathbb{Z} \times \mathbb{R} \times \mathbb{R}$ defined by

$$P(x, t) = (\theta, r, t) = (\phi - t, r, t). \qquad (6.8)$$

Thus the time–extended (V, w) system (6.1) under this coordinate system is given by

$$\dot{\theta} = 0$$
$$\dot{r} = g(\theta, r)$$
$$\dot{t} = 1$$

for some g depending on the P.

Note that unit for θ and t is ms and r is dimensionless.

6.2.3   Perturbed Morris–Lecar system in the new coordinate system

Now if the time–extended (V, w) system is perturbed, for example, it is forced, with the resulting system given by $(\dot{x}, \dot{t}) = \tilde{F}(x, t)$, then under the new coordinate system it is of the form

$$\dot{\theta} = \Theta(\theta, r, t)$$
$$\dot{r} = R(\theta, r, t)$$
$$\dot{t} = 1,$$

which is given by

$$(\dot{\theta}, \dot{r}, \dot{t}) = [D_{Q(\theta, r, t)} P] \cdot \tilde{F}(Q(\theta, r, t)) \qquad (6.9)$$

with $Q = P^{-1}$. The linearised equation in the new coordinate system is of the form

$$\delta\dot\theta = \Theta_\theta\delta\theta + \Theta_r\delta r + \Theta_t\delta t$$
$$\delta\dot r = R_\theta\delta\theta + R_r\delta r + R_t\delta t$$
$$\delta\dot t = 0, \qquad\qquad (6.10)$$

which is given by

$$(\delta\dot r, \delta\dot r, \delta\dot t) = [D_{Q(\theta,r,t)}P] \cdot [D_{Q(\theta,r,t)}\tilde F] \cdot [D_{(\theta,r,t)}Q](\delta\theta, \delta r, \delta t). \qquad (6.11)$$

Note that only the R_r term will be required in the implementation so we do not need to compute the whole of (6.11).

Practically, it is easier to evaluate the function Q rather than P. So to estimate the Jacobian DP, we can make use of the relation $D_{Q(\theta,r,t)}P = [D_{(\theta,r,t)}Q]^{-1}$ and it is easier to estimate DQ.

Note that since the linearised isochrons can overlap, for example, possibly at $(V, w) = (20, 0.1)$ see Figure 6.2, the amplitude of the forcing f in equation (6.1) must be restricted to a certain magnitude otherwise the coordinate change becomes singular. A trial and error method can be employed to determine the range of valid magnitude for f. If we set $f = A$ where A is a constant we take it to be a valid amplitude if the perturbed limit cycle due to this constant forcing does not lie beyond the overlaps of the linear isochrons. By increasing $|A|$ from 0 and following the previous step we can determine a range of valid amplitude A.

6.3 Algorithms adapted to the new coordinate system

To numerically estimate the invariant cylinder for the forced Morris–Lecar system we need to adapt the above algorithms to the time–extended (V, w) coordinate system. In particular, we need to consider the evaluation of $R(\theta, r, t)$, $R_r(\theta, r, t)$ and $\Theta(\theta, r, t)$ in the algorithms whenever they are called. For these, we need to compute $Q(\theta, r, t)$ and numerically estimate the Jacobian $[D_{(\theta,r,t)}Q]^{-1} = D_{Q(\theta,r,t)}P$ and then evaluate for the relevant components of (6.9) and (6.11) using the given forced equation $\tilde F$ and its derivative $D\tilde F$.

Thus the key step is in computing $Q(\theta, r, t)$ which is straightforward. The adjoint method can be used to output an array containing time (phase ϕ) versus linearised isochrons, while the limit cycle can also be stored as an array containing time versus the (V, w) coordinate of γ. Thus given (θ, r, t), it is easy to work out the corresponding (V, w, t) coordinate given the two arrays of data, see Figure 6.2. Note that the arrays can be produced in a separate algorithm and then loaded into **Algorithm 3** where the function Q and the above calculations can be appropriately added. There should be an extra output of **Algorithm 3** in the (V, W, t) coordinate (by applying Q) to give a cylinder.

6.3.1 Rescaling w

As seen in Figure 6.2, γ is squashed in the w–direction. Thus in the numerical implementations we will rescale this variable so that width and height of the limit cycle has similar order. We will rescale by $w \rightarrow 400w$, i.e. use the variable u where $w = 400u$ and relabel $u = w$.

6.4 Periodic, two–frequency–periodic and modified Poisson spike train inputs

We will consider the forced Morris–Lecar neuron by a forcing, f, in the V direction given by

$$\dot{V} = F_1(V, w) + f(t)$$
$$\dot{w} = F_2(V, w), \tag{6.12}$$

where f is periodic, two–frequency–periodic or a modified Poisson spike train. We note that the method can also deal with forcing that depends on the state V and w which may be more realistic.

6.4.1 Periodic forcing

Here we take

$$f(t) = 2 + 5\sin((2\pi/T + \omega_1)t) \tag{6.13}$$

where T is the period of the Morris–Lecar oscillator and $\omega_1 = 0.1 \; rad/ms$, representing the frequency difference of the forcing and the neuron.

Contraction rate of T and $\hat{T}$

To estimate the contraction rate we will consider the two initial graphs $\rho_1 \equiv 0$ and $\rho_2 \equiv -20$. From the 3–D Figure 6.4 we have the estimates $|T\rho_1 - T\rho_2| = 0.8$ and $|\rho_1 - \rho_2| = 20$. Thus the contraction rate of T has the estimate

$$c_T = 0.04. \tag{6.14}$$

In the case of $\hat{T}$, from Figure 6.5 we can obtain a similar estimate

$$c_{\hat{T}} = 0.04. \tag{6.15}$$

As we can see in Figure 6.4 A and C, there is a noticeable difference between the invariant cylinders $T\rho_1$ and $T\rho_2$ in both the new coordinate system and the time–extended (V, w) coordinate system. In some region of the cylinder $T\rho_2$ given in blue shown in Figure 6.4 C, we can clearly see red points (from the other cylinder $T\rho_1$) protruding outwardly. Similar observation can be seen for $\hat{T}$ in Figure 6.5 A and C.

	T	$\hat{T}$
Contraction rate	0.04	0.04
ρ_1	$\{r = 0\}$	$\{r = 0\}$
ρ_2	$\{r = 20\}$	$\{r = 20\}$
$|\rho_1 - \rho_2|$	20	20
$|T\rho_1 - T\rho_2|$	0.8	0.8
grid area $(t \times \theta)$	$[-10, 0] \times [0, 2\pi]$	$[-10, 0] \times [0, 2\pi]$
grid cell $= |\Delta t| \times |\Delta \theta|$	0.04×0.04	0.04×0.04
s^*	10.00001	10.00001
dt	0.0125	0.0125
δt	0.01	0.01
Newton error	0.05	–
Approx. run time for first iterate	3 hours	3 hours

Table 6.1: Results from Algorithm A and B where two surfaces are iterated. Quantitative details of both algorithms are also included.

Iterates of T and $\hat{T}$

We check how close T and $\hat{T}$ estimate the invariant manifold by taking just the first iterate of $\rho_1 \equiv 0$.

From the numerical results (see the 3–D Figure 6.6), we have

$$|T\rho_1 - T^2\rho_1| = 0.08. \tag{6.16}$$

So the second iterate of ρ_1 is very close to the first iterate. Furthermore, from eye–inspection of Figure 6.6 C, we can see that the two cylinders $T\rho_1$ and $T^2\rho_1$ in the time–extended (V, w) coordinate system are very close to each other. Similar numerical results were obtained for $\hat{T}$ as seen in Figure 6.7. Thus the first iterate of ρ_0 is a good estimate for the invariant manifold.

	T	$\hat{T}$
ρ_1	$\{r = 0\}$	$\{r = 0\}$
$|T\rho_1 - T^2\rho_1|$	0.08	0.08
grid area $(t \times \theta)$	$[-10, 0] \times [0, 2\pi]$	$[-10, 0] \times [0, 2\pi]$
grid cell $= |\Delta t| \times |\Delta\theta|$	0.08×0.08	0.04×0.04
s^*	10.00001	10.00001
dt	0.0325	0.0125
δt	0.03	0.0041
Newton error	0.05	–
Approx. run time for first iterate	3 hours	3 hours
Approx. run time for second iterate	9 hours	9 hours

Table 6.2: Results from Algorithm A and B where two surfaces are iterated. Quantitative details of both algorithms are also included.

Synchronisation

We searched for a value of ω_1 which causes the collapse of dynamics on the invariant manifold estimated by $T\rho_1$. We found that for $\omega_1 = 0.1\ rad/ms$, synchronisation takes place as is shown in Figure 6.8. Figure 6.8A shows a generic trajectory (purple) starting near the repeller (blue) at $t = -90\ ms$, which significantly deviates away by the time $t = -45\ ms$. However, in Figure 6.8B, the generic trajectory eventually approaches the attractor (red) by the time $t = 0$. In theoretical neuroscience, it may be of interest to depict this in the (V, t) plane as the voltage time series, which is of greater relevance. This is given in Figure 6.8C where the invariant cylinder is also shown.

6.4.2 Two–frequency–periodic forcing

Here we take the forcing to be

$$f(t) = 5\sin((2\pi/T + \omega_1)t) + 3\sin((2\pi/T + \omega_2)t + 1.5) \qquad (6.17)$$

which could represent a combination of two periodic forcings with a phase shift of 1.5. Note that more complicated types of forcing can be considered, for example the amplitudes given by 5 and 3 can be a time–dependent factor or even depend on the states V and w for a more realistic forcing.

Fixing $\omega_2 = -0.12\ rad/ms$, we found that for $|\omega_1| = 0.02\ rad/ms$ synchronisation takes place as depicted in Figure 6.3A. However, synchronisation begins to disappear when we increase to $|\omega_1| = 0.1\ rad/ms$ as shown in Figure 6.3B a generic trajectory (purple) starts from the right hand side of a "saddle node" (red) at time $t = -90\ ms$, which deviates away by time $t = -45\ ms$, which then approaches the "saddle" attractor from the left hand side by time $t = 0\ ms$. See Table 6.3 for a summary of the type of dynamics on the invariant cylinder by varying $|\omega_1|$.

Frequency difference $|\omega_1|$	Dynamics on cylinder
> 0.1	no collapse of dynamics
< 0.1	collapsing of dynamics exist

Table 6.3: Summary of results from varying $|\omega_1|$

6.4.3 Numerical results for periodic forcing

To view in 3–D, hold the figures at arm's length then cross your eyes until the two red dots meet horizontally. Otherwise, ignore the pictures in the right column for 2–D images.
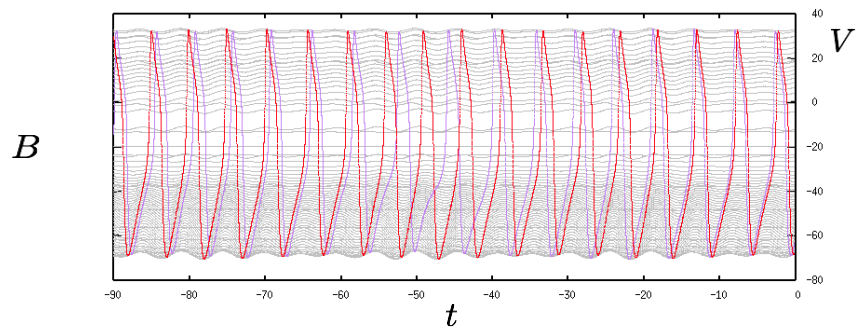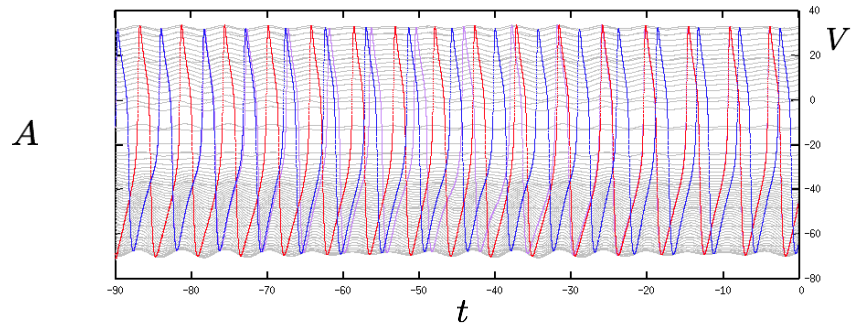
Figure 6.3: A: Synchronisation on the cylinder, blue – repeller, red – attractor, purple – generic trajectory. B: No synchronisation, red – "saddle" attractor, purple– generic trajectory.
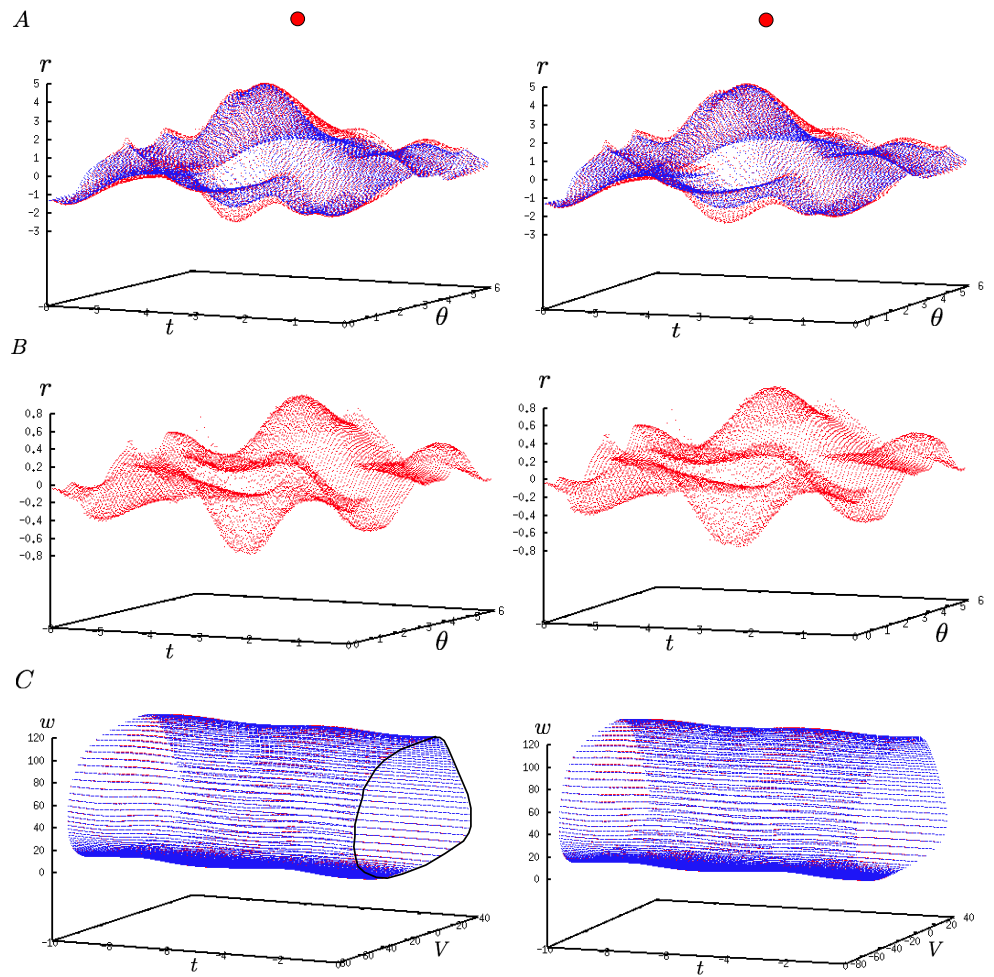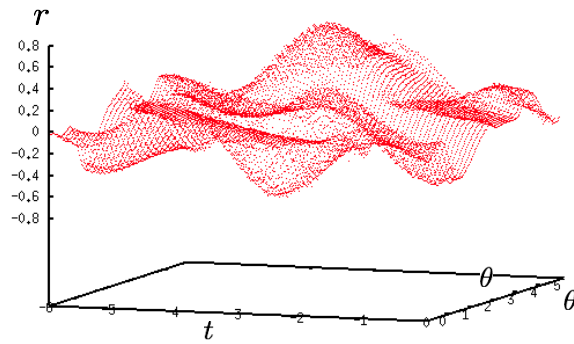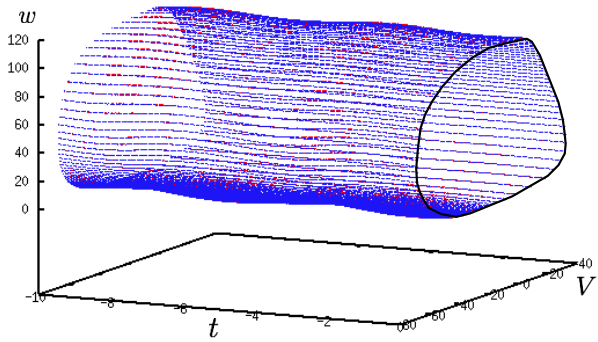
3D effect: cross your eyes until the two red circles meet.

Figure 6.4: A and C: red – $T\rho_1$, blue – $T\rho_2$ (hand drawn black circle in C is a visual aid.) B: Difference between $T\rho_1$ and $T\rho_2$ where $\rho_1 \equiv 0$ and $\rho_2 \equiv -20$.
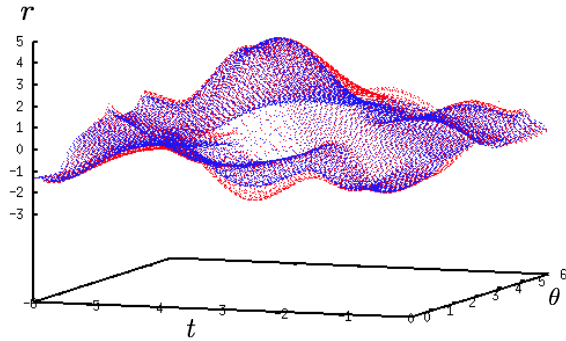
A : red $- \hat{T}\rho_1$, blue $- \hat{T}\rho_2$ where $\rho_1 \equiv 0$ and $\rho_2 \equiv -20$.

B: Difference between $\hat{T}\rho_1$ and $\hat{T}\rho_2$.

C : red $- \hat{T}\rho_1$, blue $- \hat{T}\rho_2$ where $\rho_1 \equiv 0$ and $\rho_2 \equiv -20$.

Figure 6.5: Numerical results from implementing the Graph Transform method $- \hat{T}$ (hand drawn black circle in C is a visual aid).
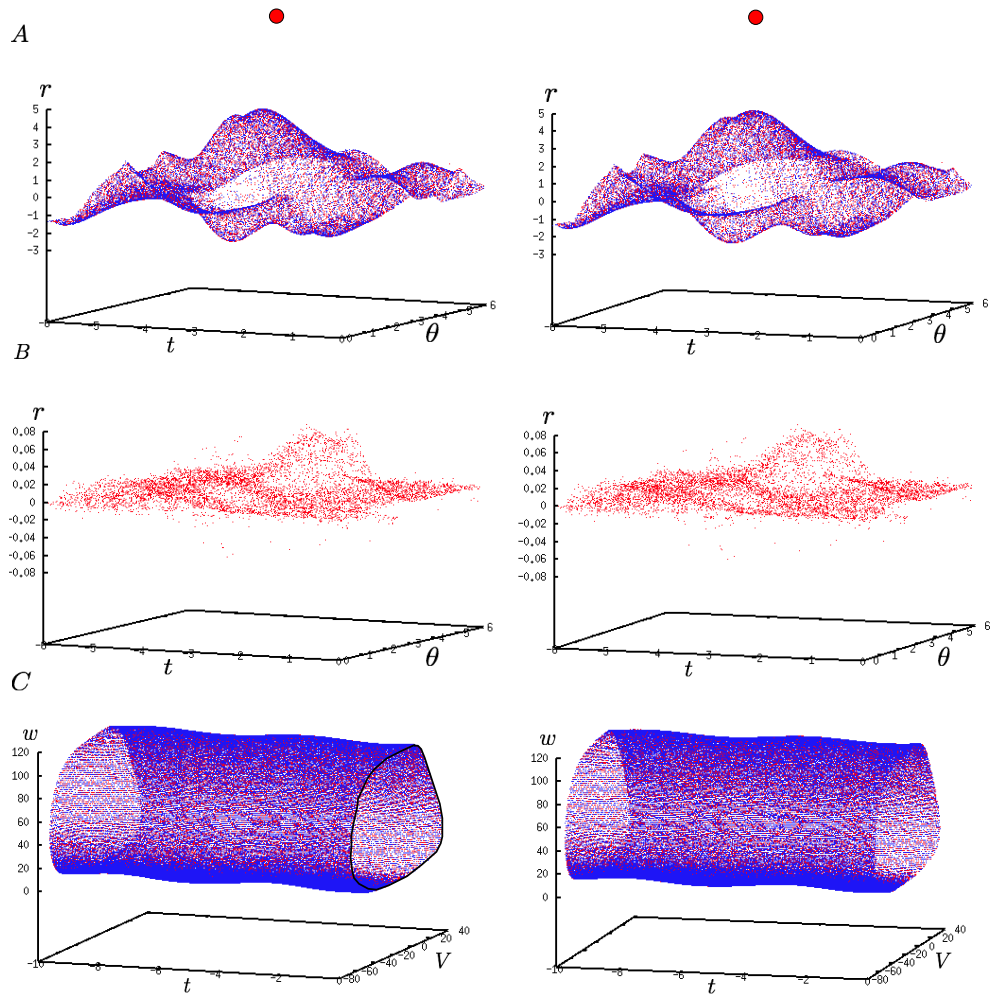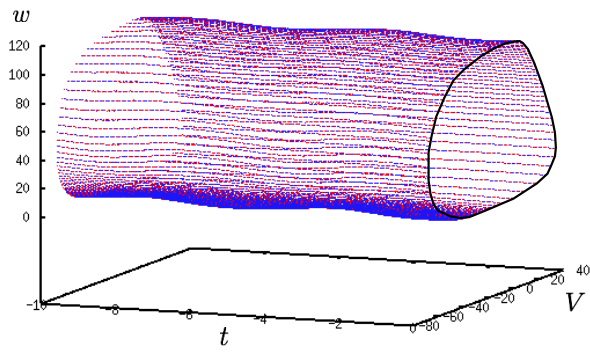
3D effect: cross your eyes until the two red circles meet.

Figure 6.6: A and C: red – $T\rho_1$, blue – $T^2\rho_1$ (hand drawn black circle in C is a visual aid.) B: Difference between $T\rho_1$ and $T^2\rho_1$ where $\rho_1 \equiv 0$.
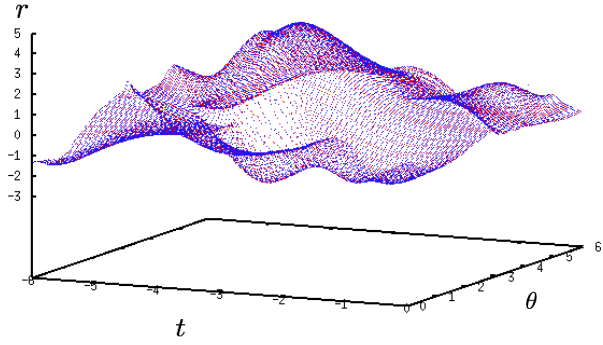
$A : \text{red} - \hat{T}\rho_1, \text{ blue} - \hat{T}^2\rho_1 \text{ where } \rho_1 \equiv 0.$
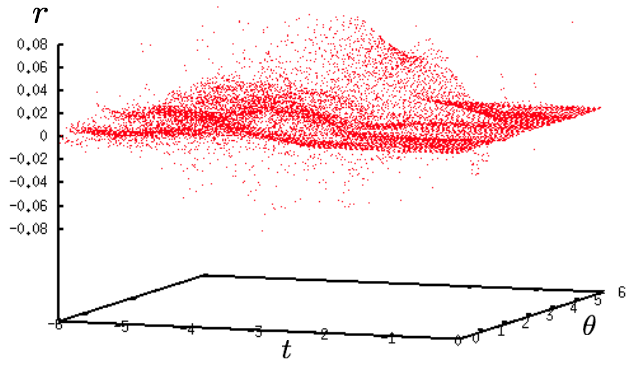
B: Difference between $\hat{T}\rho_1$ and $\hat{T}^2\rho_1$ where $\rho_1 \equiv 0$.

$C : \text{red} - \hat{T}\rho_1, \text{ blue} - \hat{T}^2\rho_1 \text{ where } \rho_1 \equiv 0.$

Figure 6.7: Numerical results from implementing the Graph Transform method $-\hat{T}$ (hand drawn black circle in C is a visual aid).

111
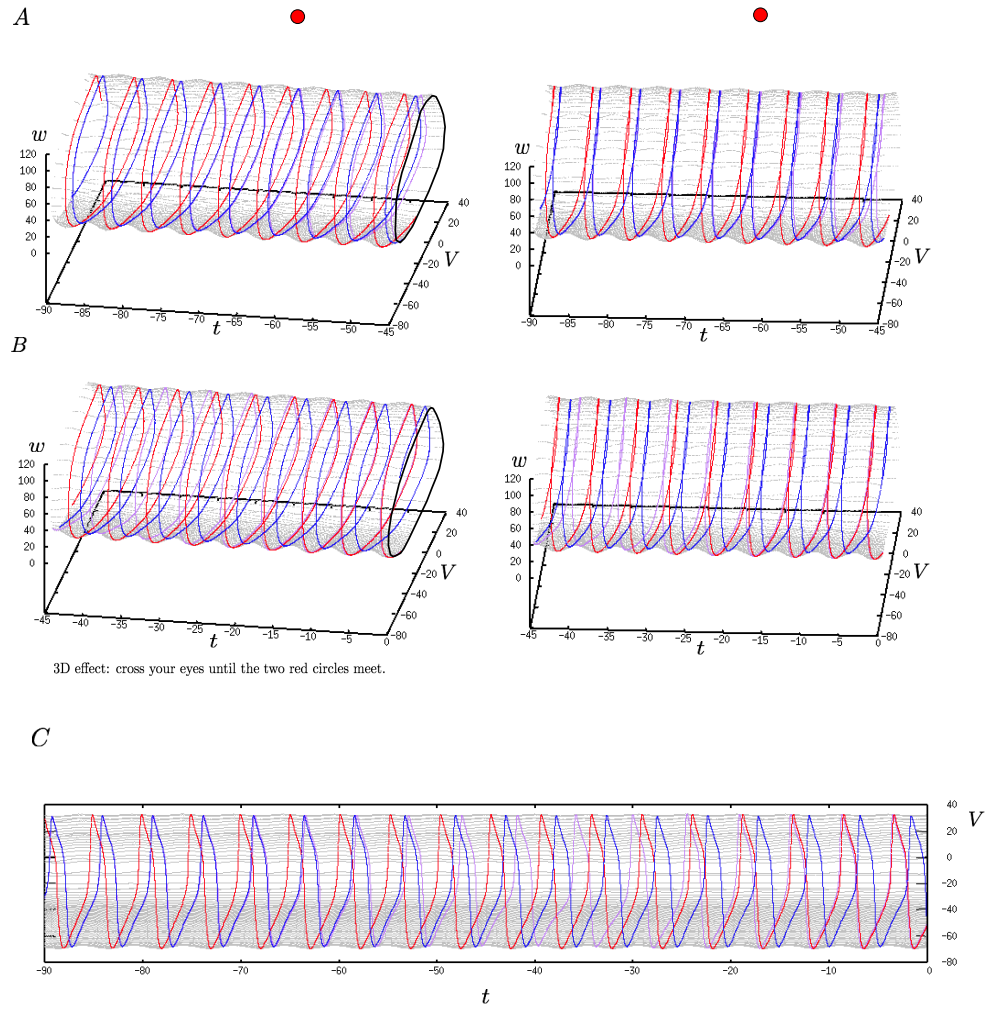
Figure 6.8: A and B: Synchronisation on the cylinder, blue – repeller, red – attractor, purple – generic trajectory (hand drawn black circles are visual aids). C: Voltage versus time plot depicting synchronisation.

6.4.4 Modified Poisson spike train

A neuron can receive signals from another neuron (KS01) where the signal is seen as the forcing and can be modelled as spikes which we model here with shape as shown in Figure 6.4.4. One can use a Hodgkin–Huxley type model
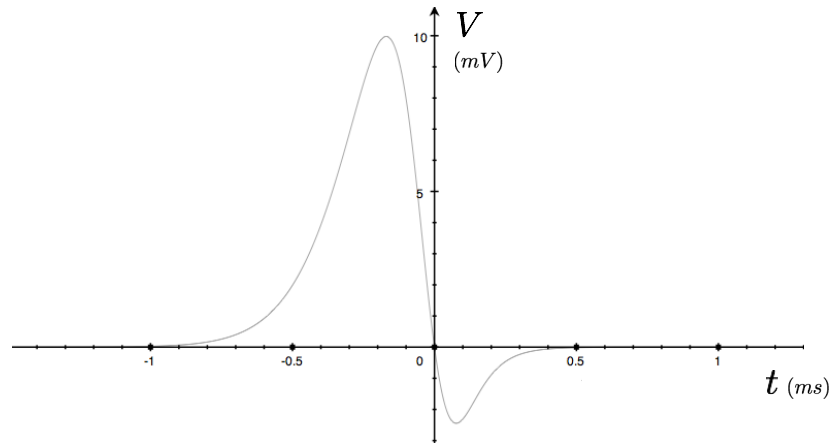

Figure 6.9: The shape of a spike signal from other neurons.

to produce a similar spike shape. However, we generated this spike from the following equation

$$S(t) = 100e^{-\pi(1+\tanh(t/0.5))}\sin(\pi(1+\tanh(t/0.2))), \qquad (6.18)$$

which mimics the shape quite well (KS01).

We can model the arrival of the signals as a modified Poisson process which is essentially a train of spikes that arrives randomly with some average time difference Δt. The Poisson distribution is given by

$$P(S_k \leq t) = 1 - \sum_{i=0}^{k-1} \frac{(\lambda t)^i}{i!} e^{-\lambda t} \qquad (6.19)$$

where $P(S_k \leq t)$ is the probability of observing the kth spike before time $t \geq 0$ and λ is the frequency of the observation.

Now to obtain a train of spikes, taking $k = 1$ in the Poisson distribution (6.19)

113

and rearranging we have

$$t = -\frac{1}{\lambda} \log(1 - x), \tag{6.20}$$

where $x = P(S_1 \leq t)$ and t is interpreted as the time difference between two consecutive spikes. Then by producing a sequence of random numbers $x_i \in [0, 1]$ one can produce a sequence, t_i, of time differences. We wish to consider a spike train with average time difference, between successive spikes, of

$$\Delta t = 5.6 \approx T \tag{6.21}$$

where T is the period of the Morris–Lecar neuron. Note that $\lambda = 1/\Delta t$. If the spikes are too close to each other the invariant cylinder may not persist as the perturbation may be too big. However, if the spikes are too far from each other there will not be much change in the dynamic. So we will restrict $x_i \in [0.53, 0.7]$ which would give a sequence $t_i \in [4.23, 6.74]$. Let us denote the spike train by $P(t)$, then we take the forcing

$$f(t) = P(t).$$

Contraction rate of T and $\hat{T}$

To estimate the contraction rate we will consider the two initial graphs $\rho_1 \equiv 0$ and $\rho_2 \equiv -20$. From the 3–D Figure 6.10 we have the estimates $|T\rho_1 - T\rho_2| = 0.8$ and $|\rho_1 - \rho_2| = 20$. Thus for the contraction rate of T we have the estimate

$$c_T = 0.04. \tag{6.22}$$

In the case of $\hat{T}$, from Figure 6.11 we can obtain a similar estimate

$$c_{\hat{T}} = 0.04. \tag{6.23}$$

As we can see in Figure 6.10 A and C, there is a noticeable difference between the invariant cylinders $T\rho_1$ and $T\rho_2$ in both the new coordinate system and the time–extended (V, w) coordinate system. In some region of the cylinder $T\rho_2$ given in blue shown in Figure 6.10 C, we can clearly see red points (from the other cylinder $T\rho_1$) protruding outwardly. One can see where the input spike caused the most perturbation of the cylinder as seen in Figure 6.10 C, i.e. the region where the red points protrude. Similar observation can be seen for $\hat{T}$ in Figure 6.11 A and C.

	T	$\hat{T}$
Contraction rate	0.04	0.04
ρ_1	$\{r = 0\}$	$\{r = 0\}$
ρ_2	$\{r = -20\}$	$\{r = -20\}$
$\|\rho_1 - \rho_2\|$	20	20
$\|T\rho_1 - T\rho_2\|$	0.8	0.8
grid area $(t \times \theta)$	$[-10, 0] \times [0, 2\pi]$	$[-10, 0] \times [0, 2\pi]$
grid cell $= \|\Delta t\| \times \|\Delta \theta\|$	0.04×0.04	0.04×0.04
s^*	10.00001	10.00001
dt	0.0125	0.0125
δt	0.01	0.01
Newton error	0.05	–
Approx. run time for first iterate	3 hours	3 hours

Table 6.4: Results from Algorithm A and B where two surfaces are iterated. Quantitative details of both algorithms are also included.

Iterates of T and $\hat{T}$

We check how close T and $\hat{T}$ estimate the invariant manifold by taking just the first iterate of $\rho_0 \equiv 0$.

From the numerical results (see the 3–D Figure 6.12), we have

$$|T\rho_1 - T^2\rho_1| = 0.08. \tag{6.24}$$

So the second iterate of ρ_1 is very close to the first iterate. Furthermore, from eye–inspection of Figure 6.12 C, we can see that the two cylinders $T\rho_1$ and $T\rho_2$ in the time–extended (V, w) coordinate system are very close to each other. Similar numerical results were obtained for $\hat{T}$ as seen in Figure 6.13. Thus the first iterate of ρ_0 is a good estimate for the invariant manifold.

	T	$\hat{T}$
ρ_1	$\{r = 0\}$	$\{r = 0\}$
$\|T\rho_1 - T^2\rho_1\|$	0.08	0.08
grid area $(t \times \theta)$	$[-10, 0] \times [0, 2\pi]$	$[-10, 0] \times [0, 2\pi]$
grid cell $= \|\Delta t\| \times \|\Delta\theta\|$	0.02×0.02	0.02×0.02
s^*	10.00001	10.00001
dt	0.0325	0.0125
δt	0.03	0.0041
Newton error	0.05	–
Approx. run time for first iterate	8 hours	8 hours
Approx. run time for second iterate	9 hours	9 hours

Table 6.5: Results from Algorithm A and B where two surfaces are iterated. Quantitative details of both algorithms are also included.

Synchronisation

We found that for $\Delta t = 5.6$, synchronisation takes place as is shown in Figure 6.14. The Figure 6.14A shows a generic trajectory (purple) starting near the repeller (blue) at $t = -180 \, ms$, which significantly deviates away by the time $t = -140 \, ms$. Then as seen in Figure 6.14B, it begins to move towards the attractor (red) for $t \in [-110, -70]$ and then eventually approaches the attractor by the time $t = 0$, as shown in Figure 6.14C. In theoretical neuroscience, it may be of interest to depict this in the (V, t) plane as the voltage time series is of greater relevance. This is given in Figure 6.15 where the invariant cylinder (grey) is also shown. Note that the small indentations at the bottom of the cylinder correspond to the arrival of spikes.

We also investigated other values of Δt and found that for some $|\Delta t|$ significantly bigger than the period T of the Morris–Lecar oscillator, synchronisation does not take place. For those values, the Morris–Lecar oscillator does have an invariant manifold where synchronisation appears to take place for a period of time, but loses this property in a later period of time. This can be explained by the randomness of the input. If the random spikes arrive at a frequency near to that of the intrinsic frequency then the neuron tries to synchronise to the signal for that period of time. Due to randomness, there is a period of time where the signal arrives at frequencies that are far from the intrinsic frequency thus the neuron could not synchronise with the signal for that period of time.

6.4.5 Numerical results for spike train input

To view in 3–D, hold the figures at arm's length then cross your eyes until the two red dots meet horizontally. Otherwise, ignore the pictures in the right column for 2–D images.
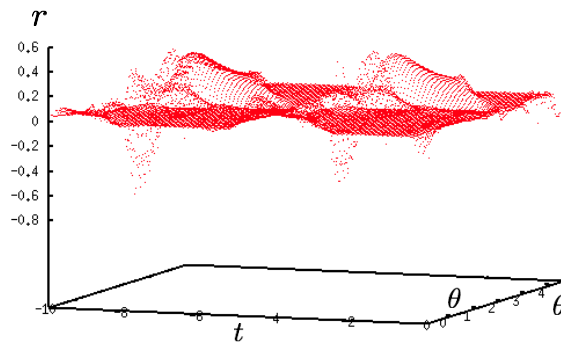
A

B

C
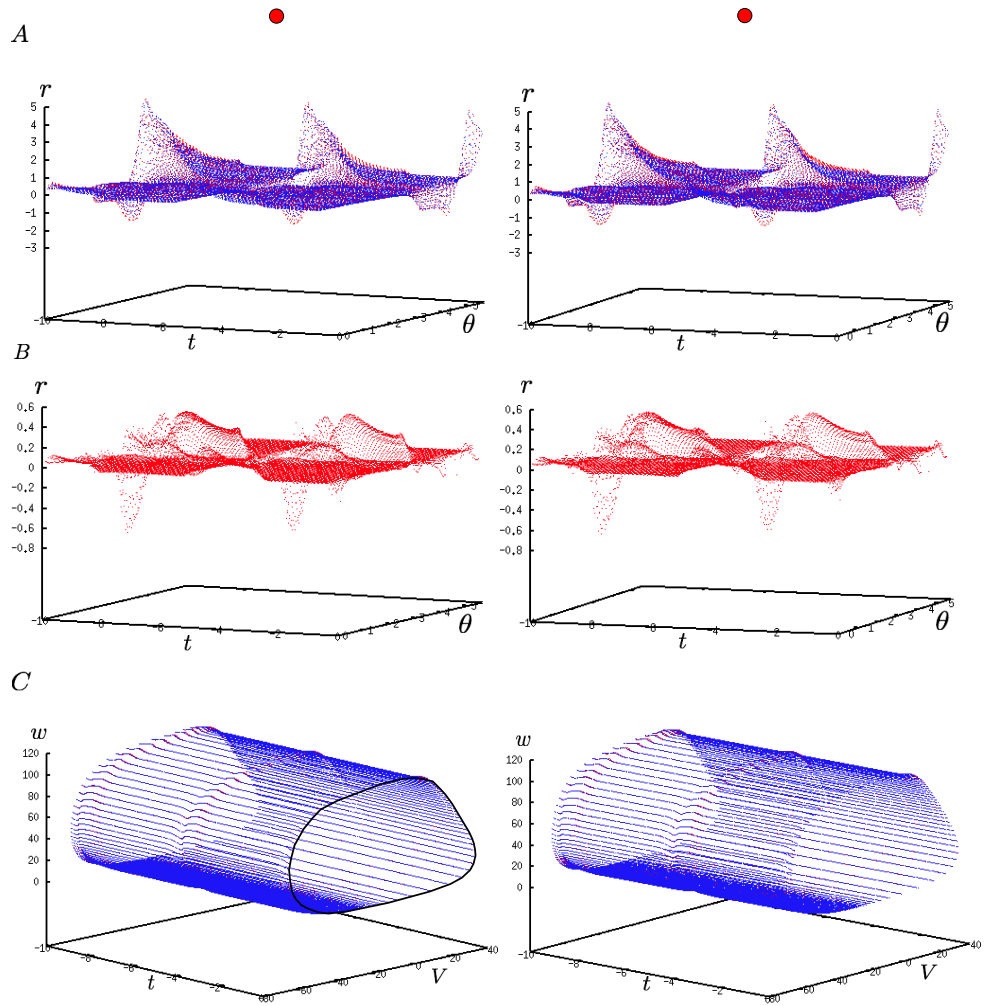
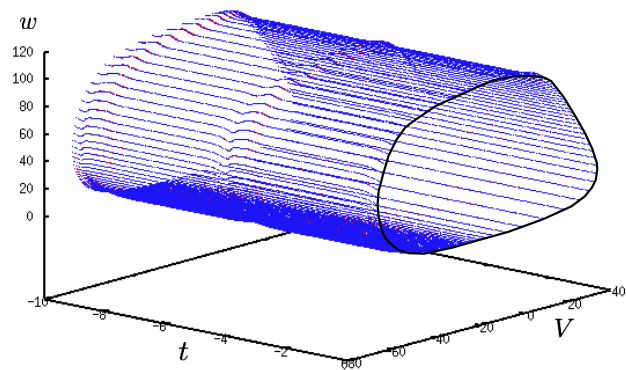3D effect: cross your eyes until the two red circles meet.

Figure 6.10: A and C: red – $T\rho_1$, blue – $T\rho_2$ (hand drawn black circle in C is a visual aid.) B: Difference between $T\rho_1$ and $T\rho_2$ where $\rho_1 \equiv 0$ and $\rho_2 \equiv -20$.

118
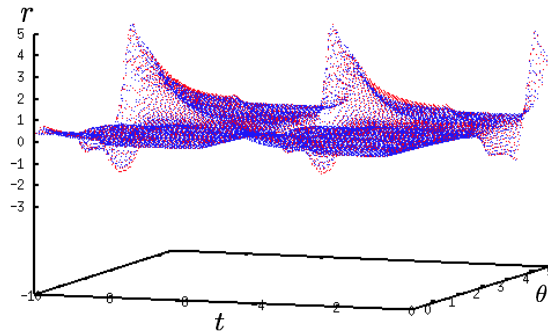
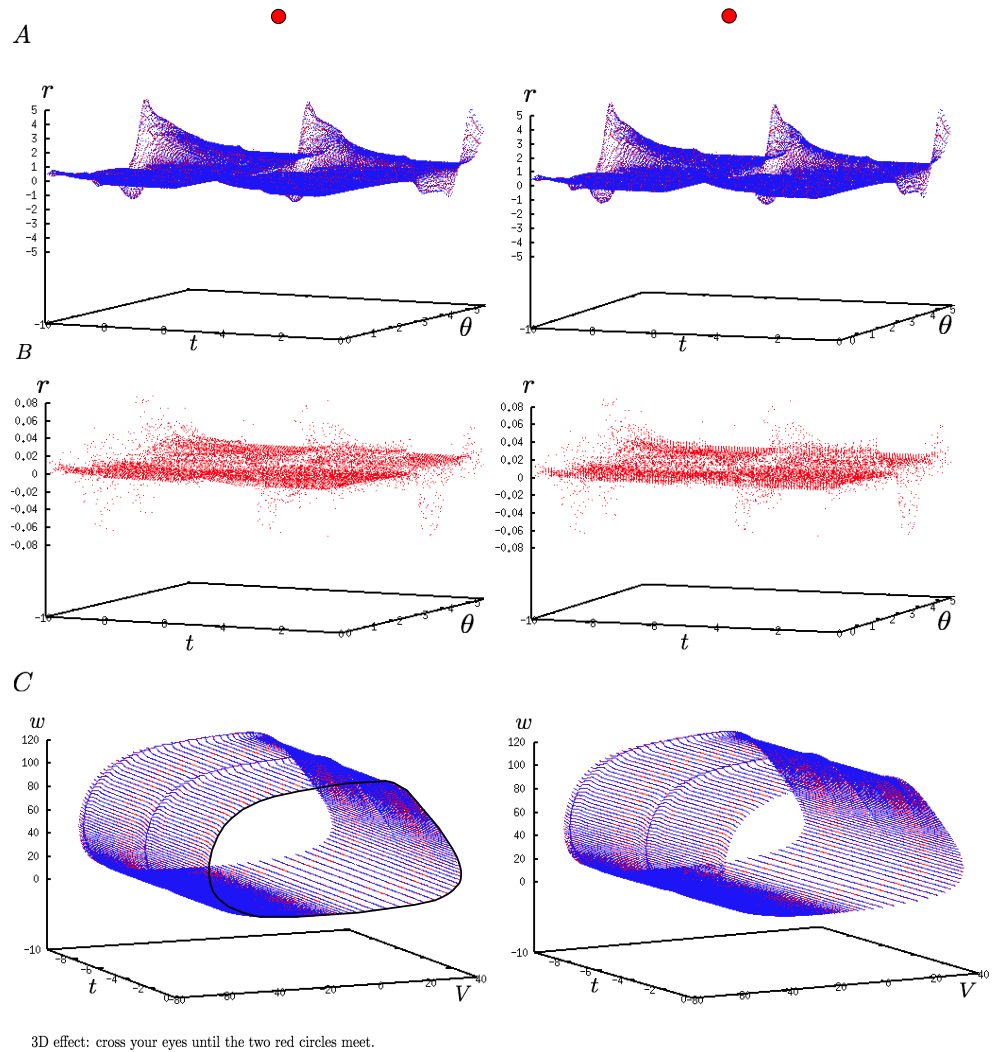A : red $-\hat{T}\rho_1$, blue $-\hat{T}\rho_2$ where $\rho_1 \equiv 0$ and $\rho_2 \equiv -20$.

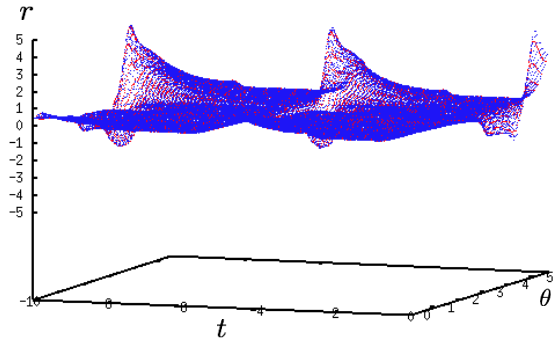B: Difference between $\hat{T}\rho_1$ and $\hat{T}\rho_2$.

C : red $-\hat{T}\rho_1$, blue $-\hat{T}\rho_2$ where $\rho_1 \equiv 0$ and $\rho_2 \equiv -20$.

Figure 6.11: Numerical results from implementing the Graph Transform method $-\hat{T}$ (hand drawn black circle in C is a visual aid).
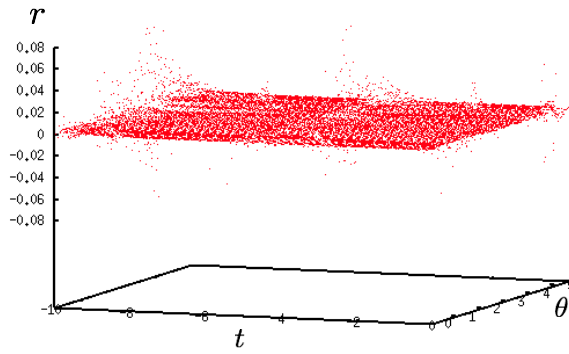
119

A

B

C

3D effect: cross your eyes until the two red circles meet.
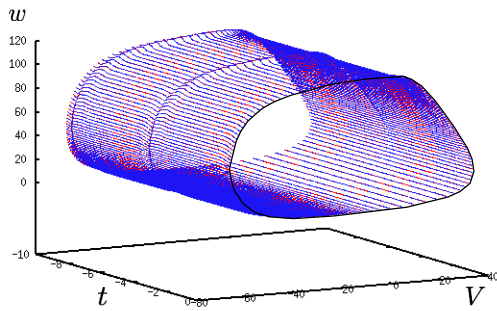
$$(6.25)$$

Figure 6.12: A and C: red – $T\rho_1$, blue – $T^2\rho_1$ (hand drawn black circle in C is a visual aid.) B: Difference between $T\rho_1$ and $T^2\rho_1$ where $\rho_1 \equiv 0$.

120

$A : \text{red} - \hat{T}\rho_1, \ \text{blue} - \hat{T}^2\rho_1 \text{ where } \rho_1 \equiv 0.$
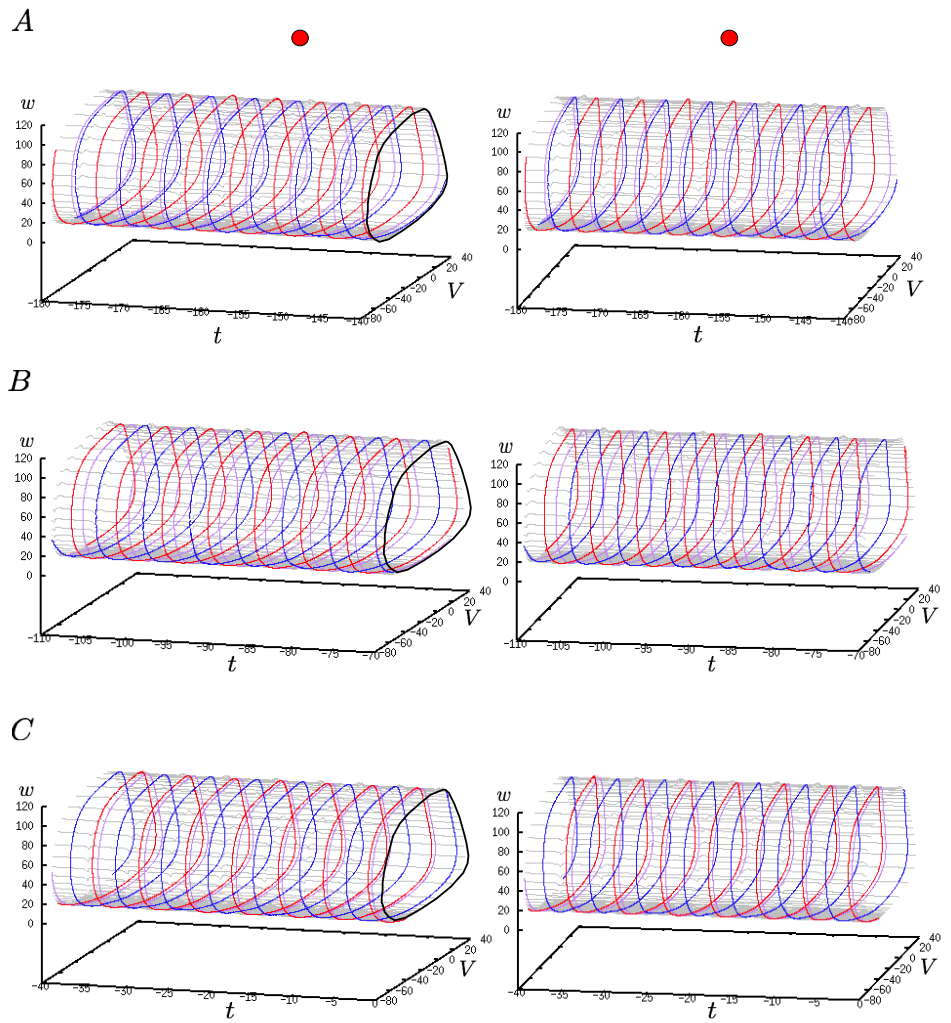

B: Difference between $\hat{T}\rho_1$ and $\hat{T}^2\rho_1$ where $\rho_1 \equiv 0$.

$C : \text{red} - \hat{T}\rho_1, \ \text{blue} - \hat{T}^2\rho_1 \text{ where } \rho_1 \equiv 0.$

Figure 6.13: Numerical results from implementing the Graph Transform method $- \hat{T}$ (hand drawn black circle in B is a visual aid).

121

A

B

C

3D effect: cross your eyes until the two red circles meet.

Figure 6.14: A,B and C are different time sections of the cylinder where synchronisation takes place. blue – repeller, red – attractor, purple – generic trajectory.
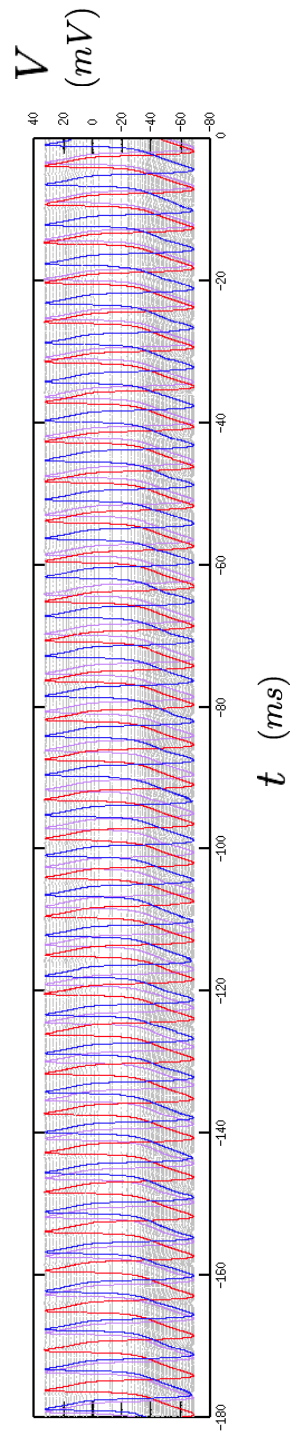
Figure 6.15: Voltage versus time plot of synchronisation: blue – repeller, red – attractor, purple – generic trajectory.

Chapter 7

Conclusions and Discussions

7.1 Uniform hyperbolicity

Given a linear time dependent system it was shown in Chapter 2 that the invertibility of its associated linear operator L implies the system has exponential dichotomy. The proof is similar to that of (Cop78) although the proof presented here deals with the whole of $\mathbb{R}$ instead of the "half lines" $\mathbb{R}_\pm$ as in (Cop78). The response of the system to a forcing is the inverse of L applied to the forcing which is given by a convolution. In addition, if the forcing is exponentially increasing with rate not too large, the response to the system is shown to be bounded by an exponentially increasing function with the same rate.

Uniformly hyperbolic set of systems arising from a time dependent vector field u was studied where each system was essentially defined by an initial point y_0 – the time dependent matrix for the system is evaluated on the trajectory of u passing through y_0 at time t_0. It was shown that the projections in the exponential dichotomy, thus the splittings, varies Hölder continuously with the initial point y_0. Given extra conditions, in particular if the rate for the exponential dichotomy is strictly greater than half the Lipschitz constant of u with respect to y, the splittings vary Lipschitz with y_0. In comparison, for hyperbolic autonomous systems which has a connection with exponential dichotomy, (Pal00) showed the splittings vary continuously with the points on the compact hyperbolic set. However, the result presented here is in the non–compact setting.

Chapter 2 was completed with a perturbation result. In particular if the vector field $\tilde{u}$ is a small enough perturbation of u, the set of perturbed systems arising from $\tilde{u}$ is also a uniformly hyperbolic set.

7.2 Normal hyperbolicity

Normally hyperbolic non–autonomous system was studied in Chapter 3 where the standard definition of normal hyperbolicity was shown to imply the definition given in the context of the thesis. The definition of normal hyperbolicity given here is based on two operators that allows the hyperbolic rates to vary with time thus is more general in this aspect.

By considering the time extended space the invariant manifold becomes non–compact and two approaches were developed to obtain these manifolds. The first was based on Dan Henry (Hen81) given in Theorem3.2.2 which is a path–wise method that avoids the graph transform thus is very advantageous. The improvement here is that the consideration of spectral gap is avoided here, however the result is based on Assumptions 2 which is restrictive and an improvement on this would be constructive. The smoothness and normal hyperbolicity of the manifold was not shown here and it would be valuable to show this in future work. The second approach is a hybrid of path–wise and graph transform which was given as Conjecture 1 and possible steps of the proof were outlined. It would be useful to construct a complete proof for this conjecture. This method was tested numerically with model systems in Chapter 5 and 6 which gave good results. The standard approach called the Graph Transform based on (HPS77, Fen71) was given as Theorem 3.2.3 and was also tested in Chapter 5 and 6 which gave similar results to the hybrid method. It would be beneficial to run numerical tests on the path–wise approach to compare with the other two as it could potentially be faster.

Comparisons of the approaches and recent work by (BOV97, GV04, BHV03) was given. The main contrast is that the work here is not restricted to non–compact invariant manifolds.

7.3 Synchronisations

Given that the invariant manifold can be obtained for a normally hyperbolic non–autonomous system by Chapter 3, it is of great interest to study the dynamic on the invariant manifold which was the subject of Chapter 4. In the case of non–autonomous oscillators the collapse of dynamic can be a desired property such as in phase locked loops (Bre96) where the event is termed synchronisation. By Chapter 3, to study synchronisation on the invariant manifold it is enough to study the time dependent center system of equation. In particular for the case of a $1 - D$ oscillator, synchronisation was defined and conditions were found for synchronisation to occur and proved in Theorem 4.1.1. In contrast, Ku-

ramoto's phase model does not include time dependency (Kur84). Conditions for a special form of synchronisation termed "reliability" as in (LSBY09) were considered in the context of non–autnomous oscillators. In higher dimensional systems such as many interacting oscillators, synchronisation was also defined. A schematic of how these oscillators could synchronise were given which serves as an outline for possible future approach to studying synchronisation as an aggregation process. It would be beneficial to find conditions for synchronisation to take to place in the many oscillators case.

A valuable future research direction could be to numerically verify the theory of synchronisation in Chapter 4 and in particular, numerically approximate the robustness region of synchronisation for a forced oscillator as in (BM03). It would be worthwhile to complete the extension of this theory to the case of two oscillators and develop the percolation idea for many oscillators.

7.4 Applications

The approaches to computing invariant manifolds given in Chapter 3 are applied to an individual normally hyperbolic oscillator in Chapter 5. In particular, assuming the unperturbed normally hyperbolic oscillator has a normally hyperbolic manifold $\rho_0 \equiv 0$ it was shown in Theorem 5.1.1 that the weakly forced oscillator also has an invariant manifold. Pseudo–codes to compute the perturbed manifold were outlined and the C++ header files of the numerical simulations were given.

The approaches, in particular that of Conjecture 1 and the Graph Transform of Theorem 3.2.3, were tested numerically on a $2 - D$ attracting normally hyperbolic oscillator under a quasi–periodic forcing with various parameter regimes. Note that although the quasi–periodic case can be studied with standard approaches that computes compact invariant manifold (BOV97) by appropriate extension of coordinate system, it is used here in the non–compact setting to demonstrate the capability of the method developed in this thesis.

In the application to the simple 2–D oscillator we found the contraction rate of our method T and that of Graph Transform $\hat{T}$ (HPS77) are very similar in value where both are roughly 7.5×10^{-5}. This is contrary to what we would expect – that is our method has a faster contraction rate as it depends on the coordinate system. However, the main reason for the comparable contraction rate is because we took a long time–T map for the Graph Transform method, i.e. as long as the time needed in the integration for the estimate of the Green's function for our method (see **Algorithm 1**). But a longer time–T map implies

a faster contraction for the Graph Transform $\hat{T}$.

The implementation of $\hat{T}$ runs marginally faster than that of T because our method has an extra step in evaluating the Green's function for each Newton step (see **Algorithm 2**), although this is not too computationally expensive. However, the method $\hat{T}$ for general systems that also have normal expanding directions would require extra computation in taking the intersection to obtain the invariant manifold (see Theorem 3.2.3). In contrast, the advantage with our method is that it directly computes the invariant manifold which could be further explored numerically if time permitted.

We found the first iterate of the zero graph $\rho_0 \equiv 0$ is a sufficiently good estimate for the invariant manifold. We investigated the dynamic on the invariant manifold and depending on the parameters of the forcing, no synchronisation, "saddle node" synchronisation (onset of synchronisation) and synchronisation can take place.

We explored the frequency difference between that of the forcing and the oscillator and found that synchronisation takes place for frequency difference below the value 0.1. We saw that for frequency difference equal to 0.2 there is no synchronisation and the oscillator is essentially independent to the forcing.

To further test the methods in computing invariant manifolds it would be valuable to test it on a higher dimensional system such as two coupled oscillators.

Note that no optimisation steps were taken in any computations in this and the next chapter. Further work to improve computational efficiency might be beneficial. Note that the computations were performed on a MacBook Pro laptop with Intel Core i7 2GHz processor.

7.5   Morris–Lecar oscillator

The approaches to computing invariant manifolds given in Chapter 3 was also applied to the Morris–Lecar oscillator in Chapter 6. Under certain parameter regimes the biophysically relevant equation exhibit an attracting limit cycle. The adjoint method was used to compute the linear isochrons of the limit cycle which was used to define a local coordinate system around the cycle. This was useful in the computer coding since the methods presented in Chapter 3 assume a coordinate system around the unperturbed manifold, the limit cycle in this case.

Various forcing to the Morris–Lecar oscillator were studied here. In the case of periodic forcing, both methods of computing the invariant manifold showed similar contraction rate of 0.04. The dynamic on the invariant manifold was studied and in particular it was found that when the frequency difference between the forcing and that of the oscillator was 0.1 rad/ms, the oscillator synchronises. In the case of two–frequency–periodic forcing, under certain parameters relating to frequency difference, a "saddle node" type synchronisation takes place where trajectories are attracted to a "saddle node" for some time then deviates from it.

A modified Poisson spike train was applied to the Morris–Lecar oscillator and the perturbed invariant manifold was also computed. The contraction rate of the two methods in computing the invariant manifold was both 0.04. When the average time difference between spikes is 5.6 ms, which is close to the oscillator period of 5.59992 ms, the dynamic on the invariant manifold synchronises. Note that this case of forcing, which has random feature, can not be dealt with using standard methods that computes compact invariant manifold such as (BOV97). As far as I know, this is the first time that an invariant cylinder is computed in a non–compact setting.

There are several further analyses that could be carried out. For example one can consider forcing with a noise component which can be biologically realistic. It may be of physiological interest to investigate forcing that give rise to more than one synchronised trajectory.

Bibliography

[ACP10] G. Alberti, M. Csörnyei, and D. Preiss. Differentiability of lipschitz functions, structure of null sets, and other problems. *Proceedings of the International Congress of Mathematicians*, 2010.

[BHV03] H. Broer, A. Hagen, and G. Vegter. Multipurpose algorithms for invariant manifolds. *Dynamics of Continuous, Discrete and Impulsive Systems*, 2003.

[BM03] Z. Bishnani and R.S. MacKay. Safety criteria for aperiodically forced systems. *Dynamical Systems: An International Journal*, 18:107–129(23), June 2003.

[BMH04] E. Brown, J. Moehlis, and P. Holmes. On the phase reduction and response dynamics of neural oscillator populations. *Neural Comp.*, 16(161-172), 2004.

[BOV97] H.W. Broer, H.M. Osinga, and G. Vegter. Algorithms for computing normally hyperbolic invariant manifolds. *Z. angew. Math. Phys.*, 48(480-524), 1997.

[Bre96] V. Paul Brennan. *Phase-locked loops : principles and practice.* Macmillan press LTD, 1996.

[BRS99] R.J. Butera, J. Rinzel, and J.C. Smith. Models of respiratory rhythm generation in the pre-bötzinger complex. ii. populations of coupled pacemaker neurons. *J Neurophysiology*, 1999.

[Cop78] W.A. Coppel. *Dichotomies in stability theory.* Lecture Notes in Mathematics. Springer, 1978.

[dlVP52] Ch. de la Vallée Poussin. *L'approximation des fonctions d'une variable ré elle.* Gauthier-Villars, Paris, 1952.

[EK84] B. Ermentrout and N. Kopell. Frequency plateaus in a chain of weakly coupled oscillators. *SIAM J. Math. Anal.*, 15(215-237), 1984.

[Eld12] J. Eldering. *Persistence of noncompact Normally Hyperbolic Invariant Manifolds in bounded geometry.* PhD thesis, Utrecht University, 2012.

[Fen71] Neil Fenichel. Persistence and smoothness of invariant manifolds for flows. *Indiana University Mathematics Journal*, 21(3), 1971.

[FN06] Feldman and Del Negro. Looking for inspiration: new perspectives on respiratory rhythm. *Nature Review Neuroscience*, 7:232–241, 2006.

[GH83] J. Guckenheimer and P. Holmes. *Nonlinear Oscillations, Dynamical Systems, and Bifurcations of Vector Fields.* Springer Verlag, Berlin, 1983.

[Guc75] J. Guckenheimer. Isochrons and phaseless sets. *J. Math. Biol., 1: 259-273.*, 1975.

[GV04] J. Guckenheimer and E. Vladimirsky. A fast method for approximating invariant manifolds. *SIAM Journal of Applied Dynamical Systems*, 3, 2004.

[Hen81] D. Henry. *Geometric theory of semilinear parabolic equations.* Springer Verlag, Berlin Heidelberg New York, 1981.

[HPS77] M.W. Hirsch, C.C. Pugh, and M. Shub. *Invariant Manifolds*, volume 583 of *Lecture Notes in Mathematics.* Springer Verlag, 1977.

[HS74] M.W. Hirsch and S. Smale. *Differential equations, dynamical systems, and linear algebra.* Elsevier/Academic Press, 1974.

[Izh07] E.M. Izhikevich. *Dynamical Systems in Neuroscience.* The MIT press, 2007.

[Kat76] T. Kato. *Perturbation theory for linear operators.* Berlin : Springer-Verlag, 1976.

[KS01] J. Keener and J. Sneyd. *Mathematical Physiology.* Springer, 2001.

[Kur84] Y. Kuramoto. *Chemical Oscillations, Waves and Turbulence.* Springer-Verlag, 1984.

[Leb09] H. Lebesgue. *Sur les intégrales singulières*, volume 25-117. Ann. Fac. Sci. Univ. Toulouse, 1909.

[LSBY09] K.K. Lin, E. Shea-Brown, and L.-S. Young. Reliability of coupled oscillators. *Journal of Nonlinear Science*, 19(497-545), 2009.

[Mil] http://info.arup.com/millenniumbridge/.

[ML81] C. Morris and H. Lecar. Voltage oscillations in the barnacle giant muscle fiber. *Biophys J 35:193-213*, 1981.

[MM10] A. Margheri and R. Martins. Generalized synchronization in linearly coupled time periodic systems. 249:3215–3232, 2010.

[Pal00] K. Palmer. *Shadowing in Dynamical Systems*. Kluwer Academic Publishers, 2000.

[PKS08] S.A. Prescott, Y.D. Koninck, and T.J. Sejnowski. Biophysical basis for three distinct dynamical mechanisms of action potential initiation. *PLos computational biology*, 2008.

[PRK01] A. Pikovsky, M. Rosenblum, and J. Kurths. *Synchronization*. Cambridge, 2001.

[SD09] Ö. Suvak and A. Demir. *Computing quadratic approximations for the isochrons of oscillators: a general theory and advanced numerical methods*. ACM, 2009.

[Str01] S. Strogatz. *Nonlinear Dynamics and Chaos: With Applications to Physics, Biology, Chemistry, and Engineering*. Westview Press, 2001.

[Str04] S. Strogatz. *Sync: the emerging science of spontaneous order*. Penguin Books, 2004.

[WHM94] S. Wiggins, G. Haller, and I. Mezic. *Normally hyperbolic invariant manifolds in dynamical systems*. Springer, 1994.

[Win80] A Winfree. *The Geometry of Biological Time*. Springer Verlag, New York, 1980.